



STANISŁAW WYBRANIEC

# TRANSFORMATIONS AND VISUALIZATION OF POTENTIAL FIELD DATA

---

POLISH GEOLOGICAL INSTITUTE SPECIAL PAPERS 1

WARSZAWA 1999



## TABLE OF CONTENTS

Introduction . . . . .	8
Transformations . . . . .	8
Transformation operators . . . . .	10
Differentiation . . . . .	10
Integration . . . . .	11
Analytical continuation . . . . .	11
New transformations . . . . .	11
Fractional differentiation and integration . . . . .	11
Hilbert transforms and directional scalar decomposition . . . . .	12
Design of digital filters . . . . .	13
1D digital filters . . . . .	13
Symmetric filters . . . . .	13
Symmetric transductor . . . . .	13
Vertical differentiator . . . . .	14
Vertical bi-differentiator . . . . .	14
Upward continuator . . . . .	15
Downward continuator . . . . .	15
Anti-symmetrical filters . . . . .	15
Anti-symmetrical transductor (Hilbert transformer) . . . . .	15
Horizontal (anti-symmetric) differentiator . . . . .	16
2D digital filters . . . . .	16
The Fourier-Hankel transform . . . . .	16
The 2D Fourier transform in polar co-ordinates . . . . .	17
2D digital filter design . . . . .	18
2D symmetric filters . . . . .	18
2D anti-symmetric filters . . . . .	20
Visualization . . . . .	20
Colour space and its co-ordinates . . . . .	21
Colour scales for scalar fields . . . . .	21
Shaded-relief . . . . .	23
Vector fields and vectorial images . . . . .	23
Other vectorial images . . . . .	24
Implementation . . . . .	24
Conclusions . . . . .	25
References . . . . .	25
Transformacje i wizualizacja danych pól potencjalnych . . . . .	26
Plates . . . . .	29



## ***Address of the Editor-in-Chief***

*It is an honour and a real pleasure to announce the commencement by the Polish Geological Institute of the new publication series: **the Polish Geological Institute Special Papers**. The series is intended to make available, in English language, the synthetic results of the Institute's vast studies on various problems of geology of Poland, in the form of monographs or collection of monographic papers, to the international, geological audience.*

*It has always been the Institute's ambition to enrich the treasury of geological sciences, on the internal, Polish scale but also on broader, world-wide scale, with the most important results of the Institute's numerous scientific and applied geological projects.*

*Initially, the Institute's publications, published fully in Polish, were provided with English summaries and the English translation of the explanations of figures, tables, photos, etc.*

*During the last ten years, the Institute's merited quarterly, **Kwartalnik Geologiczny**, was turned into the periodical, **Kwartalnik Geologiczny/Geological Quarterly**, published fully in English language.*

*The second highly regarded Institute's publication series, **Prace Panstwowego Instytutu Geologicznego** (*Memoirs of the Polish Geological Institute*), presenting for many years the synthetic scientific results in the form of monographs, started during the last years to publish some positions in English. However, after giving some thoughts to the effectiveness of such a mixed, Polish-English series, it was decided to leave **Prace PIG** to the Polish edition of the Institute's monographs, and to start a completely new series of such publications as fully English edition. **The Polish Geological Institute Special Papers** are implementing that decision in practice.*

*Despite the general philosophy of publishing, first of all, the results of the Institute's scientists studies, it is also intended to open the series for geologists from other befriended geological institutions, as well as for the proceedings of some international seminars organised in Poland.*

*It is my true belief and a real hope that the new publication series of the Polish Geological Institute, **the Polish Geological Institute Special Papers**, will soon develop the collection of numerous and valuable positions which will gain the international interest and appreciation.*

*Dr. Maciej PODEMSKI*



WYBRANIEC S., 1999 — **Transformations and visualization of potential field data.** *Polish Geological Institute Special Papers* 1: 1–88.  
Stanisław Wybraniec, Polish Geological Institute, ul. Rakowiecka 4, 00-975 Warszawa, Poland. E-mail: swyb@pgi.waw.pl

**Abstract.** Transformations of potential field data is a very important step in their interpretation. It can even be treated as just another interpretation method (Blakely, 1996). The same can be said about visualization of potential field data.

The paper presents the results of studies in both fields undertaken by the author. In the transformation method a novel technique of calculating 2D digital filters was devised, based on the Fourier-Hankel transform; new methods of transformations using fractional derivatives and integrals was proposed; the importance of 3D Hilbert transform was stressed as well as its use in analytical signal transformations of non-potential data was shown. Decomposition of 2D function to directional components was defined.

On the visualization side, new methods of imaging potential field data were devised. The most promising are vectorial images. They can be used also in the case of scalar data.

Many examples of both new transformations and new method of imaging are shown, using European and Polish gravity data and Polish magnetic data.

The presented methods can also be used for non-potential field data. Images of transformed hypsographic data of Poland are presented as an example.

Key words: potential fields, transformations, digital filtering, visualization, vectorial images, Poland, Europe.

---

**Abstrakt.** Transformacje są bardzo ważnym krokiem w interpretacji pól potencjalnych. Można je nawet traktować jako niezależną metodę interpretacji (Blakely, 1996). To samo można powiedzieć o wizualizacji tych danych.

W pracy przedstawiono wyniki badań podjętych przez autora w obu tych dziedzinach. Od strony transformacji przedstawiono nowy sposób liczenia dwuwymiarowych (2D) filtrów cyfrowych bazujących na transformacji Fouriera-Hankela, opracowany przez autora i stosowany już od wielu lat w praktyce; zaproponowano nowe metody transformacji oparte na pojęciu pochodnych i całek ułamkowych; podkreślono wagę trójwymiarowej transformacji Hilberta i pojęcia sygnału analitycznego w transformacjach pól potencjalnych, a także dowolnych danych powierzchniowych; zdefiniowano pojęcie składowych kierunkowych.

Od strony wizualizacji przedstawiono nowe metody obrazowania danych pól potencjalnych, m.in. obrazy wektorowe, które można wykorzystać także do prezentacji danych skalarnych, po ich transformacji do sygnału analitycznego.

Pokazano wiele przykładów zastosowania proponowanych metod transformacji i wizualizacji z wykorzystaniem głównie danych polskich (dane grawimetryczne i magnetyczne), a także europejskich (dane grawimetryczne). Przedstawione metody można zastosować także do danych pól niepotencjalnych, co zademonstrowano na przykładzie obrazów przedstawiających transformowane dane hipsometryczne Polski.

Słowa kluczowe: pola potencjalne, transformacje, filtracja cyfrowa, wizualizacja, obrazy wektorowe, Polska, Europa.

---

## INTRODUCTION

Natural potential fields data are very important source of information about the Earth. The Earth's gravity field contains information about its whole structure. The Earth's magnetic field is an invaluable source of information about the structure of the upper part of continental crust. As in both fields the information from many geological bodies is stacked together, the main interpretation problem is to attenuate unwanted information and to enhance that from bodies we are interested in. This can be done by an appropriate transformation and additionally, by using the best methods of visualization. The author worked in both fields on several topics which he found most important.

First goal was to design a new technique for calculating 2D digital filters which are necessary in digital filtration (transfor-

mations) of potential fields, other goal was to broaden a range of transformation methods, and to use 3D Hilbert transform, and at last, to work out better visualization tools.

Several new methods worked out during these studies were proven in practice. The new technique of calculating 2D digital filters has already been used for several years. The new visualization methods were tested on European and Polish gravity and magnetic data. One important point should be stressed: almost all methods worked out for potential fields, can be also applied to non-potential field data as (for example) to hypsography. Examples from Poland's hypsographic data are presented in the paper.

## TRANSFORMATIONS

Transformation of potential fields can be seen as just another method of interpretation. It facilitates geologic interpretation by transforming field data into new, more suitable form, where useful information can be enhanced.

The basic formula for transformations in space domain (a co-ordinate system with space co-ordinates) is that of convolution:

1D convolution

$$\begin{aligned} h(x) = f(x) * g(x) &= \int_{-\infty}^{\infty} f(x')g(x-x')dx' = \\ &= \int_{-\infty}^{\infty} g(x')f(x-x')dx', \end{aligned}$$

2D convolution

$$\begin{aligned} h(x, y) = f(x, y) * g(x, y) &= \\ &= \int_{-\infty}^{\infty} f(x', y')g(x-x', y-y')dx'dy' = \\ &= \int_{-\infty}^{\infty} g(x', y')f(x-x', y-y')dx'dy'. \end{aligned}$$

It means, that transformed function  $h(x)$  or  $h(x, y)$  can be obtained by convolution with the function  $g(x)$ , or  $g(x, y)$  respectively, which are characteristic and unique for every transformation. These expressions are only for continuous functions  $f(x)$  or  $f(x, y)$ . In practice we seldom use continuous functions. Usually we deal with discrete functions of the form  $f(n\Delta x)$ , where  $\Delta x$  is an interval of discretization or sampling rate and  $n$  is an integer number. In 2D space it is  $f(n_x\Delta x, n_y\Delta y)$ . We usually set the value of  $\Delta x$  and  $\Delta y$  to 1, so our functions have a form  $f(n)$  and  $f(n_x, n_y)$ .

The discrete convolution is as follows:

1D discrete convolution

$$\begin{aligned} h(n) = f(n) * g(n) &= \sum_{k=-\infty}^{\infty} f(k)g(n-k) = \\ &= \sum_{k=-\infty}^{\infty} f(n-k)g(k), \end{aligned}$$

2D discrete convolution

$$\begin{aligned} h(n_x, n_y) = f * g &= \sum_{k_x=-\infty}^{\infty} \sum_{k_y=-\infty}^{\infty} f(k_x, k_y) \times \\ &\quad \times g(n_x - k_x, n_y - k_y) = \\ &= \sum_{k_x=-\infty}^{\infty} \sum_{k_y=-\infty}^{\infty} g(k_x, k_y) f(n_x - k_x, n_y - k_y). \end{aligned}$$

In practice we have finite functions only, so we have the following expressions:

1D finite discrete convolution (1D digital filtration)

$$h(n) = f(n) * g(n) = \sum_{k=-M}^M f(n-k)g(k),$$

2D finite discrete convolution (2D digital filtration)

$$\begin{aligned} h(n_x, n_y) = f * g &= \\ &= \sum_{k_x=-M}^M \sum_{k_y=-N}^N f(n_x - k_x, n_y - k_y) g(k_x, k_y). \end{aligned}$$

Finite discrete convolution is also called a digital filtration and function  $g$  is called a digital filter.

We must mention very important point in function theory, namely their symmetry. Every function can be symmetric (even), anti-symmetric (odd) or non-symmetric. A symmetric (even) function has a property that  $f(x) = f(-x)$ ; in anti-symmetric (odd) function we have following relation:  $f(x) = -f(-x)$ . A non-symmetric function is a sum of symmetric  $f_s(x)$  and anti-symmetric  $f_a(x)$  parts:

$$f(x) = f_s(x) + f_a(x),$$

where

$$f_s(x) = \frac{f(x) + f(-x)}{2},$$

$$f_a(x) = \frac{f(x) - f(-x)}{2}.$$

Up to now we have operated in space domain, where co-ordinates  $x$  and  $y$  are space co-ordinates. We can operate in another, very important domain — a frequency domain. We can move from space domain to frequency domain using Fourier transform:

1D Fourier transform

$$f(\omega_x) = \int_{-\infty}^{\infty} f(x) e^{-i\omega_x x} dx,$$

$$f(x) = \frac{1}{2\pi} \int_{-\infty}^{\infty} f(\omega_x) e^{i\omega_x x} d\omega_x.$$

Or in symbolic form:

$$f(\omega_x) = F[f(x)],$$

$$f(x) = F^{-1}[f(\omega_x)].$$

We can write the 1D Fourier transform in an expanded form:

where  $i = \sqrt{-1}$ .

If we show the function  $f$  as a sum of symmetric and anti-symmetric parts we have following:

$$\begin{aligned} f(\omega_x) &= \int_{-\infty}^{\infty} f(x) \cos \omega_x x dx - i \int_{-\infty}^{\infty} f(x) \sin \omega_x x dx = \\ &= \int_{-\infty}^{\infty} [f_s(x) + f_a(x)] \cos \omega_x x dx - \\ &\quad - i \int_{-\infty}^{\infty} [f_s(x) + f_a(x)] \sin \omega_x x dx = \\ &= \int_{-\infty}^{\infty} f_s(x) \cos \omega_x x dx - i \int_{-\infty}^{\infty} f_a(x) \sin \omega_x x dx, \end{aligned}$$

because integral of product of symmetric and anti-symmetric functions are zero (cosine function is symmetric and sine function is anti-symmetric).

When treating with 2D functions we use 2D Fourier transform:

Two-dimensional Fourier transform

$$f(\omega_x, \omega_y) = \int_{-\infty}^{\infty} \int_{-\infty}^{\infty} f(x, y) e^{-i(\omega_x x + \omega_y y)} dx dy,$$

$$f(x, y) = \frac{1}{4\pi^2} \int_{-\infty}^{\infty} \int_{-\infty}^{\infty} f(\omega_x, \omega_y) e^{i(\omega_x x + \omega_y y)} d\omega_x d\omega_y.$$

Or in symbolic form:

$$f(\omega_x, \omega_y) = F[f(x, y)],$$

$$f(x, y) = F^{-1}[f(\omega_x, \omega_y)].$$

Frequency domain is also called wavenumber domain, its co-ordinates are [space] frequencies.

The variables  $\omega_x, \omega_y$ , are called angular frequencies or wavenumbers, the other used frequency variables are  $v_x, v_y$  called simply frequency. The inverse of frequency  $v_x$  is wavelength  $\lambda_x$ . Relation between these variables is as follows:

$$\omega_x = 2\pi v_x, v_x = \frac{\omega_x}{2\pi}, \lambda_x = \frac{2\pi}{\omega_x} = \frac{1}{v_x}.$$

The Fourier transform of the function is called a spectrum. The spectrum of continuous function is also continuous and usually infinite. The spectrum of the discrete function is a periodical continuous function. The period of the spectrum is  $2\pi/\Delta x$ . It means, that if the highest frequency is  $\omega_x^N$ ,

$$2\omega_x^N = \frac{2\pi}{\Delta x} \text{ so } \omega_x^N = \frac{\pi}{\Delta x} \text{ or } v_x^N = \frac{1}{2\Delta x}.$$

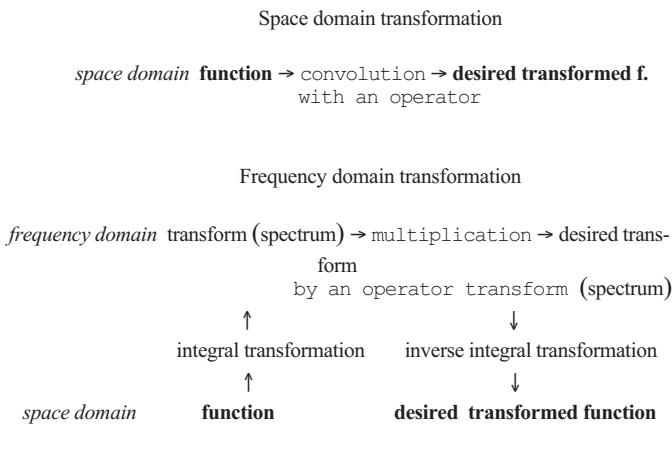
So the highest frequency of a discrete function,  $\omega_x^N$  or  $v_x^N$ , called the Nyquist frequency, is closely related to the interval of discretization (sampling rate). In case of normalized frequency where  $\Delta x = 1$ , the Nyquist frequency  $\omega_x^N = \pi$ , and  $v_x^N = 0.5$ . We can easily obtain the expressions for the shortest or the Nyquist wavelength for the discrete function:  $\lambda_x^N = 2\Delta x$ , and for the normalized function ( $\Delta x = 1$ )  $\lambda_x^N = 2$ .

In frequency domain convolution has very interesting form, from the infinite integral it changes to simple multiplication of the spectra:

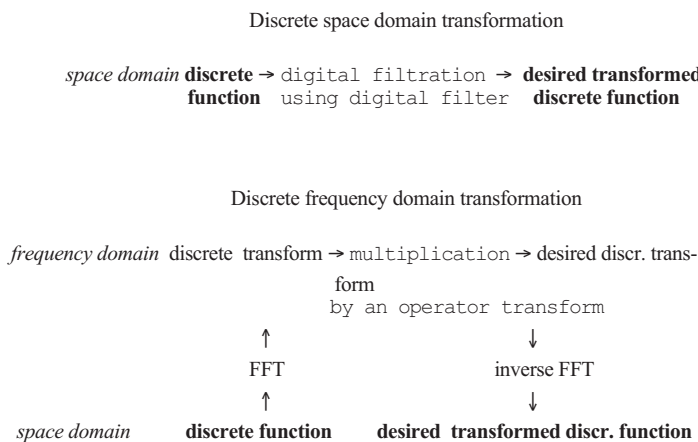
$$\begin{array}{ccc} \text{Space domain} & \xrightarrow{\text{convolution } f * g,} & \\ & \downarrow & \\ \text{Frequency domain} & \xrightarrow{\text{multiplication } f g.} & \end{array}$$

So transformations can be done using two methods. First, in space domain, we can use appropriate digital filter (space domain operator) to convolve with a given function to obtain

a desirable transformation. Another way is to operate in frequency domain or wavenumber domain. First we must enter the frequency domain using some integral transform, e.g. Fourier one. Then multiply the function transform by an appropriate frequency domain operator to obtain a desirable transformation. In the end we must exit frequency domain by inverse integral transform.



The above formulae holds in case of continuous functions. As we said, in practice we deal with discrete functions, so in this case we use discrete analogue of convolution — digital filtration and a discrete analogue of Fourier transform — a discrete Fourier transform or rather its most popular form — the fast Fourier transform (FFT). So now we will have the following relations:



As we see, the transformations base on an appropriate change of a spectrum of a function which describe field data. We can multiply the spectrum by a desirable operator in the frequency domain, or do it in the space domain by digital filtration using a filter which has desirable spectrum.

## TRANSFORMATION OPERATORS

We can use many different operators to obtain desirable transformations. It depends on what kind of information included in the field data we want to enhance. For example, if

we are interested in shallow bodies we must choose operators which strengthen high frequencies and attenuate low frequencies. If we want to eliminate noise, we must use operators for attenuating high frequencies.

There are many kinds of operators. The simplest operators are those, where we just remove chosen part of the spectrum (i.e. frequency band) without changing the rest of it. These are operators, or filters in discrete space which are used mostly in technology. We have here bandpass filters or stop-band filters. In the first case, we have lowpass filters (low frequencies are passed through and high frequencies are stopped) and highpass filters which do the opposite. These filters are not best suited for potential fields, because the spectra of body are not finite, so it is not limited to some frequency band, and it is not possible to eliminate an influence of e.g. shallow body and to left intact the spectrum of a deep one or vice versa.

## DIFFERENTIATION

Usually we use filters which change whole spectrum of the field data function in a simple way. The operation of vertical differentiation is a simplest operation of this kind. The frequency domain operator for the first vertical derivative is just

$$g_{dz}(\omega_x) = \omega_x \text{, for 1D case,}$$

and

$$g_{dz}(\omega_x, \omega_y) = \omega_x \text{, for 2D case,}$$

where

$$\omega = \sqrt{\omega_x^2 + \omega_y^2} \text{, for 2D case}$$

and

$$\omega = \sqrt{\omega_x^2} \text{, for 1D case.}$$

It means, that spectrum of the data function is linearly changed and it is a symmetrical function. In discrete data function the spectrum band below frequencies less than 1.0 is diminished gradually to zero, and above 1.0 it is increased the same way up to 3.14 at the end of the spectrum.

The higher vertical derivatives have following forms:

$$g_{dz^n}(\omega_x) = \omega_x^n \text{, for 1D case,}$$

and

$$g_{dz^n}(\omega_x, \omega_y) = \omega^n \text{, for 2D case,}$$

because differentiation is a linear operation. The higher vertical derivatives increase influence of high frequencies, also the noise, so their use is sporadic.

The horizontal differentiation has similar form:

$$g_{dx}(\omega_x) = i\omega_x \text{, for 1D case,}$$

and

$$g_{dx}(\omega_x, \omega_y) = i\omega_x,$$

$$g_{dy}(\omega_x, \omega_y) = i\omega_y, \text{ for 2D case},$$

or in general form (for 2D case):

$$g_{dx^n dy^m}(\omega_x, \omega_y) = (i\omega_x)^n (i\omega_y)^m.$$

Horizontal differentiation of an odd order is an anti-symmetric operation.

In a more general form differentiation operation has a following operator in 2D case:

$$g_{dx^n dy^m dz^l}(\omega_x, \omega_y) = (i\omega_x)^n (i\omega_y)^m \omega^l.$$

### INTEGRATION

The integration is an inverse operation to the differentiation, so we can easily find formulae for an integral operators in frequency domain:

$$g_{Iz}(\omega_x) = \frac{1}{\omega}, \text{ for 1D case},$$

and

$$g_{Iz}(\omega_x, \omega_y) = \frac{1}{\omega}, \text{ for 2D case.}$$

For horizontal integrals spectra we have following expressions:

$$g_{Ix}(\omega_x) = \frac{1}{i\omega_x} = \frac{-i}{\omega_x}, \text{ for 1D case},$$

and

$$g_{Ix}(\omega_x, \omega_y) = \frac{1}{i\omega_x} = \frac{-i}{\omega_x},$$

$$g_{Iy}(\omega_x, \omega_y) = \frac{1}{i\omega_y} = \frac{-i}{\omega_y}, \text{ for 2D case.}$$

Where  $Iz$ ,  $Ix$  and  $Iy$  stand for integration respectively in  $z$ ,  $x$  and  $y$  directions. As in differentiation we can use several times this operation (if it is possible), so we can formulate multiple integration operators as follows:

$$g_{Iz^n}(\omega_x) = \frac{1}{\omega^n},$$

$$g_{Ix^n}(\omega_x) = \frac{1}{i^n \omega_x^n} = \frac{-i^n}{\omega_x^n}, \text{ for 1D case},$$

and for 2D case

$$g_{Iz^n}(\omega_x, \omega_y) = \frac{1}{\omega^n},$$

$$g_{Ix^n}(\omega_x, \omega_y) = \frac{1}{i^n \omega_x^n} = \frac{-i^n}{\omega_x^n},$$

and

$$g_{Iy^n}(\omega_x, \omega_y) = \frac{1}{i^n \omega_y^n} = \frac{-i^n}{\omega_y^n}.$$

### ANALYTICAL CONTINUATION

Analytical continuations are another important transformations. Potential fields as analytical functions can be recalculated on another level. We can have upward or downward continuation. Frequency operators for these transformations are as follows:

$$g_{cont}(\omega_x) = e^{\omega h}, \text{ for 1D case,}$$

and

$$g_{cont}(\omega_x, \omega_y) = e^{\omega h}, \text{ for 2D case.}$$

where  $h$  is distance to the new level, and it is positive in downward continuation.

### NEW TRANSFORMATIONS

There are also other different transformations used for special purposes, e.g. reduction to the pole and pseudogravity transformations in magnetics. They are well documented for example in the Blakely's textbook (Blakely, 1996), so we will not discuss it here. Now we will introduce new transformations which can be very useful in some cases.

### Fractional differentiation and integration

First we will propose new transformations based on the above formulas and a notion of fractional derivatives and integrals (Samko *et al.*, 1987). We will not go too deep into mathematical theory of fractional differentiation and integration, but use their forms in frequency domain. As anyone can guess the general formulas are as follows:

for fractional differentiation:

$$g_{dz^{m/n}}(\omega_x) = \omega^{m/n}, \text{ for 1D case,}$$

and

$$g_{dz^{m/n}}(\omega_x, \omega_y) = \omega^{m/n}, \text{ for 2D case;}$$

and for fractional integration:

$$g_{Iz^{m/n}}(\omega_x) = \frac{1}{\omega^{m/n}}, \text{ in 1D case,}$$

and

$$g_{Iz^{m/n}}(\omega_x, \omega_y) = \frac{1}{\omega^{m/n}}, \text{ in 2D case.}$$

There is a problem when we want to find a fractional derivative or integral along  $x$  or  $y$  axis, because we should have following expressions:

$$g_{dx^{m/n}}(\omega_x) = (i\omega_x)^{m/n} = i^{m/n} \omega_x^{m/n}, \text{ in 1D case,}$$

or

$$g_{dx^{m/n}}(\omega_x, \omega_y) = (i\omega_x)^{m/n} = i^{m/n} \omega_x^{m/n},$$

or

$$g_{dy^{m/n}}(\omega_x, \omega_y) = (i\omega_y)^{m/n} = i^{m/n} \omega_y^{m/n}, \text{ in 2D case}$$

and we've got a problem with the first part of the right side expression. But for our purposes we can formulate it differently:

Fractional horizontal differentiation:

$$g_{dx^{m/n}}(\omega_x) = i\omega_x^{m/n}, \text{ for 1D case,}$$

and

$$g_{dx^{m/n}}(\omega_x, \omega_y) = i\omega_x^{m/n},$$

and

$$g_{dy^{m/n}}(\omega_x, \omega_y) = i\omega_y^{m/n}, \text{ for 2D case.}$$

Fractional horizontal integration:

$$g_{Ix^{m/n}}(\omega_x) = \frac{1}{i\omega_x^{m/n}} = \frac{-i}{\omega_x^{m/n}}, \text{ for 1D case}$$

and

$$g_{Ix^{m/n}}(\omega_x, \omega_y) = \frac{1}{i\omega_x^{m/n}} = \frac{-i}{\omega_x^{m/n}},$$

and

$$g_{Iy^{m/n}}(\omega_x, \omega_y) = \frac{1}{i\omega_y^{m/n}} = \frac{-i}{\omega_y^{m/n}}, \text{ for 2D case}$$

and we can use Hilbert transform to calculate one component from another.

### Hilbert transforms and directional scalar decomposition

**2D Hilbert transform** has following form:

$$g(x') = \frac{1}{\pi} \int_{-\infty}^{\infty} \frac{f(x)}{x' - x} dx,$$

$$f(x) = \frac{1}{\pi} \int_{-\infty}^{\infty} \frac{g(x')}{x' - x} dx'.$$

In symbolic form:

$$g(x') = \text{Hi}[f(x)],$$

$$f(x) = \text{Hi}^{-1}[g(x')].$$

Hilbert transform is a convolution integral:

$$g(x') = f(x) * \frac{1}{\pi x}.$$

Very interesting transformations are connected with the Hilbert transform. It plays an important role in the potential field theory. Let's begin with 2D case. We will define Cartesian co-ordinate system as follows: first co-ordinate axis looking downward will be signed as  $w$ . The second co-ordinate axis named  $x$ , will have direction to the right. If we take components of potential field vector in the frequency domain, and the potential  $V$  has a spectrum  $V$ , its gradient will be a vector with components  $V_w, V_x$  and following spectra  $V_w, V_x$ :

$$V_w = \omega V, V_x = i\omega_x V.$$

We see, that the operator for changing one component to other is just  $i$  sign  $\omega$ , because

$$\text{sign}(x) = \frac{x}{|x|},$$

and it is an operator of Hilbert transform in frequency domain. We can say, that in 2D space components of potential field form a Hilbert transform pair. Moreover, if we see this 2D space as a complex one, and potential field will form a complex function (Nabighian, 1972, 1974)

$$W = V_w(w, x) + iV_x(w, x).$$

**Hilbert transform in 3D.** We can define Hilbert transform also in 3D (Nabighian, 1984; Pedersen, 1989; Roest *et al.*, 1992). We can assume, that components of 3D potential field are related to each other by 3D Hilbert transform. Let's use the co-ordinate system similar as in 2D expanded by third (horizontal) axis  $y$ . We will have following spectra of components  $V_w, V_x$  and  $V_y$ :

$$V_w = \omega V, V_x = i\omega_x V, V_y = i\omega_y V.$$

As

$$\omega = \sqrt{\omega_x^2 + \omega_y^2},$$

and

$$\omega_x = \cos \varphi \omega, \omega_y = \sin \varphi \omega,$$

we can write in polar co-ordinates:

$$V_w = \omega V, V_x = i \cos \varphi \omega V, V_y = i \sin \varphi \omega V.$$

We see, that operators for changing vertical component to horizontal ones are  $i \cos \varphi$  and  $i \sin \varphi$ .

So we can say that they are frequency representations (spectra) or frequency operators of 3D Hilbert transform.

If we use these transforms to horizontal components we will have:

$$F[Hi_x[Vx]] = -\cos^2 \varphi \omega V,$$

and

$$F[Hi_y[Vy]] = -\sin^2 \varphi \omega V.$$

If we add these transformations we will obtain:

$$\begin{aligned} F[Hi_x[Vx]] + F[Hi_y[Vy]] &= -\cos^2 \varphi \omega V - \\ &- \sin^2 \varphi \omega V = -(\cos^2 \varphi + \sin^2 \varphi) \omega V = -\omega V. \end{aligned}$$

The result is a vertical derivative with negative sign. It is an important result obtained first by Nabighian (1984). It shows, that vertical derivative is a sum of respective Hilbert transforms of horizontal derivatives with negative sign. The filter with the spectrum  $-\cos^2 \varphi$  will be called a Hilbert bi-transformer.

It can lead us to very interesting decomposition, namely directional scalar decomposition of a 2D function.

Thesis: Every 2D function  $f(x,y)$ , which has a Fourier transform can be decomposed to two directional components  $f_\alpha(x,y)$ ,  $f_{\alpha+\pi/2}(x,y)$ , connected with a direction angle  $\alpha$ , such, that

$$f(x,y) = f_\alpha(x,y) + f_{\alpha+\pi/2}(x,y).$$

Prove: Let's denote the Fourier transform of the function  $f(x,y)$  as a  $f(\omega_x, \omega_y)$ , or in polar co-ordinates —  $f(\omega, \varphi)$ . Let's make two new functions  $f_\alpha(x,y)$  and  $f_{\alpha+\pi/2}(x,y)$  with the spectra  $\cos^2(\varphi + \alpha) f(\omega, \varphi)$  and  $\cos^2(\varphi + \alpha + \pi/2) f(\omega, \varphi)$  respectively.

As  $\cos(\varphi + \pi/2) = \sin \varphi$ , we have:

$$\begin{aligned} \cos^2(\varphi + \alpha) f + \sin^2(\varphi + \alpha) f &= \\ &= (\cos^2(\varphi + \alpha) + \sin^2(\varphi + \alpha)) f = f. \end{aligned}$$

As the sum of spectra of functions  $f_\alpha(x,y)$  and  $f_{\alpha+\pi/2}(x,y)$  is identical to the spectrum of the function  $f(x,y)$  it proves, that the same is true about functions.

So we have proved, that function  $f(x,y)$  could be shown as the sum of two directional components differing by  $\pi/2$  radians, or  $90^\circ$ . As the angle  $\alpha$  is arbitrary, there is infinite number of such decompositions.

## DESIGN OF DIGITAL FILTERS

There are many methods of designing digital filters (see e.g. Rabiner, Gold, 1975; Oppenheim, Schafer, 1975; Cappellini *et al.*, 1978; Szabatin, 1982; Dębski, Niewiadomski, 1993). They usually deal with the functions in time domain, so they concen-

trate on 1D digital filtering. The main topic of 2D digital filtering covered in literature is picture processing (Huang, 1975, Lim, 1990; Dudgeon, Mersereau, 1984). There are also publications which deal with geophysical data in general (Mesko, 1984; Bath, 1974) and potential field data (Baranov, 1975; Ku *et al.*, 1971). Here we will apply a method best suited for potential fields, and this method can be used both in 1D and 2D digital filters. We are beginning with 1D filters:

## 1D DIGITAL FILTERS

First we must determine the frequency characteristic for the operator defining our transformation. If we limit the operation spectrum from  $-p$  to  $p$ , we will obtain the spectrum of the continuous filter. By using inverse Fourier transform we will get an expression for continuous filter. After changing continuous variable  $x$  to discrete variable  $n$  we obtain our digital filter.

### Symmetric filters

In symmetric filters  $g(-n)$  equals  $g(n)$ , it means, that shape of filter for negative  $n$  mirrors that with positive  $n$ .

#### SYMMETRIC TRANSDUCTOR

Let's show it on the simplest example. The simplest 1D digital filter is a filter which does not change the shape of the input function but only changes its pass band. We will call it a symmetric transductor —  $g_{ST}(n)$ . So we will have a full transductor (all-band pass) —  $g_{STf}(n)$ , lowpass transductor —  $g_{STl}(n)$ , highpass transductor —  $g_{STh}(n)$  and bandpass transductor —  $g_{STb}(n)$ .

Let's determine the analytic expressions for these filters. We must calculate inverse transform from the filter spectrum:

$$g_{ST}(x) = \frac{1}{2\pi} \int_{-\infty}^{\infty} g_{ST}(\omega_x) e^{i\omega_x x} d\omega_x,$$

and

$$g_{ST}(0) = \frac{1}{2\pi} \int_{-\infty}^{\infty} g_{ST}(\omega_x) d\omega_x.$$

In this case the filter spectrum is as follows:

$$\begin{aligned} g_{ST}(\omega_x) &= 1, \text{ for } \omega_{x1} < \omega_x < \omega_{x2}, \text{ and } -\omega_{x2} < \omega_x < -\omega_{x1}, \\ &= 0, \text{ for all other cases.} \end{aligned}$$

The above integrals are equivalent to following ones. Because it is symmetric filter we use cosine kernel function.

$$g_{ST}(x) = \frac{1}{\pi} \int_{\omega_{x1}}^{\omega_{x2}} g_{ST}(\omega_x) \cos \omega_x x d\omega_x = \frac{1}{\pi} \int_{\omega_{x1}}^{\omega_{x2}} \cos \omega_x x d\omega_x,$$

$$g_{ST}(0) = \frac{1}{\pi} \int_{\omega_{x1}}^{\omega_{x2}} g_{ST}(\omega_x) d\omega_x$$

The solution of the first integral is

$$g_{ST}(x) = \frac{1}{\pi} \left| \frac{\sin \omega_x x}{x} \right|_{\omega_{x1}}^{\omega_{x2}},$$

and the second

$$g_{ST}(0) = \frac{1}{\pi} \left| \omega_x \right|_{\omega_{x1}}^{\omega_{x2}}.$$

Substituting  $n$  for  $x$ , and for  $\omega_{x1}$  and  $\omega_{x2}$  the appropriate frequency limits, we obtain expressions for versions of the symmetric transducer:

All-band pass symmetric transducer,  $g_{STf}(n)$ ,  $\omega_{x1} = 0.0$ ,  $\omega_{x2} = \pi$

$$g_{STf}(0) = 1.0,$$

$$g_{STf}(n) = 0.0, \text{ for } n \neq 0.$$

As we see, all-band pass symmetrical transducer has only one, central element which equals 1. It means, that it really does not change the input function, passing all frequencies.

Lowpass symmetric transducer,  $g_{STl}(n)$ ,  $\omega_{x1} = 0.0$ ,  $\omega_{x2} = \omega_{x0}$

$$g_{STl}(0) = \frac{\omega_{x0}}{\pi},$$

$$g_{STl}(n) = \frac{\sin \omega_{x0} n}{\pi n}, \text{ for } n \neq 0.$$

Highpass symmetrical transducer,  $g_{STh}(n)$ ,  $\omega_{x1} = \omega_{x0}$ ,  $\omega_{x2} = \pi$

$$g_{STh}(0) = 1 - \frac{\omega_{x0}}{\pi},$$

$$g_{STh}(n) = -\frac{\sin \omega_{x0} n}{\pi n}, \text{ for } n \neq 0.$$

Bandpass symmetrical transducer,  $g_{STb}(n)$ ,  $\omega_{x1}, \omega_{x2}$

$$g_{STb}(0) = \frac{\omega_{x2} - \omega_{x1}}{\pi},$$

$$g_{STb}(n) = \frac{\sin \omega_{x2} n - \sin \omega_{x1} n}{\pi n}, \text{ for } n \neq 0.$$

Using this technique we can obtain expressions for other filters. For brevity we will present only all-band pass and band pass filters. The other versions can be deduced very easily.

#### VERTICAL DIFFERENTIATOR

It is a filter for obtaining first vertical derivative. We know already, that frequency characteristic for this operation is just  $\omega$ .

$$g_{VD}(0) = \omega.$$

All-band pass vertical differentiator,  $g_{Vdf}(n)$ ,  $\omega_{x1} = 0.0$ ,  $\omega_{x2} = \pi$

$$g_{Vdf}(0) = \frac{\pi}{2},$$

$$g_{Vdf}(n) = -\frac{2}{\pi n^2}, \text{ for } n \neq 0, \text{ odd};$$

$$g_{Vdf}(n) = 0, \text{ for } n \neq 0, \text{ even.}$$

Bandpass vertical differentiator,  $g_{Vdb}(n)$ ,  $\omega_{x1}, \omega_{x2}$

$$g_{Vdb}(0) = \frac{1}{2\pi} (\omega_{x2}^2 - \omega_{x1}^2)$$

$$g_{Vdb}(n) = \frac{1}{\pi} \left[ \frac{\omega_{x2}^2 \sin \omega_{x2} n}{\omega_{x2} n} - \frac{\omega_{x2}^2}{2} \left( \frac{\sin \frac{\omega_{x2} n}{2}}{\frac{\omega_{x2} n}{2}} \right)^2 - \frac{\omega_{x1}^2 \sin \omega_{x1} n}{\omega_{x1} n} + \frac{\omega_{x1}^2}{2} \left( \frac{\sin \frac{\omega_{x1} n}{2}}{\frac{\omega_{x1} n}{2}} \right)^2 \right], \text{ for } n \neq 0.$$

#### VERTICAL BI-DIFFERENTIATOR

It is a filter for calculation of the second vertical derivative. Its frequency characteristic is  $\omega^2$ . Using our technique we obtain the following expressions for all-band pass filter and bandpass filter:

All-band pass vertical bi-differentiator,  $g_{Vbf}(n)$ ,  $\omega_{x1} = 0.0$ ,  $\omega_{x2} = \pi$

$$g_{Vbf}(0) = \frac{\pi^2}{3},$$

$$g_{Vbf}(n) = \frac{2}{n^2}, \text{ for } n \neq 0, \text{ even},$$

$$g_{Vbf}(n) = -\frac{2}{n^2}, \text{ for } n \neq 0, \text{ odd.}$$

Bandpass vertical bi-differentiator,  $g_{Vbb}(n)$ ,  $\omega_{x1}, \omega_{x2}$

$$g_{Vbb}(0) = \frac{1}{3\pi} (\omega_{x2}^3 - \omega_{x1}^3)$$

$$g_{VBB}(n) = \frac{\omega_{x2}^2 \sin \omega_{x2} n}{\pi n} + \frac{2\omega_{x2} \cos \omega_{x2} n}{\pi n^2} - \frac{2\sin \omega_{x2} n}{\pi n^3} - \frac{\omega_{x1}^2 \sin \omega_{x1} n}{\pi n} - \frac{2\omega_{x1} \cos \omega_{x1} n}{\pi n^2} + \frac{2\sin \omega_{x1} n}{\pi n^3}, \text{ for } n \neq 0.$$

## UPWARD CONTINUATOR

It is a filter performing calculation of analytic function on a higher level. The frequency characteristic

$$g_{UC}(\omega_x) = e^{-\omega_x h},$$

where  $h$  is a distance to the higher level.

Using our technique of calculation we obtain the following expressions for this filter:

All-band pass upward continuator,  $g_{UCf}(n)$ ,  $\omega_{x1} = 0.0$ ,  $\omega_{x2} = \pi$

$$g_{UCf}(0) = \frac{1}{\pi h} (1 - e^{-\pi h}),$$

$$g_{UCf}(n) = \frac{h}{\pi(h^2 + n^2)} (1 - e^{-\pi h}), \text{ for } n \neq 0, \text{ even},$$

$$g_{UCf}(n) = \frac{h}{\pi(h^2 + n^2)} (1 + e^{-\pi h}), \text{ for } n \neq 0, \text{ odd}.$$

Bandpass upward continuator,  $g_{UCb}(n)$ ,  $\omega_{x1}$ ,  $\omega_{x2}$ 

$$g_{UCb}(0) = \frac{1}{\pi h} (e^{-\omega_{x1} h} - e^{-\omega_{x2} h}),$$

$$g_{UCb}(n) = \frac{1}{\pi(h^2 + n^2)} [e^{-\omega_{x2} h} (n \sin \omega_{x2} n - h \cos \omega_{x2} n) - e^{-\omega_{x1} h} (n \sin \omega_{x1} n - h \cos \omega_{x1} n)], \text{ for } n \neq 0.$$

## DOWNWARD CONTINUATOR

This filter is used for transformation of a function to the lower level. Its spectrum is

$$g_{DC}(\omega_x) = e^{\omega_x h},$$

where  $h$  is a distance to the new level.

After calculations we get the following expressions:

All-band pass downward continuator,  $g_{DCf}(n)$ ,  $\omega_{x1} = 0.0$ ,  $\omega_{x2} = \pi$

$$g_{DCf}(0) = \frac{e^{\pi h} - 1}{\pi h},$$

$$g_{DCf}(n) = \frac{h}{\pi(n^2 + h^2)} (e^{\pi h} - 1), \text{ for } n \neq 0, \text{ even},$$

$$g_{DCf}(n) = \frac{h}{\pi(n^2 + h^2)} (e^{\pi h} + 1), \text{ for } n \neq 0, \text{ even}.$$

Bandpass downward continuator,  $g_{DCb}(n)$ ,  $\omega_{x1}$ ,  $\omega_{x2}$ 

$$g_{DCb}(0) = \frac{1}{\pi h} (e^{\omega_{x2} h} - e^{\omega_{x1} h}),$$

$$g_{DCb}(n) = \frac{1}{\pi(n^2 + h^2)} [(n \sin \omega_{x2} n + h \cos \omega_{x2} n) e^{\omega_{x2} h} - (n \sin \omega_{x1} n + h \cos \omega_{x1} n) e^{\omega_{x1} h}], \text{ for } n \neq 0.$$

**Anti-symmetrical filters**

In anti-symmetrical filters  $g(-n)$  equals  $-g(n)$ . It means, that central element  $g(0)$  must always equal zero. Let's calculate several anti-symmetrical filters:

ANTI-SYMMETRICAL TRANSDUCTOR  
(HILBERT TRANSFORMER)

This filter changes symmetry of a function. The symmetrical function becomes anti-symmetrical and vice versa. In literature it is called a Hilbert transformer or a quadrature filter. For an analogy to symmetrical transductor, we can call it also an anti-symmetrical transductor.

The spectrum of this filter is

$$g_{AT}(\omega_x) = \frac{i\omega_x}{\omega} = i \operatorname{sign} \omega_x,$$

because we define a signum function as follows (as we have already shown):

$$\operatorname{sign} x = \frac{x}{|x|}.$$

Using the same technique as in symmetrical filters we obtain the following expressions for this filter:

All-band pass anti-symmetrical transductor (Hilbert trans-former),  $g_{ATf}(n)$ ,  $\omega_{x1} = 0.0$ ,  $\omega_{x2} = \pi$

$$g_{ATf}(0) = 0.0,$$

$$g_{ATf}(n) = \frac{2}{\pi n}, \text{ for } n > 0, \text{ odd},$$

$$g_{ATf}(n) = 0.0, \text{ for } n > 0, \text{ even},$$

$$g_{ATf}(-n) = -g_{ATf}(n).$$

Band pass anti-symmetrical transductor (Hilbert trans-former),  $g_{ATb}(n)$ ,  $\omega_{x1}$ ,  $\omega_{x2}$

$$g_{ATb}(0) = 0.0,$$

$$g_{ATb}(n) = \frac{1}{\pi n} (\cos \omega_{x2} n - \cos \omega_{x1} n), \text{ for } n > 0,$$

$$g_{ATb}(-n) = -g_{ATb}(n).$$

### HORIZONTAL (ANTI-SYMMETRIC) DIFFERENTIATOR

This filter performs horizontal differentiation. The frequency operator for this operation is  $i\omega_x$ . After similar calculations as before, we obtain the following expressions for ideal filter of this sort:

All-band pass horizontal differentiator,  $g_{HDf}(n)$ ,  $\omega_{x1} = 0.0$ ,  $\omega_{x2} = \pi$

$$g_{HDf}(0) = 0.0,$$

$$g_{HDf}(n) = \frac{1}{n}, \text{ for } n > 0, \text{ even,}$$

$$g_{HDf}(n) = -\frac{1}{n}, \text{ for } n > 0, \text{ odd,}$$

$$g_{HDf}(-n) = -g_{HDf}(n).$$

Band pass horizontal differentiator:  $g_{HDb}(n)$ ,  $\omega_{x1}$ ,  $\omega_{x2}$

$$g_{HDb}(0) = 0.0,$$

$$g_{HDb}(n) = \frac{1}{\pi} \left( \frac{\omega_{x2} \cos \omega_{x2} n}{n} - \frac{\sin \omega_{x2} n}{n^2} - \frac{\omega_{x1} \cos \omega_{x1} n}{n} + \frac{\sin \omega_{x1} n}{n^2} \right), \text{ for } n > 0,$$

$$g_{HDb}(-n) = -g_{HDb}(n).$$

### 2D DIGITAL FILTERS

The design of 2D digital filters is much more complicated than the 1D filters. In textbooks about digital filters several techniques are discussed (see e.g. Lim, 1990), but they are not suited for potential field needs. In this field interesting results were obtained by Baranov (1975), but his method is quite complicated and restricted to simple transformations. The problem is, that 2D filters ought to have circular symmetry and we ought to work in space with that symmetry, it means with polar co-ordinates, not Cartesian. But 2D Fourier transform is for Cartesian space, so we must find an analogue of 2D Fourier transform for a space with polar co-ordinates.

First we will give formulae of Hankel transforms which will be used later on:

Hankel transform of zero order (see e.g. Bracewell, 1965):

$$f(\rho) = \int_0^\infty f(r) J_0(\rho r) dr,$$

$$f(r) = \int_0^\infty f(\rho) J_0(\rho r) d\rho,$$

where  $J_0(\cdot)$  is a Bessel function of first kind and zero order (McLachlan, 1955; Korenev, 1971).

In symbolic form:

$$f(\rho) = H_0[f(r)],$$

$$f(r) = H_0^{-1}[f(\rho)].$$

Hankel transform of n-th order:

$$f(\rho) = \int_0^\infty f(r) J_n(\rho r) dr,$$

$$f(r) = \int_0^\infty f(\rho) J_n(\rho r) d\rho,$$

where  $J_n(\cdot)$  is a Bessel function of the first kind and n-th order.

In symbolic form:

$$f(\rho) = H_n[f(r)],$$

$$f(r) = H_n^{-1}[f(\rho)].$$

### The Fourier-Hankel transform

We must realise, that the 2D Fourier transform is not universal tool for 2D functions. If we deal with functions with circular symmetry, we ought to use polar co-ordinates rather than Cartesian ones. Let's try to find what transform we ought to use in polar co-ordinates.

Let's write Fourier transform of the function  $f(x)$  in the following form:

$$F[f(x)] = f(\omega_x) = \int_{-\infty}^{\infty} f(x) e^{-i\omega_x x} dx \quad (1)$$

and its inversion in the form

$$F^{-1}[f(\omega_x)] = f(x) = \frac{1}{2\pi} \int_{-\infty}^{\infty} f(\omega_x) e^{i\omega_x x} d\omega_x \quad (2)$$

The two-dimensional Fourier transform in Cartesian co-ordinates of the function  $f(x,y)$  can be written as

$$\begin{aligned} F[f(x,y)] &= f(\omega_x, \omega_y) = \\ &= \frac{1}{2\pi} \int_{-\infty}^{\infty} \int_{-\infty}^{\infty} f(x,y) e^{-i(x\omega_x + y\omega_y)} dx dy, \end{aligned} \quad (3)$$

and its inverse transform as

$$\begin{aligned} F^{-1}[f(\omega_x, \omega_y)] &= \\ &= \frac{1}{2\pi} \int_{-\infty}^{\infty} \int_{-\infty}^{\infty} f(\omega_x, \omega_y) e^{i(x\omega_x + y\omega_y)} d\omega_x d\omega_y. \end{aligned} \quad (4)$$

As we see, in Cartesian co-ordinates the 2D Fourier transform is obtained easily from 1D transform and if  $f(x,y)$  can be shown as simple product

$$f(x, y) = f(x) \cdot f(y),$$

then

$$F[f(x) \cdot f(y)] = f(\omega_x) \cdot f(\omega_y).$$

(see e.g. Bracewell, 1965).

Let's consider functions in polar co-ordinates  $r, \varphi$ . Let's begin with a function of circular symmetry, depending only on a radial variable  $r$  —  $f(r)$ , and find a form of Fourier transform of this function in polar co-ordinates.

The relation between Cartesian and polar co-ordinates is in space domain as follows:

$$x = r \cos \varphi, \quad y = r \sin \varphi,$$

where

$$r = \sqrt{x^2 + y^2},$$

and

$$\varphi = \arctan \frac{y}{x}.$$

In frequency domain we have following formulae:

$$\omega_x = \omega \cos \psi, \quad \omega_y = \omega \sin \psi,$$

where

$$\omega = \sqrt{\omega_x^2 + \omega_y^2},$$

and

$$\psi = \arctan \frac{\omega_y}{\omega_x}.$$

Substituting polar co-ordinates in (3), and taking into account, that

$$dx dy = 2\pi r dr d\varphi,$$

we obtain

$$\begin{aligned} F[f(r, \varphi)] &= f(r) = \int_0^\infty \int_0^{2\pi} f(r) e^{-ir\omega \cos(\varphi - \psi)} r dr d\varphi = \\ &= \int_0^\infty r f(r) \int_0^{2\pi} e^{-ir\omega \cos \varphi} d\varphi dr. \end{aligned} \quad (5)$$

As we know

$$\int_0^{2\pi} e^{-ix \cos \varphi} d\varphi = 2\pi J_0(x),$$

where  $J_0(x)$  is a Bessel function of first kind and zero order. So we see that transform  $F[f(r)]$  is a Hankel transform of zero order:

$$\begin{aligned} F[f(r)] &= H_0[f(r)] = f_0^H(\omega) = \\ &= \int_0^\infty f(r) J_0(\omega r) r dr. \end{aligned} \quad (6)$$

The inversion of the Hankel transform of the zero order has following form

$$H_0^{-1}[f_0^H(\omega)] = f(r) = \int_0^\infty f_0^H(\omega) J_0(\omega r) \omega d\omega. \quad (7)$$

Generally the Hankel transform of  $n$  order has a form

$$H_n[f(r)] = f_n^H(\omega) = \int_0^\infty f(r) J_n(\omega r) r dr, \quad (8)$$

and its inversion is

$$H_n^{-1}[f_n^H(\omega)] = f(r) = \int_0^\infty f_n^H(\omega) J_n(\omega r) \omega d\omega. \quad (9)$$

## THE 2D FOURIER TRANSFORM IN POLAR CO-ORDINATES

Let's take an arbitrary function in polar co-ordinates  $f(r, \varphi)$ . We can observe, that this function is periodical with reference to angular variable  $\varphi$ , because

$$f(r, \varphi + 2\pi k) = f(r, \varphi), \quad k = 0, \pm 1, \pm 2, \dots$$

So we can expand this function to Fourier series:

$$f(r, \varphi) = \sum_{n=-\infty}^{\infty} f_n(r) e^{in\varphi} \quad (10)$$

where

$$f_n = \frac{1}{2\pi} \int_0^{2\pi} f(r, \varphi) e^{-in\varphi} d\varphi.$$

Let's re-write the formula (5)

$$F[f(r, \varphi)] = \int_0^\infty \int_0^{2\pi} f(r, \varphi) e^{-ir\omega \cos(\varphi - \psi)} r dr d\varphi,$$

and (10):

$$f(r, \varphi) = \sum_{n=-\infty}^{\infty} f_n(r) e^{in\varphi}.$$

Substituting the latter to the first we obtain

$$\begin{aligned} F[f(r, \varphi)] &= \sum_{n=-\infty}^{\infty} f_n^h(\omega) = \\ &= \int_0^{2\pi} \int_0^\infty \sum_{n=-\infty}^{\infty} f_n(r) e^{in\varphi} e^{-ir\omega \cos(\varphi - \psi)} r dr d\varphi. \end{aligned} \quad (11)$$

The frequency angular variable is a discrete one as the function  $f(r, \varphi)$  is periodical, so in the place of  $\psi$  we should

use  $n$ . In the above formula we can change the order of summation and for one arbitrary value  $n$  we can write

$$\begin{aligned} f_n^h(\omega) &= \int_0^\infty \int_0^{2\pi} f_n(r) e^{in\varphi} e^{ir\omega \cos(\varphi-n)} r dr d\varphi = \\ &= \int_0^\infty f_n(r) \left[ \int_0^{2\pi} e^{-ir\omega \cos\varphi} e^{in\varphi} d\varphi \right] r dr. \end{aligned} \quad (12)$$

It is known (see e.g. McLachlan, 1955), that

$$\int_0^{2\pi} e^{iz \cos\varphi} e^{in\varphi} d\varphi = i^n 2\pi J_n(z),$$

so

$$\begin{aligned} \int_0^{2\pi} e^{-iz \cos\varphi} e^{in\varphi} d\varphi &= i^n 2\pi J_n(-z) = i^n (-1)^n 2\pi J_n(z) = \\ &= (-i)^n 2\pi J_n(z), \end{aligned} \quad (13)$$

because

$$J_n(-z) = J_{-n}(z) = (-1)^n J_n(z).$$

As a result we obtain

$$f_n^h(\omega) = (-i)^n 2\pi \int_0^\infty f_n(r) J_n(\omega r) r dr. \quad (14)$$

We see, that it is a Hankel transform of the  $n$ -th order. Substituting  $f_n(r)$  in the integral by the formula (11) we get

$$f_n^h(\omega) = (-i)^n \int_0^\infty \int_0^{2\pi} f(r\varphi) e^{-in\varphi} J_n(\omega r) r dr d\varphi. \quad (15)$$

It is one arbitrary element of an infinite series

$$\begin{aligned} H[f(r, \varphi)] &= f^{FH}(\omega, n) = \sum_{n=-\infty}^{\infty} f_n^h(\omega) = \\ &= \sum_{n=-\infty}^{\infty} (-i)^n \int_0^\infty \int_0^{2\pi} f(r, \varphi) e^{-in\varphi} J_n(\omega r) r dr d\varphi. \end{aligned} \quad (16)$$

Inversion of the transform in the expression (14) is as follows:

$$f_n(r) = \frac{i^n}{2\pi} \int_0^\infty f_n^h(\omega) J_n(\omega r) \omega d\omega,$$

and remembering that

$$f(r, \varphi) = \sum_{n=-\infty}^{\infty} f_n(r) e^{in\varphi},$$

we can obtain full expression for the inverse transform

$$\begin{aligned} H^{-1}[f^{FH}(\omega, n)] &= f(r, \varphi) = \\ &= \sum_{n=-\infty}^{\infty} \frac{i^n e^{in\varphi}}{2\pi} \int_0^\infty f_n^h(\omega) J_n(\omega r) \omega d\omega. \end{aligned} \quad (17)$$

The integral transform expressed in formulae (16) and (17) can be called the Fourier-Hankel transform.

We have proved that an analogue of the 2D Fourier transform in polar co-ordinates is an infinite series of Hankel transforms.

## 2D digital filter design

### 2D SYMMETRIC FILTERS

Now we can approach the problem. Let's begin with the symmetrical filters with circular symmetry (not dependent on angular variable). After determining the spectrum of the operation  $g(\omega)$  we will use the first element of the inverse Fourier-Hankel transform to calculate the expression for a continuous filter and after changing to discrete variables, we obtain the filter:

$$g(r) = \frac{1}{2\pi} \int_0^\infty g(\omega) J_0(\omega r) \omega d\omega,$$

where  $g(\omega)$  is a filter spectrum define by the formula

$$\begin{aligned} g(\omega) &= g(\omega), \text{ for } 0.0 \leq \omega_1 < \omega < \omega_2 \leq \pi \\ &= 0.0, \text{ for all other cases.} \end{aligned}$$

It means, that above integral is equivalent to the following one:

$$g(r) = \frac{1}{2\pi} \int_{\omega_1}^{\omega_2} g(\omega) J_0(\omega r) \omega d\omega.$$

After solving the integral we substitute the appropriate frequency limits and discrete variables  $n_x$  and  $n_y$  for  $r$ , remembering that

$$r = \sqrt{n_x^2 + n_y^2}.$$

If the integral has no analytic solution, we can solve it by numerical integration using one of several known methods. We used a method published by Baranov (1975) based on the Romberg's algorithm.

Below are examples of analytical expressions for several different 2D symmetrical filters.

**2D symmetric transductor.** Let's make calculations for symmetrical transductor, using the above technique, analogue to that in 1D filter design. The integral is as follows:

$$g(r) = \frac{1}{2\pi} \int_0^\infty g_{ST}(\omega) J_0(\omega r) \omega d\omega,$$

where

$$\begin{aligned} g_{ST}(\omega) &= 1.0 \text{ for } \omega_1 < \omega < \omega_2, \\ &= 0.0 \text{ for all other cases.} \end{aligned}$$

So we have in reality following integrals:

$$g_{ST}(r) = \frac{1}{2\pi} \int_{\omega_1}^{\omega_2} \omega J_0(\omega r) d\omega,$$

$$g_{ST}(0) = \frac{1}{2\pi} \int_{\omega_1}^{\omega_2} \omega d\omega.$$

The solution is as follows:

$$g_{ST}(r) = \frac{1}{2\pi} \left| \frac{\omega J_1(\omega r)}{r} \right|_{\omega_1}^{\omega_2},$$

$$g_{ST}(0) = \frac{1}{2\pi} \left| \frac{\omega^2}{2} \right|_{\omega_1}^{\omega_2}.$$

Using this solution we can obtain expressions for different versions of that filter:

All-band pass 2D symmetrical transductor,  $g_{STf}(n_x, n_y)$ ,  $\omega_1 = 0.0$ ,  $\omega_2 = \pi$

$$g_{STf}(0,0) = \frac{\pi}{4},$$

$$g_{STf}(n_x, n_y) = \frac{J_1\left(\pi\sqrt{n_x^2 + n_y^2}\right)}{2\sqrt{n_x^2 + n_y^2}}, \text{ for } n_x, n_y \neq 0.$$

Bandpass 2D symmetrical transductor,  $g_{STb}(n_x, n_y)$ ,  $\omega_1$ ,  $\omega_2$

$$g_{STb}(0,0) = \frac{\omega_2^2 - \omega_1^2}{4\pi},$$

$$g_{STb}(n_x, n_y) = \frac{\omega_2 J_1\left(\omega_2 \sqrt{n_x^2 + n_y^2}\right)}{2\pi\sqrt{n_x^2 + n_y^2}} - \frac{\omega_1 J_1\left(\omega_1 \sqrt{n_x^2 + n_y^2}\right)}{2\pi\sqrt{n_x^2 + n_y^2}}, \text{ for } n_x, n_y \neq 0.$$

**2D vertical differentiator.** As we already know, this filter performs vertical differentiation and its frequency characteristic is  $\omega$ . Using the technique shown above we can calculate expressions for this filter. We will skip calculations and show results for:

All-band pass 2D vertical differentiator,  $g_{Vdf}(n_x, n_y)$ ,  $\omega_1 = 0.0$ ,  $\omega_2 = \pi$

$$g_{Vdf}(n_x, n_y) = \frac{\pi J_1(\pi r)}{2r} - \frac{\pi}{4r} [J_1(\pi r)H_0(\pi r) - J_0(\pi r)H_1(\pi r)], \text{ for } r \neq 0,$$

$$r = \sqrt{n_x^2 + n_y^2}.$$

$H_0(z)$  and  $H_1(z)$  are Struve functions (see e.g. Abramowitz, Stegun, 1964).

Bandpass 2D vertical differentiator,  $g_{VDb}(n_x, n_y)$ ,  $\omega_1, \omega_2$

$$g_{VDb}(0,0) = \frac{\omega_2^3 - \omega_1^3}{6\pi},$$

$$g_{VDb}(n_x, n_y) = \frac{\omega_2^2 J_1(\omega_2 r)}{2\pi r} - \frac{\omega_2}{4r^2} [J_0(\omega_2 r)H_0(\omega_2 r) - J_1(\omega_2 r)H_1(\omega_2 r)] - \frac{\omega_1^2 J_1(\omega_1 r)}{2\pi r} + \frac{\omega_1}{4r^2} [J_1(\omega_1 r)H_0(\omega_1 r) - J_0(\omega_1 r)H_1(\omega_1 r)],$$

for  $r \neq 0$ .

**2D vertical bi-differentiator.** This filter, as we know from its 1D version, is for obtaining the second vertical derivative. Its frequency characteristic is

$$g_{VB} = \begin{cases} \omega^2, & \text{for } 0.0 \leq \omega_1 < \omega < \omega_2 \leq \pi, \\ 0.0, & \text{for all other cases.} \end{cases}$$

We must then solve following integrals:

$$g_{VB}(0) = \frac{1}{2\pi} \int_{\omega_1}^{\omega_2} \omega^3 d\omega,$$

$$g_{VB}(r) = \frac{1}{2\pi} \int_{\omega_1}^{\omega_2} \omega^3 J_0(\omega r) d\omega.$$

These integrals can be solved and we obtain following analytic expressions for two versions of this filter:

All-band pass 2D vertical bi-differentiator,  $g_{VBF}(n_x, n_y)$ ,  $\omega_1 = 0.0$ ,  $\omega_2 = \pi$

$$g_{VBF}(0,0) = \frac{\pi^3}{8},$$

$$g_{VBF}(n_x, n_y) = \frac{\pi}{r^2} J_0(\pi r) + \left( \frac{\pi^2}{2r} - \frac{2}{r^3} \right) J_1(\pi r), \text{ for } r \neq 0.$$

Bandpass 2D vertical bi-differentiator,  $g_{VBB}(n_x, n_y)$ ,  $\omega_1, \omega_2$

$$g_{VBB}(n_x, n_y) = \frac{\omega_2^2}{\pi r^2} J_0(\omega_2 r) + \left( \frac{\omega_2^3}{2\pi r} - \frac{2\omega_2}{\pi r^3} \right) J_1(\omega_2 r) - \frac{\omega_1^2}{\pi r^2} J_0(\omega_1 r) + \left( \frac{\omega_1^3}{2\pi r} - \frac{2\omega_1}{\pi r^3} \right) J_1(\omega_1 r), \text{ for } r \neq 0.$$

**2D vertical integrator.** This filter performs vertical integration and its spectrum is  $1/\omega$ . After solving appropriate integrals we will obtain following expressions for this filter:

All-band pass 2D vertical integrator,  $g_{Vf}(n_x, n_y), \omega_1 = 0.0, \omega_2 = \pi$

$$g_{Vf}(0,0) = 10,$$

$$g_{Vf}(n_x, n_y) = \frac{J_0(\pi r)}{2} + \frac{\pi}{4} [J_1(\pi r)H_0(\pi r) - J_0(\pi r)H_1(\pi r)], \text{ for } r \neq 0.$$

Bandpass 2D vertical integrator,  $g_{Vb}(n_x, n_y), \omega_1, \omega_2$

$$g_{Vb}(0,0) = \frac{\omega_2 - \omega_1}{\pi},$$

$$g_{Vb}(n_x, n_y) = \frac{\omega_2}{2\pi} J_0(\omega_2 r) + \frac{\omega_2}{4} [J_1(\omega_2 r)H_0(\omega_2 r) - J_0(\omega_2 r)H_1(\omega_2 r)] - \frac{\omega_1}{2\pi} J_0(\omega_1 r) - \frac{\omega_1}{4} [J_1(\omega_1 r)H_0(\omega_1 r) - J_0(\omega_1 r)H_1(\omega_1 r)],$$

for  $r \neq 0$ .

## 2D ANTI-SYMMETRIC FILTERS

2D anti-symmetric filters have spectra from the second element of the Fourier-Hankel series:  $g(\omega, 1)$ . We will use following integral for calculating these filters:

$$g(r, \varphi) = \frac{1}{2\pi} \cos \alpha \cos \varphi \int_{\omega_1}^{\omega_2} g(\omega, 1) J_1(\omega r) \omega d\omega + \frac{1}{2\pi} \sin \alpha \sin \varphi \int_{\omega_1}^{\omega_2} g(\omega, 1) J_1(\omega r) \omega d\omega,$$

where  $\alpha$  is an azimuth of symmetry.

After similar calculations as shown above we can obtain following results for simplest 2D anti-symmetric filters:

**2D anti-symmetric transductor (2D Hilbert transformer).** This filter changes the symmetry of the 2D function. From z-component we can obtain x- or y-component.

All-band pass 2D Hilbert transformer,  $g_{HTf}(n_x, n_y), \omega_1 = 0.0, \omega_2 = \pi, \alpha = 0.0$

$$g_{HTf}(0, n_y) = 0.0.$$

$$g_{HTf}(n_x, n_y) = \frac{n_x}{2r^2} \left\{ J_0(\pi r) \left( 1 - \frac{1}{r} \right) - \frac{\pi}{2} [J_1(\omega r)H_0(\omega r) - J_0(\omega r)H_1(\omega r)] \right\},$$

for  $n_x > 0$ ,

and

$$g(-n_x, n_y) = -g(n_x, n_y), \text{ for } n_x < 0.$$

**2D anti-symmetric differentiator.** This filter is used for calculating a horizontal derivative in chosen direction. The analytic expression for these filters is very simple. We show as an example expression for all-band pass filter.

All-band pass 2D anti-symmetric differentiator,  $g_{ADf}(n_x, n_y), \omega_1 = 0.0, \omega_2 = \pi, \alpha = 0.0$

$$g_{ADf}(0, n_y) = 0.0.$$

$$g_{ADf}(n_x, n_y) = \frac{n_x}{2r^2} [\pi J_2(\pi r)], \text{ for } n_x > 0,$$

and

$$g(-n_x, n_y) = -g(n_x, n_y), \text{ for } n_x < 0.$$

## VISUALIZATION

The result of geophysical survey, especially in potential fields, are data scattered on surveyed area. When we measure one quantity, we obtain a set of points in 3D space  $\{x, y, w\}$ , where  $x, y$  are space co-ordinates ( $z$  co-ordinate is thought to be unimportant) and  $w$  is measured quantity. If we treat  $w$  as a third space co-ordinate we may say that the data represent a surface in 3D space, a 3D object, a relief which can be compared to terrain relief. So visualization of scalar fields can use the same techniques as those used in relief visualization.

The known methods are as follows:

**1.** 2D or conventional image — contour image (map).

The measured quantity is shown on image (map) by contours, coloured or not.

**2.** 2-1/2D image — shaded-relief image.

On this image its three-dimensionality is shown by shades. It is a shaded-relief image. It shows 3D object from vertical.

**3.** 3D image — perspective view image.

In this case the 3D surface (relief) can be seen from any point of view. It is a perspective view.

**4.** 3-1/2D image — animated shaded relief.

We can call in such a way an image 2-1/2D changing in time. So it is an animation of an image where parameters of illumination are changing in time: azimuth and/or elevation of illumination source.

**5.** 4-D image — animated perspective view.

It is an animation of 3D image, where point of view is changing in time.

Additionally we can speak about 1-1/2D image in the case of gray-tone shaded relief, where some information about measured quantity is lost.

The digital revolution in which we live, have brought new methods in data presentation. Computer graphics and colour displays and printers make use of colour affordable to many users.

## COLOUR SPACE AND ITS CO-ORDINATES

The colour space is a 3D space. There are many mathematical models of this space (see e.g. Foley *et. al.*, 1994). We will use two of them. The first is a RGB model. It is a Cartesian co-ordinate system where co-ordinate axes are three basic colours: red–R, green–G, and blue–B. In this model the colour space is a cube. The colour is a point in this space with co-ordinates  $r, g, b$ . The range of co-ordinates is  $\{0.0, 1.0\}$ . The black colour has co-ordinates  $(0.0, 0.0, 0.0)$  and white  $(1.0, 1.0, 1.0)$ . It means, that main diagonal of colour cube is an axis of grey tones. It is a main axis of another colour co-ordinate system: the IHS (intensity, hue, saturation) model, also called VHS (value, hue, saturation) model. It can be obtained by rotating the colour RGB cube. The main diagonal of the cube becomes the vertical axis in this new model. After some modification the cube becomes an upside-down conic. In this conical co-ordinate system, which is more natural to human perception, the vertical axis is an intensity (I) axis, the radial axis is a saturation (S) axis, and the angle is a hue (H). The upper side of this colour conic is a colour circle of colours with maximal intensities (see Plate 1h). These mathematical models are continued spaces with infinity numbers of colours. In computer technology more natural model is a RGB model, because the given colour is obtained on the display as a mixture of three basic colours. In practice we also use discrete models with limited numbers of colours instead of continued models. Now a common practise in computer graphics is to use a so-called TrueColour standard, with 256 different values of every basic colour.

Below are co-ordinates of selected colours in discussed colour models:

Colour co-ordinate systems

Colour	Continued colour space		Discrete colour space
	RGB	IHS	RGB
black	$(0.0, 0.0, 0.0)$	$(0.0, \text{undefined}, 0.0)$	$(0, 0, 0)$
white	$(1.0, 1.0, 1.0)$	$(1.0, \text{undefined}, 1.0)$	$(255, 255, 255)$
red	$(1.0, 0.0, 0.0)$	$(1.0, 0.0^\circ, 1.0)$	$(255, 0, 0)$
green	$(0.0, 1.0, 0.0)$	$(1.0, 120.0^\circ, 1.0)$	$(0, 255, 0)$
blue	$(0.0, 0.0, 1.0)$	$(1.0, 240.0^\circ, 1.0)$	$(0, 0, 255)$
yellow	$(1.0, 1.0, 0.0)$	$(1.0, 60.0^\circ, 1.0)$	$(255, 255, 0)$
cyan	$(0.0, 1.0, 1.0)$	$(1.0, 180^\circ, 1.0)$	$(0, 255, 255)$
magenta	$(1.0, 0.0, 1.0)$	$(1.0, 300.0^\circ, 1.0)$	$(255, 0, 255)$
orange	$(1.0, 0.5, 0.0)$	$(1.0, 30.0^\circ, 1.0)$	$(255, 127, 0)$
violet	$(0.5, 0.0, 1.0)$	$(1.0, 270^\circ, 1.0)$	$(127, 0, 255)$
pink	$(1.0, 0.5, 0.5)$	$(1.0, 0.0^\circ, 0.5)$	$(255, 127, 127)$
brown	$(0.5, 0.5, 0.0)$	$(0.5, 60.0^\circ, 1.0)$	$(127, 127, 0)$

**Contour image.** There are many software packages which can make contour maps using PC, but this technique does not use all possibilities which has computer graphics. It was invented for manual work, but nevertheless we can modify this technique as will be shown below.

The simplest contour-like image made by computer can be an image where for every data point there will be a point on an image with the colour according to a colour scale. As the next step we can interpolate scattered data to a regular grid and for every point of the grid use the colour from the colour scale. So in this point we must discuss the problem of colour scales.

## COLOUR SCALES FOR SCALAR FIELDS

The design of a colour scale is easier using IHS model for colour space. We can use any component of this model of colour space as a base or colour scale: hue, saturation or intensity.

**Full-hue colour scales.** In this case hue changes, and saturation and intensity are constant. We must decide which hues are at the beginning and at the end of the scale. If we choose the violet as the first and last colour of our scale all negative values will have cold hues and positive — warm ones. If we standardize the measured data to the range from  $-1.2$  to  $1.2$  we will have in this case following colour scale — a relation between data values and colours (for selected data values):

Full-hue colour scale (Plate 1a)

Data value	Intensity	Hue	Saturation
1.2	constant	$270.0^\circ$	(violet)
1.0		$300.0^\circ$	(magenta)
0.8		$330.0^\circ$	
0.6		$0.0^\circ$	(red)
0.4		$30.0^\circ$	(orange)
0.2		$60.0^\circ$	(yellow)
0.0		$90.0^\circ$	(green-yellow)
-0.2		$120.0^\circ$	(green)
-0.4		$150.0^\circ$	
-0.6		$180.0^\circ$	(cyan)
-0.8		$210.0^\circ$	
-1.0		$240.0^\circ$	(blue)
-1.2		$270.0^\circ$	(violet)

**Extended full-hue colour scale.** The hue colour scale mentioned above can be extended. We can use the same hues for different values of presented quantity. Let's extend the hues for high values from  $270^\circ$  (violet) to  $180^\circ$  (cyan) and for lowest values from  $270^\circ$  to  $360^\circ$  ( $0^\circ$ ) (red). We can observe that the image with this colour scale is more vivid and is more informative and there is no danger to make a mistake when reading the image. We can use different scaling for the extended portions of this scale:

Extended full-hue colour scale (Plate 1b)

Data value	Intensity	Hue	Saturation
2.4	constant	180.0° (cyan)	constant
1.2		270.0° (violet)	
1.0		300.0° (magenta)	
0.8		330.0°	
0.6		0.0° (red)	
0.4		30.0° (orange)	
0.2		60.0° (yellow)	
0.0		90.0° (green-yellow)	
-0.2		120.0° (green)	
-0.4		150.0°	
-0.6		180.0° (cyan)	
-0.8		210.0°	
-1.0		240.0° (blue)	
-1.2		270.0° (violet)	
-2.4		360.0° (red)	

**Inverse full-hue colour scales.** There is another possibility of arranging colours in colour scale. The normal colour scale has this inconvenience, that colours for values near zero have smaller information capacity, as their discrimination power is not big. They are yellowish green and green. But we can choose different colour scale which has much bigger discrimination power near zero. We will call it an inverse full-hue colour scale. As we see below, the colours are also divided to warm and cold, but the colour order was reversed, and in the middle of the scale, for zero data value, we have hue 270° (violet).

Inverse full-hue colour scale (Plate 1c)

Data value	Intensity	Hue	Saturation
1.2	constant	90.0° (green-yellow)	constant
1.0		60.0° (yellow)	
0.8		30.0° (orange)	
0.6		0.0° (red)	
0.4		330.0°	
0.2		300.0° (magenta)	
0.0		270.0° (violet)	
-0.2		240.0° (blue)	
-0.4		210.0°	
-0.6		180.0° (cyan)	
-0.8		150.0°	
-1.0		120.0° (green)	
-1.2		90.0° (green-yellow)	

**Extended inverse full-hue colour scale.** We can also extend the inverse colour scale (as below). Because in these scales the order of colours is rather unusual it is advised to use them together with shaded relief.

Extended inverse full-hue colour scale (Plate 1d)

Data value	Intensity	Hue	Saturation
2.4	constant	180.0° (cyan)	constant
1.2		90.0° (green-yellow)	
1.0		60.0° (yellow)	
0.8		30.0° (orange)	
0.6		0.0° (red)	
0.4		330.0°	
0.2		300.0° (magenta)	
0.0		270.0° (violet)	
-0.2		240.0° (blue)	
-0.4		210.0°	
-0.6		180.0° (cyan)	
-0.8		150.0°	
-1.0		120.0° (green)	
-1.2		90.0° (green-yellow)	
-2.4		0.0° (red)	

We can make many different colour scales by changing saturation and/or intensity. Apart of colour scale with saturated colours (saturation = 1.0) we can use scales with unsaturated (pastel) colours (saturation < 1.0). But if we think that this scale is too monotonous, we can “enliven” it by varying intensity in a hue/intensity colour scale.

**Full-hue/intensity colour scale.** If intensity will vary along the scale in sinusoidal way we will obtain a contour-like image.

Full-hue/intensity colour scale (Plate 1e)

Data value	Intensity	Hue	Saturation
1.2	varying sinusoidally	270.0° (violet)	constant
0.0		90.0° (green-yellow)	
-1.2		270.0° (violet)	

**Saturation (2-hue-saturation) colour scale.** In the above scale hues varied. We can design a family of scales where saturation changes. Let's select a hue from warm colours for positive data values. In this case a hue for negative values will be a hue on the opposite side of the colour circle, i.e. which differs by 180.0°. If we standardize data values to the range from -1.0 to 1.0, we will have following relation between data values and colours, if red is selected as a positive hue:

## 2-hue/saturation colour scale (Plate 1f)

Data value	Intensity	Hue	Saturation
1.0	constant	constant 0.0°	red
0.8		0.0°	light red
0.6		0.0°	pink
0.4		0.0°	
0.2		0.0°	
0.0		0.0°/180.0° (undefined), white	0.0
-0.2		180.0°	
-0.4		180.0°	
-0.6		180.0°	
-0.8		180.0°	light cyan
-1.0		180.0°	cyan

In these scales we can also use the variable intensity to obtain contour-like images:

## 2-hue/saturation/intensity colour scale (I) (Plate 1g)

Data value	Intensity	Hue	Saturation
1.0	varying sinusoidally	30.0°	red
0.0		30.0°/210.0° (undefined), white	0.0
-1.0		210.0°	cyan

We can also make another version of saturation/intensity colour scale if we extend the saturation colour scale on both sides diminishing gradually intensity to zero:

## Saturation/intensity colour scale (II)

Data value	Intensity	Hue	Saturation
1.5	0.0	undefined	black
1.0	1.0	0.0°	red
0.0	1.0	undefined	white
-1.0	1.0	180.0°	cyan
-1.5	0.0	undefined	black

**Intensity colour scale (grey scale).** We can use also the third component of IHS colour space, the intensity. Usually it is called grey scale. In this case the image looks like a black and white photograph. We must only decide if zero intensity (black colour) shows the lowest data values or highest.

## Intensity colour scale (grey scale)

Data value	Intensity	Hue	Saturation
1.0	1.0 or 0.0	undefined	0.0
0.0	0.5	undefined	0.0
-1.0	0.0 or 1.0	undefined	0.0

## SHADED-RELIEF

As we stated before, we can treat the set of data from a certain area as a 3D object (a relief). We can illuminate this object and the shadows can reveal many details not seen otherwise. On shaded relief alone there is only relative, indirect information about data values. If we want also exact information about data values we must superimpose one of colour-scaled (or contour) image mentioned before on it, but only that, where intensity was not used. As we can see, the [grey-scale] shaded-relief and colouring are independent. We can use these techniques independently so we can use any colour scale which use only hues (full-hue colour scale or extended full-hue colour scale) or hues and saturation (2hue/saturation colour scale) and even use this possibility to show two quantities on the same image: one quantity shown as a shaded-relief and second — colour-scaled, e.g. shaded relief of gravity data with colour-scaled magnetic data.

If we use shaded-relief with colour scale we can try its modified version: instead of normal data we can apply absolute data, it means that positive and negative anomalies will look alike. The difference will be only in colours. This type of shaded-relief images is good in a case where we want stress that every anomaly positive or negative has the same importance.

The above statements are true in cases where illumination light is white, so only one component of the colour space is used in shaded-relief-intensity. We can use also colour lights as an illumination source, two or more and different light sources. A special case is when we use three — red, green and blue light sources of the same elevation with azimuths differing by 120° (Wybraniec, 1995a, 1995b; Królikowski, Wybraniec, 1996).

Shaded-relief can be treated as a **directional filtration method** because it enhances linear features perpendicular to the illumination direction, so by changing the azimuth of illumination we enhance different features on the image. Using this method we must also keep in mind that we ought to use illumination from northern directions because of human perception peculiarities. Otherwise the positive anomaly on the shaded-relief image seems to be a negative one and vice versa. It can be verified also by looking on the satellite images of mountainous regions. As they are real shaded-relief images and as a rule they are oriented as geographical maps — north upwards, they look bizarre. When we turn them upside-down, we see mountains and valleys very clearly as they should.

A special case of shaded relief is that mentioned above — illuminated by red, green and blue light sources. The obtained image is similar to horizontal vector image described below in next paragraph.

## VECTOR FIELDS AND VECTORIAL IMAGES

In geophysics we often measure vector fields. In fact, potential fields are also vector fields, but in this case the field components are interdependent, so the whole information is included in every component and there is no need to measure more than one component. Apart of vector fields we often have two (or more) data sets in the same area and it would be

desirable to image these data simultaneously. So there is the need to show two (or more) quantities in one image. We can do it by using two kinds of contours, but perception of this kind of an image is very difficult. As we said, for showing one quantity on an image, it is enough to use one component of the IHS colour space, so there are two components left which can be used for showing another quantities in the same image. The natural conclusion for showing two-dimensional vector or two-quantity data set is to use hue and saturation or in other words — a colour circle. If we show 2D vector in polar co-ordinates, every one has his radial component (length) and angular component (azimuth). We can relate the vector length to saturation and vector azimuth to hue. So every vector is bound to one colour from colour circle. We will call this kind of images — vectorial images (Wybraniec, 1997). As the third component of the colour space — the intensity — is left unused, we can use it for a shaded-relief, which can be superimposed on the vectorial image.

**2D colour scales.** We can construct different colour scales accordingly to different kind of data. First scale will be for two component data, we will call it a 2-component colour scale. It is aimed for components with mean value about zero. This colour scale ([Plate 1h](#)) is just colour circle. The components can be components of the same vector or can be different quantities. Two other colour scales are for data, where one set is that of component and other has only positive values as in a module of component. The colour scales ([Plate 1, i and j](#)) have a shape of a half-circle. We will call them component/component-module and component-module/component colour scales. If both components have only positive values, i.e. are module-like, we can show them using the third kind of 2D scales ([Plate 1, k and l](#)) — 2-component-module colour scale and inverse 2-component-module colour scale.

**Horizontal vectorial images.** As the 3D vector has three components, we can use different two component arrangements in vectorial images. First, we can use two horizontal components, which means a horizontal projection of the vec-

tor. We can call this kind of image — a horizontal vectorial image. For this purpose we must use 2-component colour scale ([Plate 1h](#)). For shaded-relief we can use a module of horizontal component.

**Vertical vectorial images.** If we take a projection of the vector on a vertical plane we will have a vertical vectorial image, but we can have also different vectorial image.

**Vertical-horizontal vectorial images.** If we take a vertical component and a module of horizontal component, we obtain a set of vectors occupying only right half of a colour circle. We must also change colour scale for this sort of colour images, to squeeze all colours into the right side of the circle. We also begin this colour scale with hue of 270 degrees (violet) to have an upper quarter of the circle with warm colours and the lower quarter — with cool colours ([Plate 1i](#)). The first component — vertical component is also used for shaded-relief.

**Horizontal-vertical vectorial images.** Another possibility in vectorial imaging is a horizontal-vertical image. In this image we use module of horizontal component and vertical component ([Plate 1j](#)). For the shaded-relief the first component — the module of horizontal component is used.

## OTHER VECTORIAL IMAGES

We can also use the concept of vectorial images in other cases, not only for vector fields data presentation. We know that the analytic signal approach gives possibility to change scalar field to a potential (read: vector) field. So we can use vectorial images even in a case of scalar fields (e.g. terrain hypsography). In this case we can use the term “analytic” vectorial image.

**Pseudo-vectorial images.** We can use vectorial image concept for showing two different quantity measured in the same area simultaneously. Because they are not a vector data, we can call this sort of images as pseudo-vectorial images. According to data type, we can use different 2D colour scales ([Plate 1, h-l](#)).

## IMPLEMENTATION

All mentioned methods of transformation and visualization were put into practice. Transformations were performed using both methods: Fourier transform method and digital filtration method.

**Transformations by Fourier transform method.** In this case the base programs were those from the USGS package (Cordell *et al.*, 1992). It is based on FTT technique and can be adapted for new transformations. All new transformations were implemented using base programs from this package.

**Transformations by digital filtration.** The main problem in digital filtration is calculating digital filters. Using the technique described above, a package of programs for this purpose have been elaborated together with Z. Petecki (Wybraniec, Petecki, 1995). They are based on calculation of integrals of Bessel functions.

These programs can calculate almost any two-dimensional filter suited for potential field purposes in reasonable time and with good accuracy. The program for convolution is then quite simple. These programs have been used for several years without any problems.

Both packages are written in FORTRAN programming language and USGS standard for grids are used in both.

**Visualization.** The FORTRAN language is not suited for graphics programming, the C (or C++) is a natural choice, but grid standard was a problem. There is no easy way to move from FORTRAN binary grids to C, and to use two grid standards — one in FORTRAN and other in C is inconvenient, as it takes much more room on hard disks. In the end, the method of reading FORTRAN grids by C programs has been found. The method of obtaining computer image of a grid is as fol-

lows: using appropriate colour scale the grid is transformed to an image: one point in a grid to one pixel in an image. The image is directly written in a TARGA format, as \*.tga file.

It creates possibility of importing the image by almost any graphic program for further processing and printing.

## CONCLUSIONS

Author presents a new approach to two important parts of geophysical interpretation: transformation of data and their visualization.

1. Transformations of 2D potential field data by digital filtering was hampered by lack of effective method of calculating of 2D digital filters. A new method based on 2D Fourier-Hankel transform, formulated by the author, was elaborated for this purpose. It enables to calculate 2D filters for all important transformations.

2. Apart from well known transformations, as derivatives, upward and downward continuation etc., an importance of new transformations was stressed. These transformations include 3D Hilbert transform described by Nabighian (1984) and new ones proposed by the author: fractional integrals and derivatives, and scalar directional decomposition.

3. An importance of visualization of potential field data is also underlined. In this field author is suggesting several improvements and new ideas. Several colour scales are proposed for scalar fields and new variants of shaded relief using colour light sources are described.

4. Quite new idea is presented for visualization of vector fields — vectorial images. Several variants of these images can be used for presentation of 3D vector fields, including potential fields.

5. All above mentioned ideas have been put into practise by writing appropriate computer programs and then testing them on field data during considerable time (in some cases

for several years). As a basis the USGS software package (Cordell *et al.*, 1992) was used and enlarged by digital filtering and visualization programs.

6. The described methods can be also used in many cases for transformations and visualization of other 2D data, not only potential field ones.

7. Many examples of the use of discussed methods of transformations and visualization are presented. The potential field examples are based on Polish gravity data ([Plates 2 to 11](#)), Polish magnetic data ([Plates 12 to 18](#)) and European gravity data ([Plates 19 to 24](#)). As an example of application of proposed methods to non-potential field data the hypsography data of Poland are shown ([Plates 25 to 30](#)).

**Acknowledgements.** Author would like to pay tribute to colleagues from USGS, Denver, Reston and Menlo Park for their help in computer programming for potential fields and stimulating discussions: Melvin Podwysocki, Lindrith Cordell, Jeffrey Phillips and others. Special thanks are due to Lindrith Cordell, USGS, Denver, who introduced me also to modern techniques of computer graphics. I would like also to thank Hans Thybo, Copenhagen University and Edward Perchuc, Polish Academy of Sciences, whose interest to my work and help were very important for me.

I would also like to mention my colleague, Zdzisław Petecki, who is an author of basic programs used in digital filtering.

## REFERENCES

- ABRAMOWITZ M., STEGUN I. A. (eds.), 1964 — Handbook of mathematical functions with formulas, graphs and mathematical tables. National Bureau of Standards, Applied Mathematics Series 55 (Russian translation). Nauka, Moskva, 1979.
- BARANOV V., 1975 — Potential fields and their transformations in applied geophysics. Gebrueder Borntraeger, Berlin (Russian translation). Nedra, Moskva, 1980.
- BATH M., 1974 — Spectral analysis in geophysics. Elsevier, Amsterdam, Oxford, New York (Russian translation). Nedra, Moskva, 1980.
- BLAKELY R. J., 1996 — Potential theory in gravity and magnetic applications. Cambridge University Press, Cambridge, New York.
- BRACEWELL R., 1965 — The Fourier transform and its application. McGraw Hill, New York (Polish translation). PWN, Warszawa, 1968.
- CAPPELINI V., CONSTANTINIDES A. G., EMILANI P., 1978 — Digital filters and their applications. Academic Press, London (Russian translation). Energoatomizdat, Moskva, 1983.
- CORDELL L., PHILLIPS J. D., GODSON R. H., 1992 — U.S. Geological Survey potential field software, version 2.0, Open-File Report 92-18. U.S.G.S., Denver.
- DĘBSKI W., NIEWIADOMSKI J., 1993 — Numerical filters. *Publ. Inst. Geophys. Pol. Acad. Sc.*, G-4 (257): 1-68.
- DUDGEON D. E., MERSEREAU R. M., 1984 — Multidimensional digital signal processing. Prentice Hall, Englewood Cliffs (Russian translation). Mir, Moskva, 1988.
- FOLEY J. D., van DAM A., FEINER S. K., HUGHES J. F., PHILLIPS R. L., 1994 — Introduction to computer graphics. Addison-Wesley, Reading. (Polish translation). WNT, Warszawa, 1995.
- HUANG T. S. (ed.), 1975 — Picture processing and digital filtering. Springer-Verlag, Berlin, Heidelberg, New York (Russian translation). Mir, Moskva, 1979.
- KORENEV B. G., 1971 — Introduction to the theory of Bessel functions. (In Russian), Nauka, Moskva (Czech translation). SNTL, Praha, 1977.
- KRÓLIKOWSKI C., PETECKI Z., 1995 — Gravimetric atlas of Poland. Państw. Inst. Geol., Warszawa.
- KRÓLIKOWSKI C., WYBRANIEC S., 1996 — Gravity and magnetic maps of Poland — historical background and modern presentation. *Publ. Inst. Geophys. Pol. Acad. Sc.*, M-18 (273): 87-92.

- KU C. C., TELFORD W. M., LIM S. H., 1971 — The use of linear filtering in gravity problems. *Geophysics*, **36**, 6: 1174–1203.
- LIM J. S., 1990 — Two dimensional signal and image processing. Prentice Hall, Englewood Cliffs.
- McLACHLAN N. W., 1955 — Bessel functions for engineers. Clarendon Press, Oxford (Polish translation). PWN, Warszawa, 1964.
- MESKO A., 1984 — Digital filtering: applications in geophysical exploration for oil. Akademiai Kiado, Budapest.
- NABIGHIAN M. N., 1972 — The analytic signal of two-dimensional magnetic bodies with polygonal cross-section: its properties and use for automatic anomaly interpretation. *Geophysics*, **37**, 3: 507–517.
- NABIGHIAN M. N., 1974 — Additional comments on the analytic signal of two-dimensional magnetic bodies with polygonal cross-section. *Geophysics*, **39**, 1: 85–92.
- NABIGHIAN M. N., 1984 — Toward a three-dimensional automatic interpretation of potential field data via generalized Hilbert transform: Fundamental relations. *Geophysics*, **49**, 6: 780–786.
- OPPENHEIM A. V., SCHAFER R. W., 1975 — Digital signal processing. Prentice Hall, Englewood Cliffs. Polish translation. Wyd. Kom. i Łączn., Warszawa, 1979; Russian translation. Sviaz', Moskva, 1979.
- PEDERSEN L. B., 1989 — Relations between horizontal and vertical gradients of potential fields. *Geophysics*, **54**, 5: 662–663.
- RABINER L. R., GOLD B., 1975 — Theory and application of digital signal processing. Prentice Hall, Englewood Cliffs (Russian translation). Mir, Moskva, 1978.
- ROEST W. R., VERHOEF J., PILKINGTON M., 1992 — Magnetic interpretation using the 3-D analytic signal. *Geophysics*, **57**, 1: 116–125.
- SAMKO S. I., KILBAS A. A., MAROCHEV O. I., 1987 — Integrals and derivatives of fractional order and some applications (in Russian). Nauka i tekhnika, Minsk.
- SZABATIN J., 1982 — Podstawy teorii sygnałów (in Polish only: Fundamentals of signal theory). Wyd. Kom. i Łączn., Warszawa.
- WYBRANIEC S., 1995a — Gravity shaded pseudo-relief of Poland (English Sum.). *Prz. Geol.*, 2: 101–106.
- WYBRANIEC S., 1995b — The pseudorelief illumination by RGB sun system—a method of multidirectional filtering (English Sum.). *Prz. Geol.*, 4: 285–290.
- WYBRANIEC S., PETECKI Z., 1995 — Pakiet programów komputerowych do filtracji i wizualizacji pól potencjalnych (in Polish, unpublished: Computer programs package for digital filtration and visualization of potential field data). Arch. Polish Geological Institute. Warszawa.
- WYBRANIEC S., 1997 — Obrazy wektorowe — nowy sposób przedstawiania danych powierzchniowych [in Polish: Vectorial images — a new method of presenting 2D data]. *Posiedz. Nauk. PIG*, **53(5)**: 42.
- WYBRANIEC S., ZHOU Sh., THYBO H., FORSBERG R., PERCHUĆ E., LEE M., DEMIANOV G. D., STRAKHOV V. N., 1998 — New map compiled of Europe's gravity field. *Eos, Transactions, American Geophysical Union*, **79**, 37: 437, 442.

## TRANSFORMACJE I WIZUALIZACJA DANYCH PÓŁ POTENCJALNYCH

W pracy przedstawiono nowe dane uzyskane w trakcie studiów nad transformacjami i technikami prezentacji danych pól potencjalnych. Transformacje pól potencjalnych wykonuje się dwoma sposobami: za pomocą przekształcenia Fouriera oraz z wykorzystaniem filtracji cyfrowej. Przekształcenie Fouriera stało się podstawowym sposobem prowadzenia transformacji pól potencjalnych od momentu opracowania bardzo efektywnej techniki liczenia tego przekształcenia, tzw. szybkiego przekształcenia Fouriera (ang. Fast Fourier Transform — FFT). Słabym punktem filtracji cyfrowej w zastosowaniu do transformacji pól potencjalnych był brak dobrych metod liczenia dwuwymiarowych filtrów cyfrowych, które w tej metodzie są zasadniczym elementem. Z tego powodu była ona coraz rzadziej stosowana. Autor przedstawia w niniejszej pracy nowy sposób konstrukcji filtrów cyfrowych zarówno jedno-, jak i dwuwymiarowych, co w rezultacie powoduje, że w wielu wypadkach stosowanie filtracji cyfrowej staje się atrakcyjne. Do konstrukcji filtrów dwuwymiarowych wykorzystano nowo zdefiniowane całkowe przekształcenie Fouriera-Hankela, będące nieskończoną sumą przekształceń Hankela, i stanowiące odpowiednik dwuwymiarowego przekształcenia Fouriera w układzie współrzędnych biegunowych.

Dzięki wspomnianej metodzie można uzyskać wzory analityczne opisujące różne filtry zarówno jedno-, jak i dwuwymiarowe. W pracy przedstawiono liczne przykłady wzorów analitycznych na filtry jedno- i dwuwymiarowe. W wielu przypadkach znalezienie wzorów analitycznych jest utrudnione lub wręcz niemożliwe, wtedy jednak filtry można obliczyć przez rozwiązywanie numeryczne odpowiednich całek. Napisano w tym celu stosowne programy komputerowe. W rezultacie istnieje możliwość konstrukcji prawie dowolnych filtrów cyfrowych.

Zakres możliwych transformacji pól potencjalnych jest szeroki. Oprócz dobrze znanych transformacji typu pochodnych pionowych, kontynuacji analitycznej w dół lub w góre autor zwraca uwagę na stosunkowo nowe transformacje związane z pojęciem tzw. sygnału analitycznego i transformacji Hilberta. Przekształcenie to pozwala obliczyć składowe poziome pola potencjalnego na podstawie składowej pionowej i odwrotnie.

Zaproponowano też nowe metody transformacji pól potencjal-

nych: pochodne i całki ułamkowe oraz składowe kierunkowe. Stwierdzono, że ułamkowe całki pionowe są przydatne do wzmacniania anomalii wielkopromiennych, co przydaje się zwłaszcza przy analizie pól magnetycznych. Transformacje wykorzystujące składowe kierunkowe stosuje się przy analizie tektonicznej obszaru.

Przykłady transformacji zaprezentowane na załączonych tablicach oparte są na obu metodach transformacji: zarówno transformacji Fouriera wykorzystującej technikę FFT, jak i filtracji cyfrowej z zastosowaniem filtrów obliczonych opisaną metodą.

Dużo uwagi poświęcono wizualizacji danych wychodząc z założenia, że jest to niezwykle istotny fragment analizy pól potencjalnych i może ona stanowić jeden ze sposobów interpretacji badań. Olbrzymie możliwości w tym zakresie stwarzają niezwykle dynamicznie rozwijającą się grafika komputerowa.

Autor przedstawił nowe metody wizualizacji danych potencjalnych. Opierając się na przestrzeni barw w systemie chroma (barwność), nasycenie i jasność opracowano szereg skal barw, które można wykorzystać do przedstawiania danych skalarnych. Nowym typem skali barw jest skala odwrócona, która wzmacnia słabe anomalie. Opracowano także sposób przedstawiania dwuwymiarowych pól wektorowych. Polega on na tym, że skalę barw dla tych obrazów stanowi koło barw. Obrazy przedstawiające takie dane nazwano obrazami wektorowymi. Dla wizualizacji danych pól potencjalnych można wykorzystać kilka wariantów obrazów wektorowych.

Napisano programy komputerowe pozwalające przedstawione metody transformacji i wizualizacji wykorzystywać w praktyce. Na 30 dołączonych tablicach pokazano różne przykłady zastosowania opisanych metod.

Na tablicy 1 uwidoczniono skale barw stosowane do przedstawiania danych skalarnych (lewa strona tablicy) i wektorowych (jej prawa strona). Dwie pierwsze skale to skale pełnochromatyczne, czyli wykorzystujące wszystkie dostępne chromy (odcienie barw). Pierwsza skala to skala normalna, natomiast druga jest skalą rozszerzoną, gdzie część kolorów zimnych wykorzystano do pokazania wartości najwyższych, a część kolorów cieplich do wartości najniższych. Następne dwie skale to skale pełnochromatyczne odwró-

cone. Jest tu odwrócona kolejność odcieni barw a granica między chromami zimnymi i cieplymi stanowi fiolet ( $270^\circ$ ), a nie chroma żółtozielona ( $90^\circ$ ), jak w poprzednich skalach. Ten rodzaj skali jest bardzo przydatny do podkreślenia słabych anomalii, które są słabo widoczne przy skalach normalnych. Następna skala to skala pełnochromatyczna normalna ze zmieniającą się sinusoidalnie jasnością, dającą obraz podobny do izoliniowego. Dwie ostatnie skale skalarne to skale dwuchromatyczne, w których wielkością zmieniającą się jest nasycenie. Ostatnia skala dodatkowo korzysta ze zmieniającej się sinusoidalnie jasności.

Prawe skale to skale dla obrazów wektorowych. Pierwszą skalę, którą stanowi koło barw stosuje się w przypadku zwykłych wektorów dwuwymiarowych. Każdy taki wektor we współrzędnych biegunowych określony jest przez swoją długość i kąt (azymut). Jeśli długość przyporządkujemy nasyceniu, a azymutowi barwność (chromę, odcień barwy), to każdemu wektorowi będzie odpowiadać określona barwa. Drugą skalę obejmującą prawą połowę koła, która zawiera jednak wszystkie barwy, stosujemy, gdy druga składowa ma tylko wartości dodatnie, czyli jest modułem. Następna skala jest podobna, ale w tym wypadku to pierwsza składowa jest modułem, także kolejność barw jest inna. Dwie ostatnie skale barw stosuje się, gdy obie składowe są modułami, przy czym w ostatniej skali barwy są odwrócone.

Pozostałe tablice (2–30) przedstawiają zastosowanie opisanych metod transformacji i wizualizacji do prezentacji polskich danych grawimetrycznych i magnetycznych, europejskich danych grawimetrycznych oraz danych hipsograficznych Polski, jako przykład danych pól nie potencjalnych.

Tablice 2 do 11 pokazują lądowe dane grawimetryczne Polski. Wykorzystano tu dane zgromadzone w bazie danych grawimetrycznych. Obraz na tablicy 2, przedstawiający anomalie Bouguera jest przekształceniem siatki regularnej 1 na 1 km, którą otrzymano po przez interpolację danych z nieregularnie położonych punktów pomiarowych. Wykorzystano w tym celu program z amerykańskiego pakietu do obróbki i interpretacji danych potencjalnych (Cordell i in., 1992). Interpolacja stosuje algorytm najmniejszej krzywizny. Obraz ten to nałożenie dwóch obrazów: obrazu kolorowego z zastosowaniem pełnochromatycznej rozszerzonej skali barw przy nasyceniu maksymalnym (1,0) oraz rzeźby cieniowanej w szarościach, oświetlanej z północy. Przyjęto też, że powierzchnia charakteryzuje się odbiciem zwierciadlanym o wykładniku 10 i współczynniku 1,0. Należy zauważyć, że skala barw nie jest równomierna. Dla części rozszerzonej zastosowano współczynnik skali 4-krotnie większy.

Analogiczne parametry obrazu zastosowano na tablicy 3, gdzie pokazano lokalne anomalie grawimetryczne z podstawowym zakresem długości fal od 2 do 60 km. Ten obraz jest także interesujący z tego powodu, że wzięto pod uwagę fakt, iż każda funkcja 2D jest sumą jej dwóch (czterech itd.) składowych kierunkowych oraz, że najdłuższa fala przestrzenna jaką jest przepuszczana w czasie filtracji cyfrowej zależy od wymiarów filtra. W tym konkretnym przypadku anomalie uzyskano poprzez sumowanie czterech składowych kierunkowych (co  $90^\circ$ ) obliczonych na drodze filtracji cyfrowej przy pomocy bi-transformatora Hilberta o wymiarach 61 na 61 wyrazów.

Tablica 4 przedstawia te same dane, ale zastosowano tu inną skalę barw, a mianowicie rozszerzoną odwróconą skalę pełnochromatyczną. Skala ta podkreśla mocniej słabe anomalie, co w wielu przypadkach jest bardzo pożądane. Widać to wyraźnie na przykładzie anomalii związanych ze strefą Koszalin–Chojnice.

Tablica 5 na pierwszy rzut oka jest bardzo podobna do tablicy 3 jednak zastosowano tu zupełnie inny rodzaj skali barw, gdyż jest to obraz wektorowy. Jest to obraz pionowo-poziomy, gdzie pierwszą składową wektora jest składowa pionowa (lokalna anomalia Bouguera) przedstawiona na tablicy 3, a drugą składową jest moduł składowej poziomej. Jest to więc pierwiastek z sumy kwadratów dwóch składowych poziomych uzyskanych na drodze filtracji cyfrowej, gdzie filtrami były odpowiednie transformatory Hilberta o

wymiarze 61 na 61 wyrazów. Na obrazie wektorowym anomalie dodatnie (lub ujemne) mają ten sam odcień barwy (chromę, barwność). Nasycenie zaś mówi o intensywności anomalii, czyli pośrednio o głębokości zalednia ciała powodującego daną anomalię. Z porównania obu obrazów, zwykłego (skalarnego) z wektorowym można wyciągnąć też wnioski o kształcie ciała.

Tablica 6 przedstawia inny rodzaj obrazu wektorowego: obraz poziomo-pionowy. Swoim wyglądem różni się on zasadniczo od poprzedniego. Wynika to z odmiennej kolorystyki podkreślającej strefy gradientowe. Są one dodatkowo wzmacnione cieniami, gdyż rzeźba cieniowana dotyczy tu modułu składowej poziomej, a nie składowej pionowej jak na poprzednim obrazie wektorowym. Obraz ten w pewnym stopniu podobny jest do obrazu na tablicy 4 z odwróconą skalą barw wzmacniającą słabe anomalie, czyli kontrasty gęstościowe.

Jeszcze inny rodzaj obrazu wektorowego widzimy na tablicy 7. Jest on zupełnie inny od poprzednich, gdyż jest to obraz wektorowy poziomy, wykorzystujący tylko składowe poziome. Chromy (barwności) są tu związane bezpośrednio z azymutem pełnej składowej poziomej wektora grawitacji. Rzeźba cieniowana, jak na tablicy 6, odzwierciedla moduł pełnej składowej poziomej.

Na tablicach 8 i 9 przedstawiono efekt nowej transformacji zaproponowanej w niniejszej pracy. Są to składowe kierunkowe. Obraz z tablicy 3 został rozłożony na dwie składowe kierunkowe: 45-stopniową (tablica 8) i 135-stopniową (tablica 9). Na tablicy 8 podkreślone są anomalie wydłużone w kierunku  $45^\circ$ – $225^\circ$ , a osiąbane w innych, natomiast na tablicy 9 wzmacnione są kierunki  $135^\circ$ – $315^\circ$ .

Dwie następne tablice pokazują obrazy wektorowe pionowo-poziome bazujące na siatce regularnej 500 na 500 m. Przy przygotowaniu tablicy 10 zastosowano te same transformacje i te same filtry co przy tablicy 4, ale rezultat jest inny z dwóch powodów. Dwa razy mniejszy bok siatki powoduje, że zakres długości fal wynosi w tym przypadku 1–30 km, a nie 2–60 km, jak na poprzednich obrazach. Pokazuje on więc anomalie bardziej lokalne pochodzące od płytowych ciał. Inną różnicą jest to, że rzeźba cieniowana dotyczy modułu składowej poziomej, a nie samej składowej. Stąd zarówno anomalie dodatnie, jak i ujemne pokazane są jako obiekty wypukłe.

Podobną manierę zastosowano przy następnej tablicy, gdzie pokazano obraz wektorowy gradientu pionowego pola grawitacyjnego. Został on obliczony za pomocą transformacji Fouriera, a następnie wygładzony w promieniu 1,5 km. W porównaniu z tablicą poprzednią pokazuje on jeszcze mniejsze anomalie, pochodzące od najpłytszych ciał, co wynika z zastosowania pierwsi pochodnej pionowej. Wygładzenie zastosowano do osłabienia zakłóceń.

Na następnych 7 tablicach pokazano obrazy przedstawiające pole magnetyczne Polski. Dane magnetyczne to dane dotyczące pola całkowitego, obejmujące dane polowe zgromadzone w bazie danych magnetycznych oraz przeliczone dane składowej pionowej pomierzone głównie w północno-wschodniej i wschodniej Polsce i w Karpatach. Przeliczenie to wykonała firma GETECH z Leeds w Wielkiej Brytanii.

Na tablicy 12 pokazano dane nietransformowane, analogicznie do danych grawimetrycznych z tablicy 2. Na północ od Karpat widoczny jest stopień wyznaczający granicę między nowym zdjęciem

*T* na północy oraz starym przeliczonym zdjęciem regionalnym składowej pionowej w Karpatach. W momencie przeliczenia, nowych pomiarów w rejonie Kielc jeszcze nie było, stąd pojawienie się tego stopnia (poprzednio go nie było). Tablica ta pokazuje problemy związane z prezentacją danych magnetycznych w Polsce. Północno-wschodnia część kraju jest silnie magnetyczna, natomiast część pozostała — bardzo słabo, dlatego trudno na jednym obrazie pokazać odpowiednio obie prowincje. Trzeba w tym celu wykonać dwa obrazy.

Na tablicy 13 zastosowano do tych samych danych skalę odwróconą. Dzięki niej bardzo wyraźnie są pokazane słabe anomalie w za-

chodniej i południowej Polsce, natomiast gorzej czytelne są dane z północno-wschodniej Polski.

Na dwóch następnych tablicach pokazano obrazy wektorowe pola magnetycznego. Na tablicy 14 uwidoczniono obraz wektorowy pionowo-poziomy. Podobnie jak w przypadku analogicznego obrazu grawimetrycznego, jest on podobny do obrazu z tablicy 12, ale słabe anomalie z południa kraju są lepiej czytelne niż na zwykłym obrazie.

Obraz wektorowy poziomo-pionowy pokazany na tablicy 15 bardzo wyraźnie pokazuje granice magnetyczne. Okazuje się, że są one bardziej skomplikowane niż się dawniej wydawało.

Na następnych trzech tablicach pokazano nowe wersje obrazów przedstawiających inną, nową transformację zaproponowaną w niżej szej pracy. Jest to pionowa całka ułamkowa. W naszym przypadku jest to całka połówkowa. Całki ułamkowe wzmacniają anomalie wielkopromienne, co łatwo zauważać na tablicy 16. Ten rodzaj transformacji jest przydatny zwłaszcza w magnetyce (ale nie tylko, co zobaczymy poniżej). Z obrazów wektorowych przedstawionych na tablicach 17 i 18, sugestynny jest zwłaszcza obraz wektorowy poziomo-pionowy z tablicy 18. Sugeruje on, że ważniejszą granicą magnetyczną na północy kraju jest linia Włocławek–Szczecin, a nie Bydgoszcz–Koszalin jak się dawniej uważało.

Na kolejnych sześciu tablicach pokazano obrazy prezentujące europejskie dane grawimetryczne. Dane te to komplikacja materiałów z różnych źródeł (zob. Wybraniec i in., 1998). Są to anomalie Bouguera na lądzie oraz anomalie wolnopowietrzne na morsach. Te ostatnie, to dane z pomiarów satelitarnych. Niestety na lądach widnieje jeszcze dużo białych plam, co wynika z trudności z dotarciem do materiałów źródłowych.

Na tablicy 19 pokazano dane bez transformacji, z zastosowaniem rozszerzonej skali pełnochromatycznej. Jak widać obraz grawimetryczny Europy, poza śródziemnomorskimi pasem alpejskim oraz Skandynawią, jest mało zróżnicowany, dlatego potrzebne są tutaj odpowiednie transformacje i metody wizualizacji. Na tablicy 20 widnieje obraz wektorowy pionowo-poziomy. Jest on bardziej zróżnicowany. Można zauważyć, że kolorystyka obrazu uzależniona jest od miąższości skorupy ziemskiej. Barwy zimne obserwuje się głównie na platformie prekambryjskiej oraz w miejscach występowania pasm górskich, czyli tam, gdzie skorupa ziemska ma większą miąższość. Na tablicy 21 pokazano obraz wektorowy poziomo-pionowy. Przedstawia on jeszcze inny aspekt tego pola grawitacyjnego. Warto tu zwrócić uwagę na dwa bloki o podwyższonych wartościach pola: blok irlandzki obejmujący także Walię i Kornwalię o prawie południkowej granicy wschodniej oraz blok duński obejmujący również część Morza Północnego, północno-wschodnie Niemcy i południowo-zachodni Bałtyk. Blok irlandzki charakteryzuje się wyraźnie oceanicznym charakterem pola grawitacyjnego, natomiast pozycja bloku duńskiego jest dość zagadkowa. Na kolejnych trzech tablicach pokazano transformację europejskiego pola grawitacyjnego. Jest to ułamkowa (połówkowa) całka pionowa pola grawitacyjnego pokazana w trzech wersjach wizualizacyjnych.

Na tablicy 22 można zobaczyć obraz skalarny z zastosowaniem rozszerzonej skali pełnochromatycznej. W porównaniu z obrazem z

tablicy 19 jest on o wiele bardziej zróżnicowany. Pozwala on wydzielać duże bloki skorupowe, które na tablicy 19 były ledwie widoczne. Jest rzeczą interesującą, że ujemna anomalia Karpat jest tu na odwrót słabiej widoczna w odróżnieniu od anomalii Alp, Iberii i Skandynawii, które uległy wzmacnieniu. Warto też zwrócić uwagę na ukraiński blok podwyższonych wartości, który łączy się prawdopodobnie poprzez Bułgarię z wyżem Morza Egejskiego oraz z wyżem pannońskim. Niestety jest tu zbyt dużo białych plam, by scharakteryzować pełniej ten bardzo ważny obszar. Obrazy wektorowe na tablicach 23 i 24 dostarczają dalszych szczegółów do charakterystyki pola grawitacyjnego Europy.

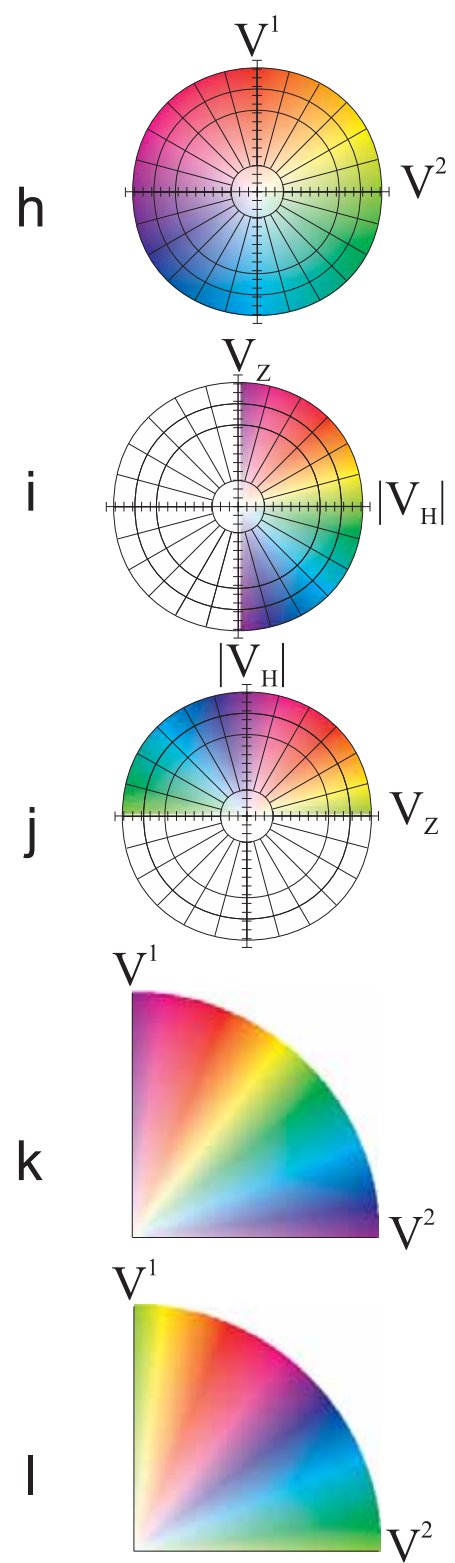
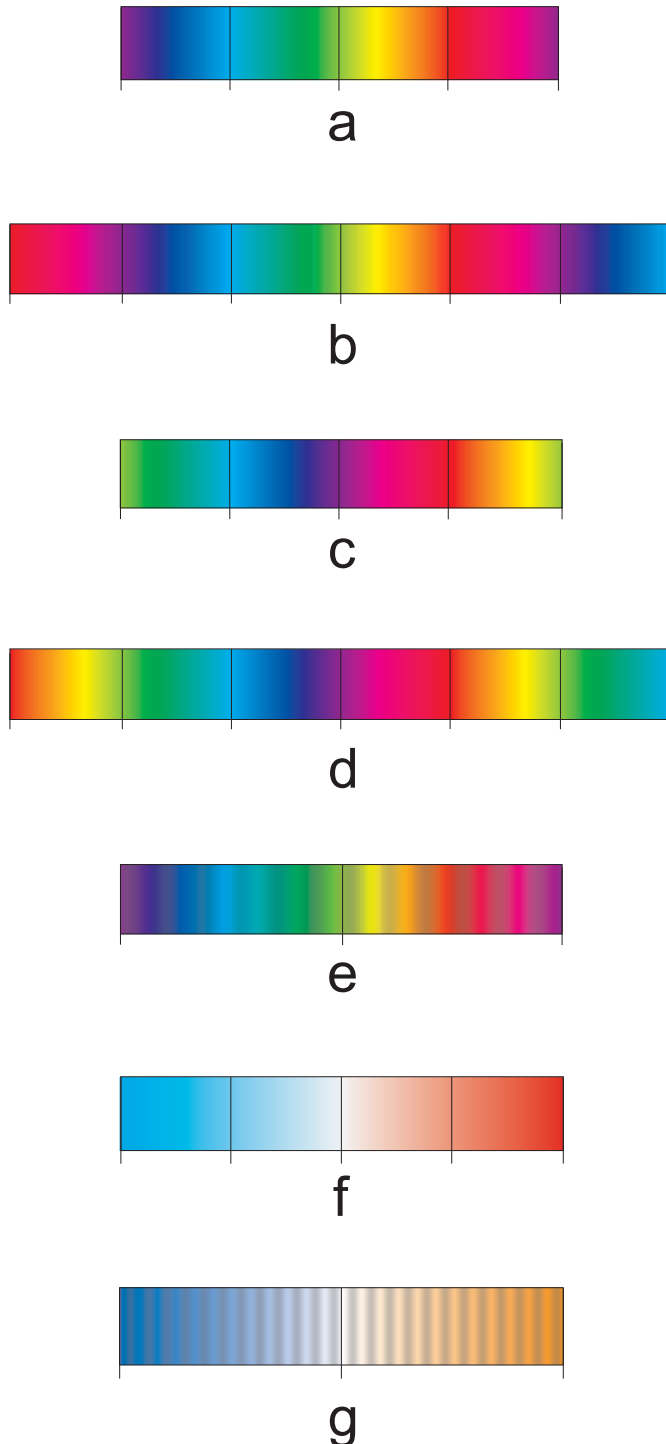
Na ostatnich sześciu tablicach pokazano, że opisane w pracy metody transformacji i wizualizacji można stosować nie tylko do danych pól potencjalnych. Jako przykład wybrano tu polskie dane hipsograficzne, czyli dane o rzeźbie terenu. Wykorzystano dane z bazy danych grawimetrycznych. Wszystkie obrazy oparte są na regularnej siatce interpolacyjnej o oczku 500 na 500 m.

Na tablicy 25 przedstawiono obraz rzeźby cieniowanej z rozszerzoną pełnochromatyczną skalą barw. Na tablicach 26 i 27 pokazano obrazy wektorowe. Założono, że funkcja opisująca rzeźbę terenu jest składową pionową pewnego pola potencjalnego. Wykorzystując metody stosowane dla pól potencjalnych można policzyć więc składowe poziome i skonstruować odpowiednie obrazy wektorowe. Pierwsze dwa obrazy wektorowe (tablice 26 i 27) otrzymano obliczając składowe poziome za pomocą transformacji Fouriera. W tym przypadku zakres długości fal przestrzennych jest ograniczony wielkością kraju, czyli jest rzędu 800 km, natomiast trzy ostatnie obrazy uzyskano stosując filtrację cyfrową z filtrami o wymiarach 61 na 61 wyrazów, czyli podstawowy zakres długości fal jest ograniczony i wynosi 2 do 30 km. Przedstawiają one więc pewnego rodzaju anomalie lokalne wysokości terenu. Obrazy na tablicach 26 i 27 są do siebie bardzo podobne, a różnią się raczej jak pozytyw od negatywu. Charakterystycznym elementem jest tu rejon wyżyn południowo-środkowych wraz z Karpatami. Jest to blok ograniczony od wschodu dolinami Sanu i środkowej Wisły, a od zachodu doliną Odry. Wyżyna Lubelska ma wyraźnie inny charakter. Na obrazie z tablicy 27 w północnej Polsce widać także delikatną siatkę cieni o kierunku generalnie NNE–SSW. Ma ona prawdopodobnie związek z kierunkiem posuwania się lądolodu w czasie ostatnich zlodowań. Ta hipoteza wymagałaby jednak weryfikacji.

Analizując obrazy z tablic 28–30 można ocenić ich przydatność w celach interpretacji geomorfologicznej i geologicznej. Wydaje się, że bardzo przydatne mogą tu być obrazy wektorowe. Obiekty geomorfologiczne są bardzo dobrze wyeksponowane na obrazie pionowo-poziomym (tablica 29), natomiast zjawiska neogeodynamiczne łatwo identyfikować na obrazie poziomo-pionowym (tablica 30), gdzie podkreślone są rejony o szybkich zmianach morfologii terenu.

Wydaje się, że załączone przykłady dostatecznie sugestynie pokazują przydatność opisanych w pracy metod transformacji i wizualizacji danych. Pomyślano wpierw jako narzędzia dla danych pól potencjalnych, mogą one służyć także do analizy i prezentacji innych danych powierzchniowych.

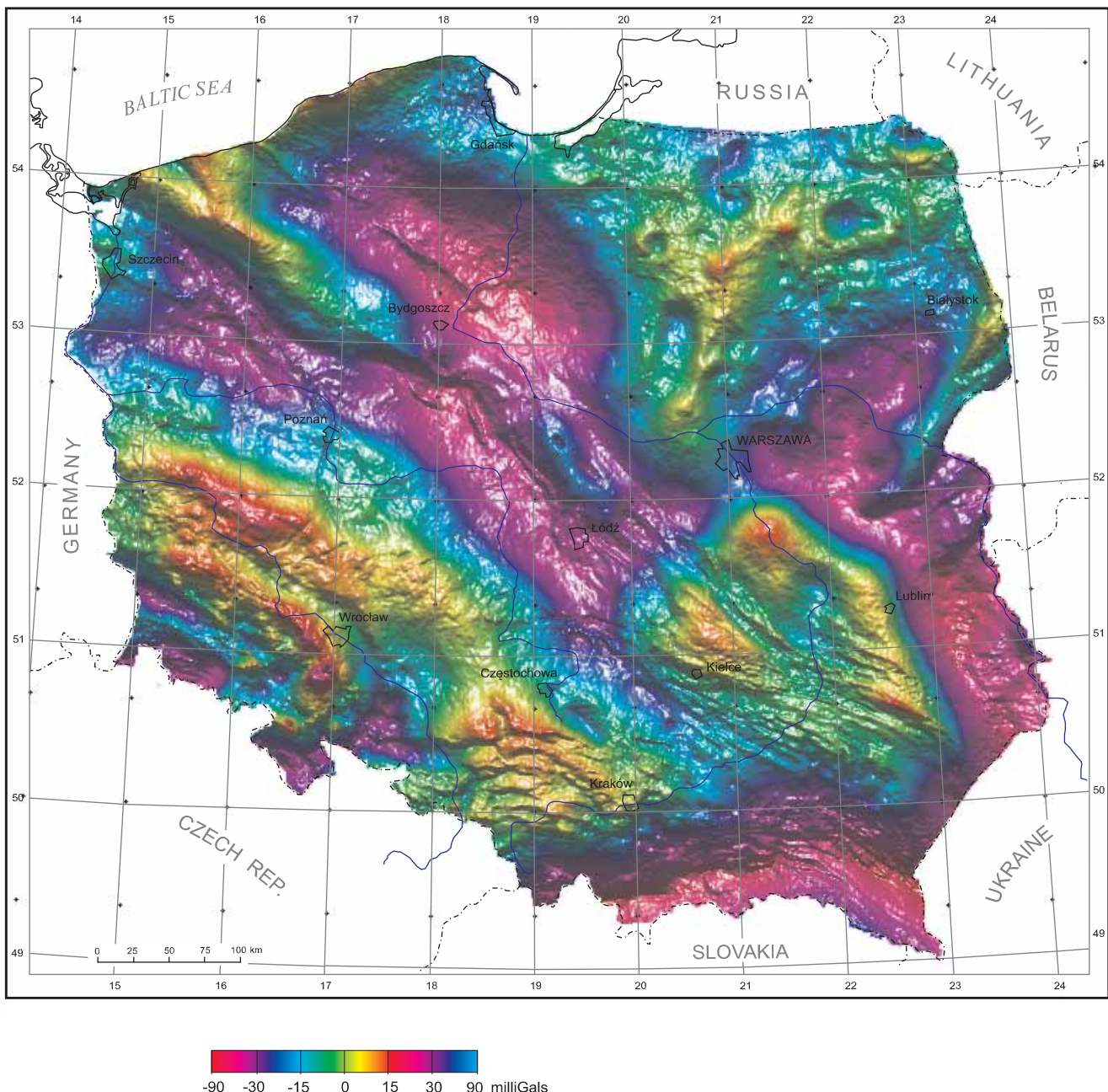
## Colour scales



**1D colour scales:** **a** — full-hue colour scale; saturation and intensity: 1.0; **b** — extended full-hue colour scale; saturation and intensity: 1.0; **c** — inverse full-hue colour scale; saturation and intensity: 1.0; **d** — extended inverse full-hue colour scale; saturation and intensity: 1.0; **e** — full-hue/intensity colour scale; saturation 1.0; **f** — 2-hue/saturation colour scale; hues:  $180^\circ$  and  $0^\circ$ , intensity 1.0; **g** — 2-hue/saturation/intensity colour scale; hues:  $210^\circ$  and  $30^\circ$ ; **2D (vector image) colour scales:** **h** — 2-component colour scale; intensity 1.0; **i** — component/component-module colour scale; intensity 1.0; **j** — component-module/component colour scale; intensity 1.0; **k** — 2-component-module colour scale; intensity 1.0; **l** — inverse 2-component-module colour scale; intensity 1.0

**PLATE 2**

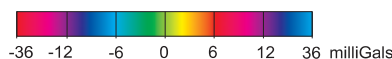
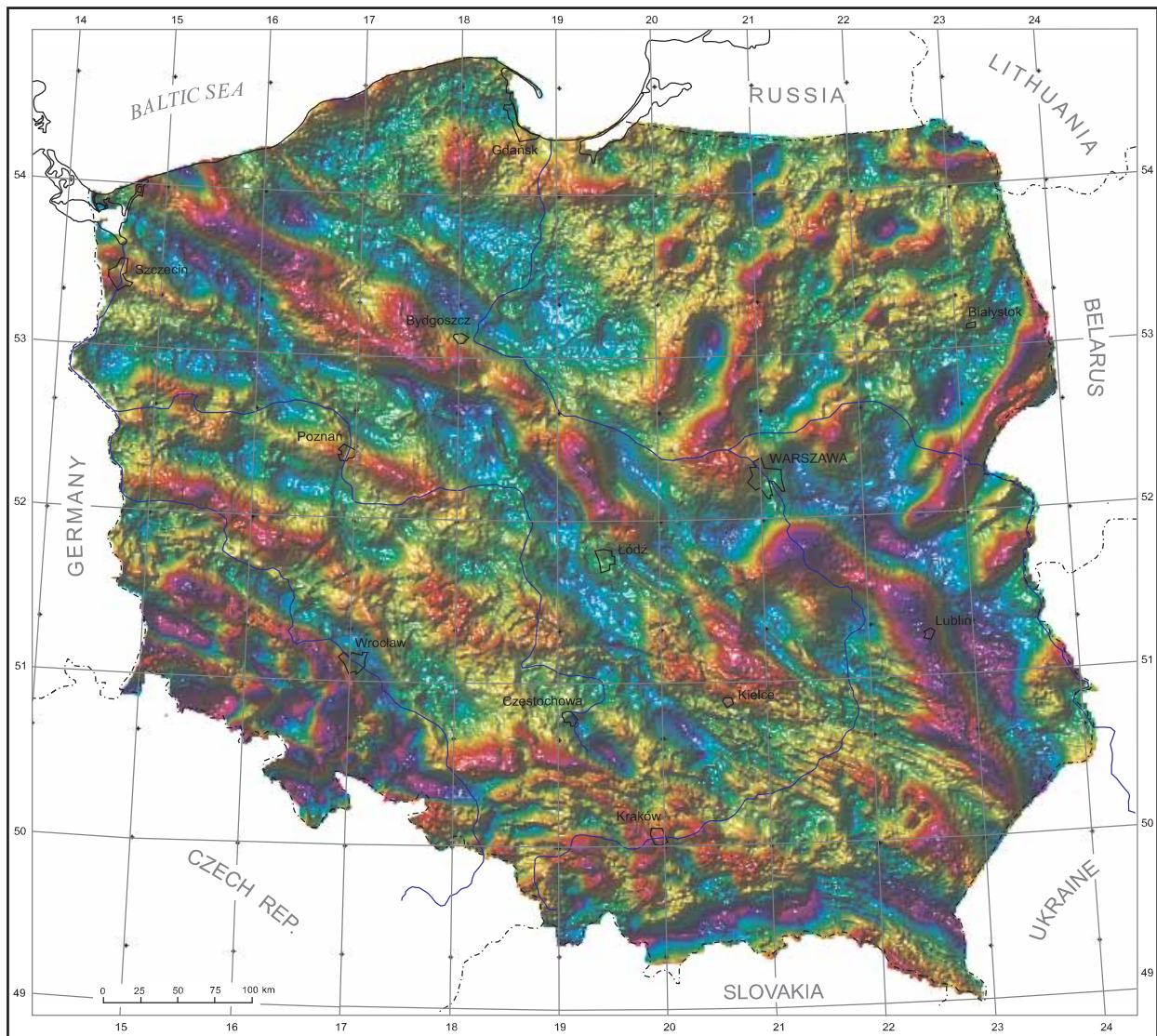
**Image of Bouguer anomaly of Poland — extended full-hue colour scale**



**Data source:** Polish onshore gravity database (see Królikowski, Petecki, 1995); **processing:** grid 1 x 1 km, gridding using minimum curvature algorithm — USGS's MINC-program; **transformation:** no; **wavelength range:** minimal — 2 km; **visualization:** superposition of scalar image with extended full-hue colour scale, and shaded relief illuminated from the north; surface mirror reflectivity: index 10, coefficient 1.0

**Remarks:** Novelty in this image is its colour scale: extended full-hue colour scale. Notice also, that for extended parts of colour scale the scaling is different, with factor x 4.

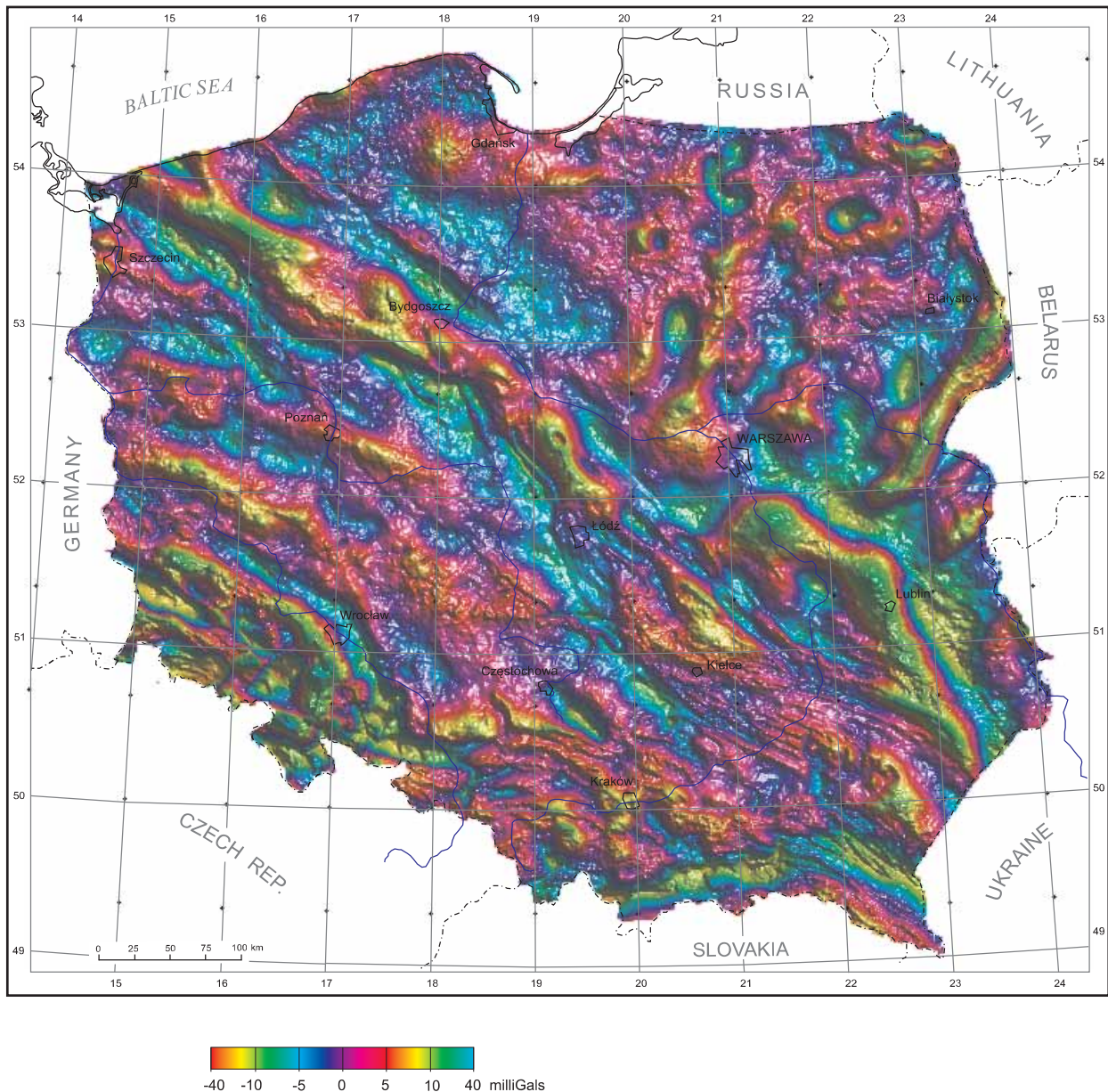
## Image of local Bouguer anomaly of Poland — extended full-hue colour scale



**Transformation:** local anomaly with basic wavelength range 2 to 60 km; **transformation technique:** sum of four directional components (every 90°), obtained by digital filtering with Hilbert bi-transformer of 61x61 dimensions; **visualization:** superposition of scalar image with extended full-hue colour scale, and shaded relief illuminated from the north; **surface mirror reflectivity:** index 10, coefficient 1.0

**Remarks:** In this image a method of obtaining local anomaly is interesting. Two facts were taken into account: a 2-D function can be composed of its two (four etc.) directional components and that basic wavelength range passed through in digital filtering depends of the dimension of the filter, but in some extent longer wavelengths are also present.

## Image of local Bouguer anomaly of Poland — extended inverse full-hue colour scale

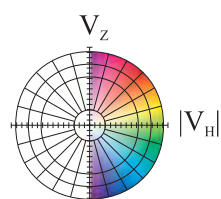
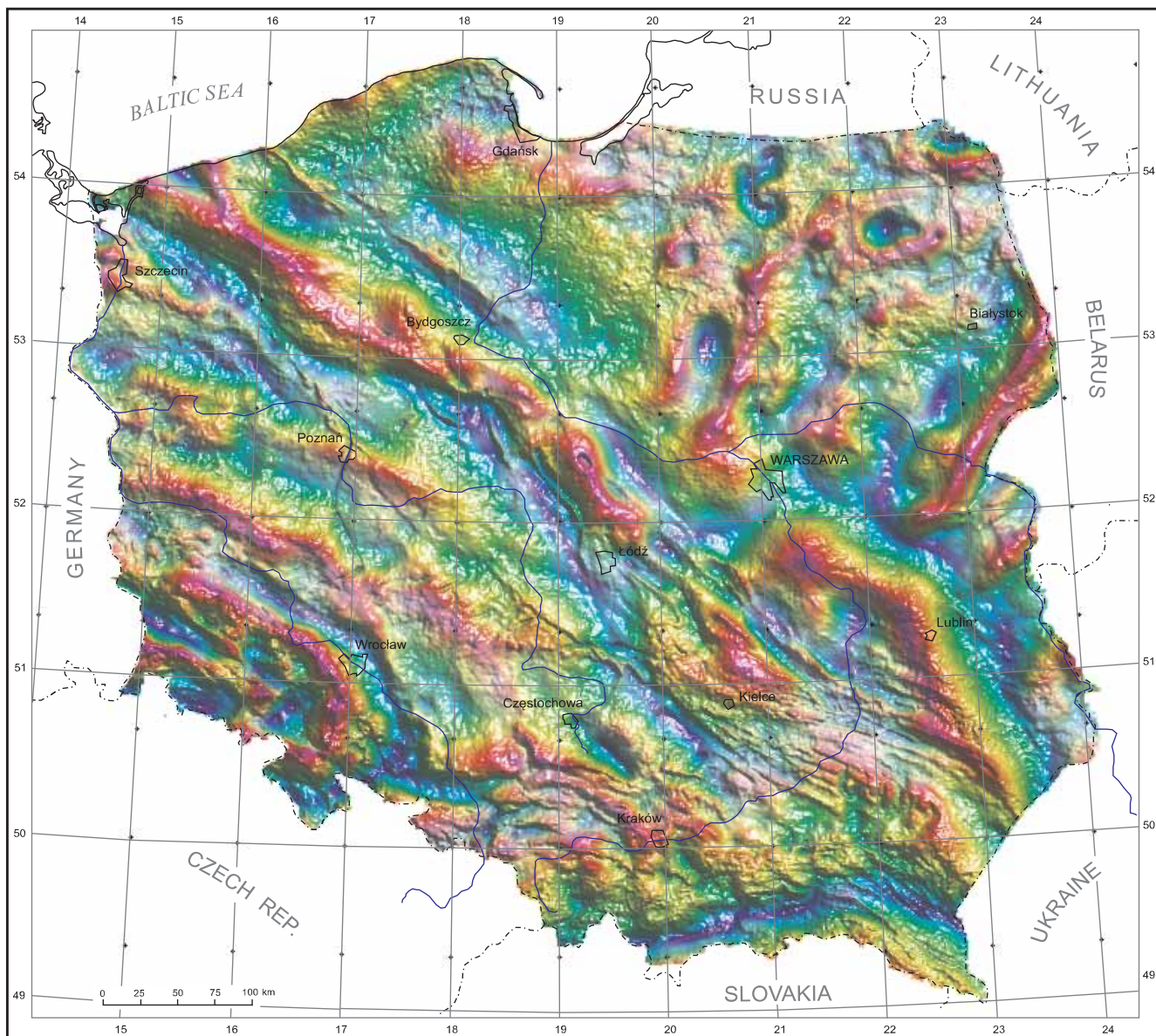


**Transformation:** local anomaly with basic wavelength range 2 to 60 km (as in Plate 3); **transformation technique:** as in Plate 3; **visualization:** superposition of scalar image with extended inverse full-hue colour scale, and shaded relief illuminated from the north-east; surface mirror reflectivity: index 10, coefficient 1.0

**Remarks:** On this image one can see effect of the new extended inverse full-hue colour scale. Its purpose is to enhance weak anomalies. Compare with [Plate 3](#).

## PLATE 5

**Vertical-horizontal vectorial image of local (basic wavelength range 2 to 60 km) Bouguer anomaly of Poland**

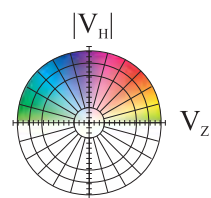
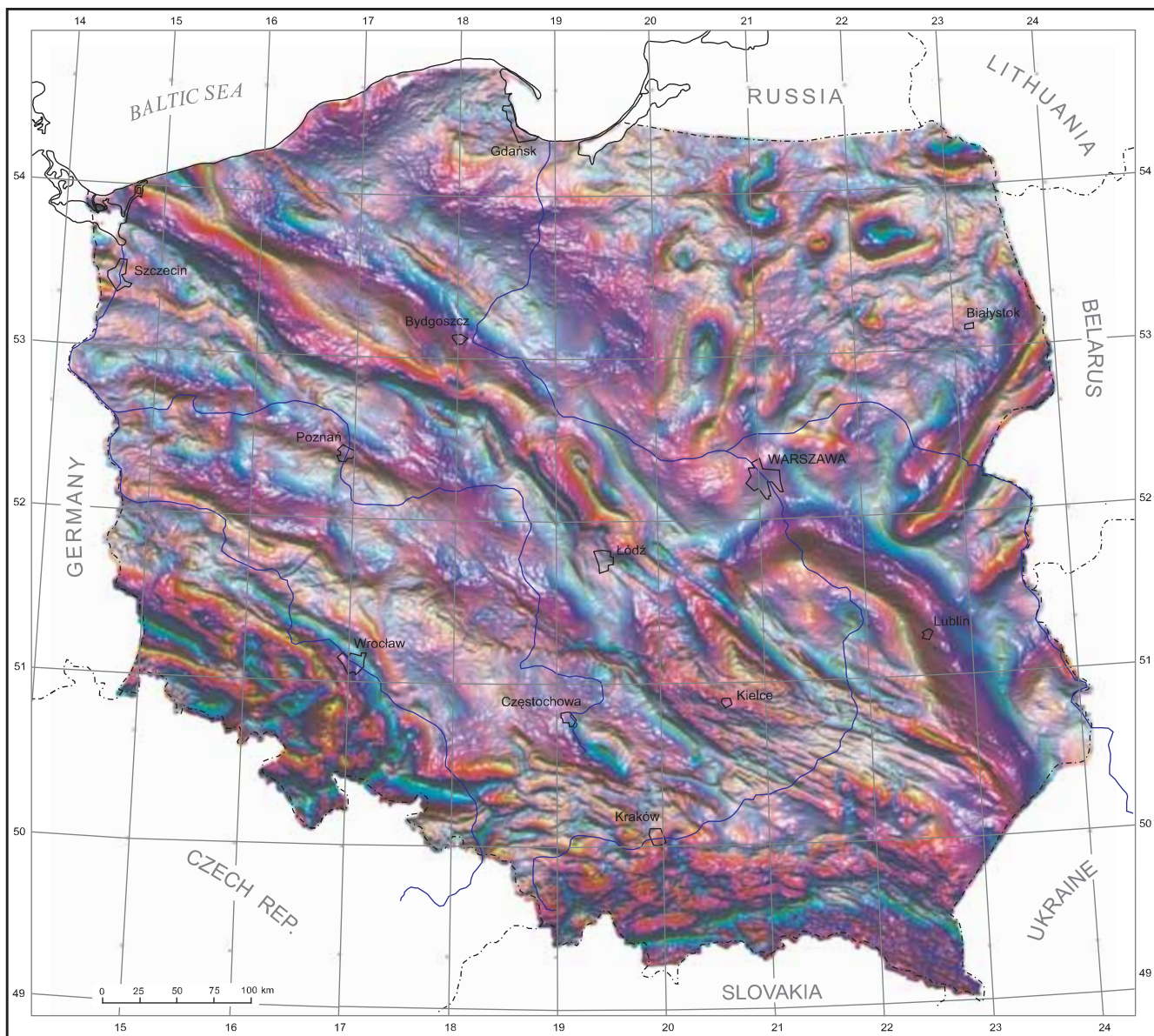


**Transformation:** local anomaly with basic wavelength range 2 to 60 km (as in Plate 3) and a module of its horizontal component; **transformation technique:** as in Plate 3 and additionally: horizontal components obtained by digital filtration using x- and y-Hilbert transformers (dimension 61x61); **visualization:** vertical-horizontal vectorial image with component/component-module colour scale (intensity 1.0) with superimposed shaded relief of local anomaly illuminated from the north-east; surface mirror reflectivity: index 10, coefficient 1.0

**Remarks:** It looks almost exactly as an image in Plate 3, but entirely different scale was used. It is a vectorial image with 2D colour scale. The main difference is that all positive (or negative) anomalies have the same hue. Intensity of anomaly influence colour saturation (e.g. anomaly from deeper body is pale).

**PLATE 6**

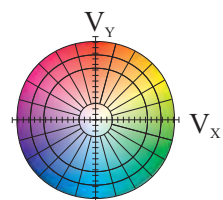
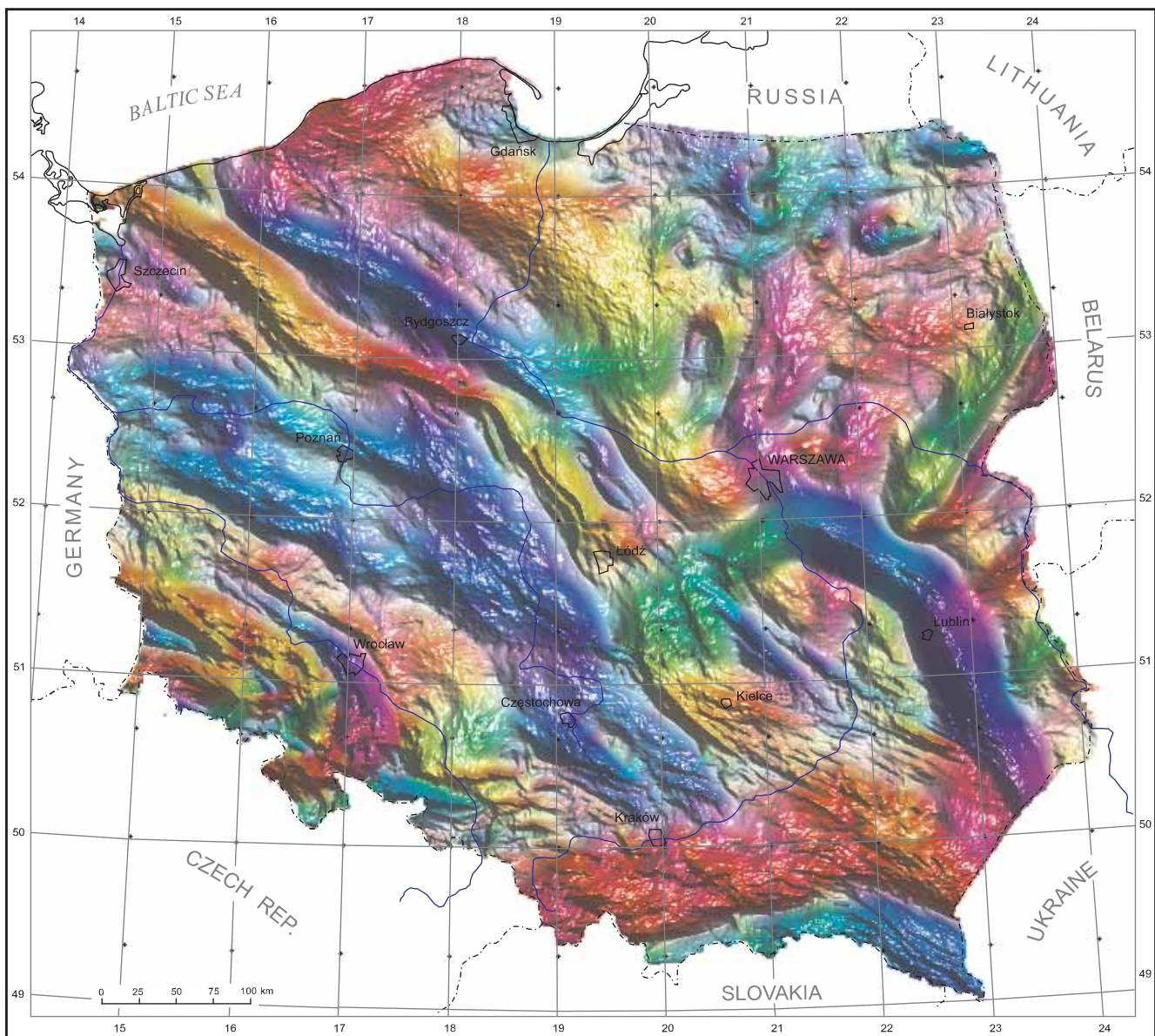
**Horizontal-vertical vectorial image of local Bouguer anomaly of Poland**



**Transformation:** local anomaly with basic wavelength range 2 to 60 km (as in [Plate 3](#)) and a module of its horizontal component (as in [Plate 5](#)); **transformation technique:** as in [Plates 3 and 5](#); **visualization:** horizontal-vertical vectorial image with component-module/component colour scale (intensity 1.0) with superimposed shaded relief of the module of horizontal component illuminated from the north; surface mirror reflectivity: index 10, coefficient 1.0

**Remarks:** This vectorial image is similar with that in [Plate 4](#) with inverse scale, because its 2-D scale is also inverse for enhancing weak anomalies. Please note, that in this image the shaded relief of the module of horizontal component is used which additionally strengthens the density contrasts boundaries.

### Horizontal vectorial image of local Bouguer anomaly of Poland

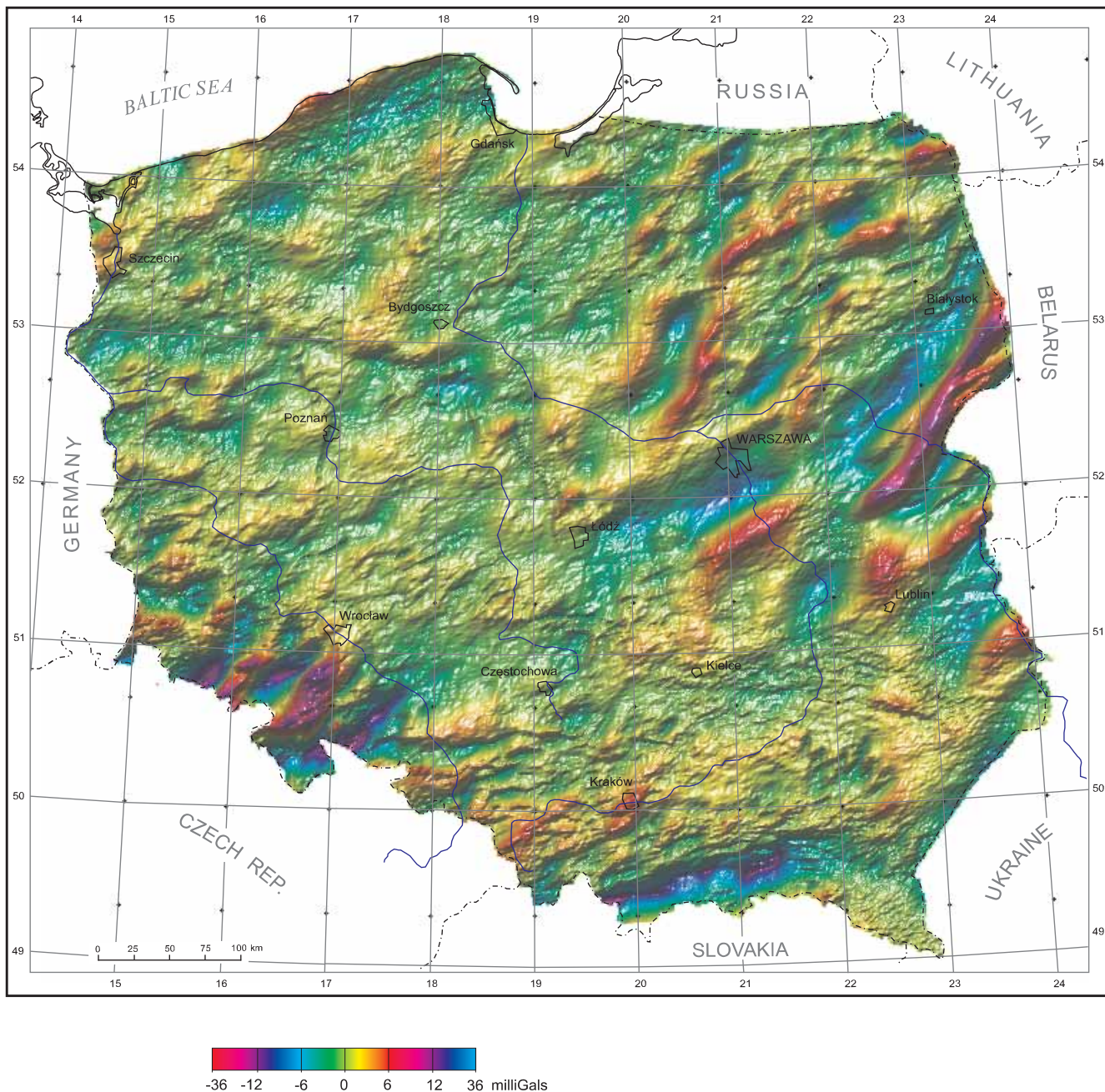


**Transformation:** horizontal components of local Bouguer anomaly with basic wavelength range 2 to 60 km; **transformation technique:** as in [Plate 5](#); **visualization:** horizontal vectorial image with two-component colour scale (intensity 1.0) with superimposed shaded relief of the module of horizontal component illuminated from the north; surface mirror reflectivity: index 10, coefficient 1.0

**Remarks:** This vectorial image is different as it based on horizontal components only, and hues are connected directly with an azimuth of full horizontal component of gravity vector.

PLATE 8

Image of directional ( $45^\circ$ ) scalar component of local Bouguer anomaly of Poland — extended full-hue colour scale

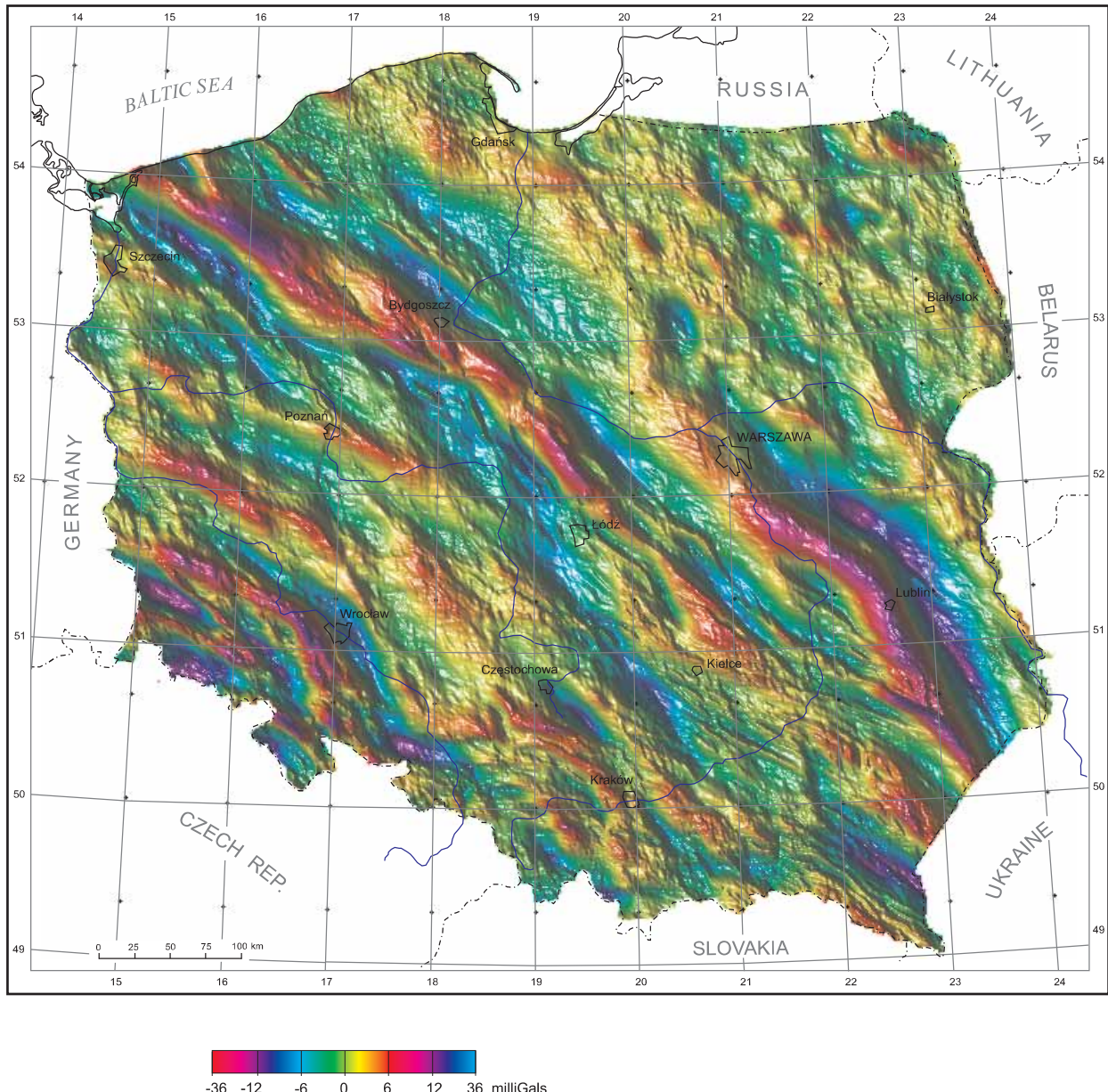


**Transformation:**  $45^\circ$ -directional scalar component with basic wavelength range 2 to 60 km; **transformation technique:** as in [Plate 3](#); **visualization:** superposition of scalar image with extended full-hue colour scale, and shaded relief illuminated from the north; surface mirror reflectivity: index 10, coefficient 1.0

**Remarks:** It is one of several new transformations proposed. It is directional component in  $45^\circ$  direction. It enhances features elongated in this and similar directions and attenuates others. Compare with the [next Plate](#).

**PLATE 9**

**Image of directional ( $135^\circ$ ) scalar component of local Bouguer anomaly of Poland — extended full-hue colour scale**

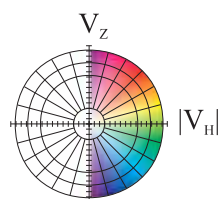
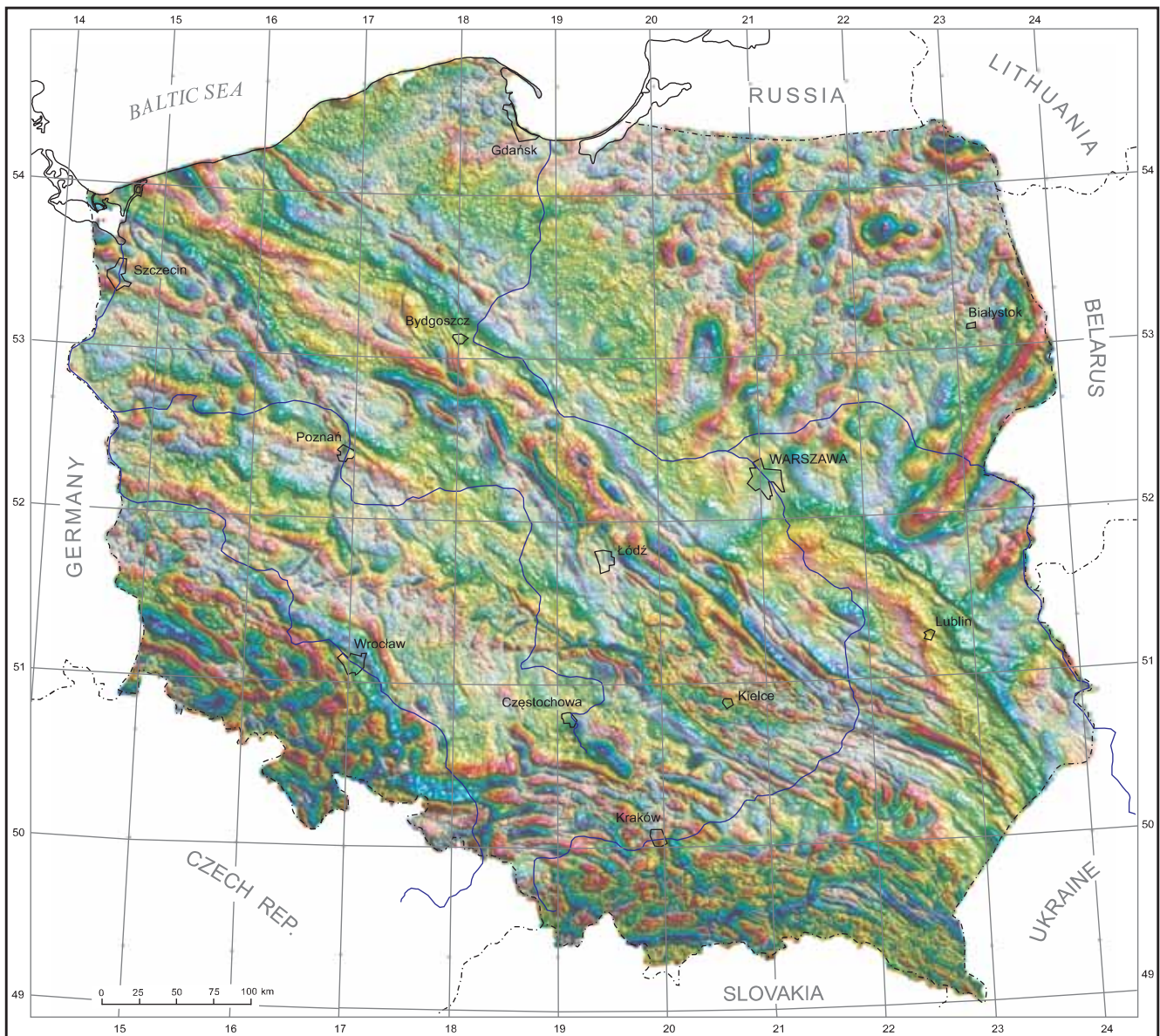


**Transformation:**  $135^\circ$ -directional component with basic wavelength range 2 to 60 km; **transformation technique:** as in [Plate 3](#); **visualization:** as in [Plate 8](#)

**Remarks:** The same kind of image as in [Plate 8](#), but the main direction is  $135^\circ$ . The sum of [Plates 8 and 9](#) gives [Plate 3](#).

PLATE 10

Vertical-horizontal vectorial image of local (basic wavelength range 1 to 30 km) Bouguer anomaly of Poland

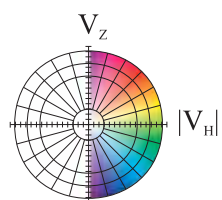
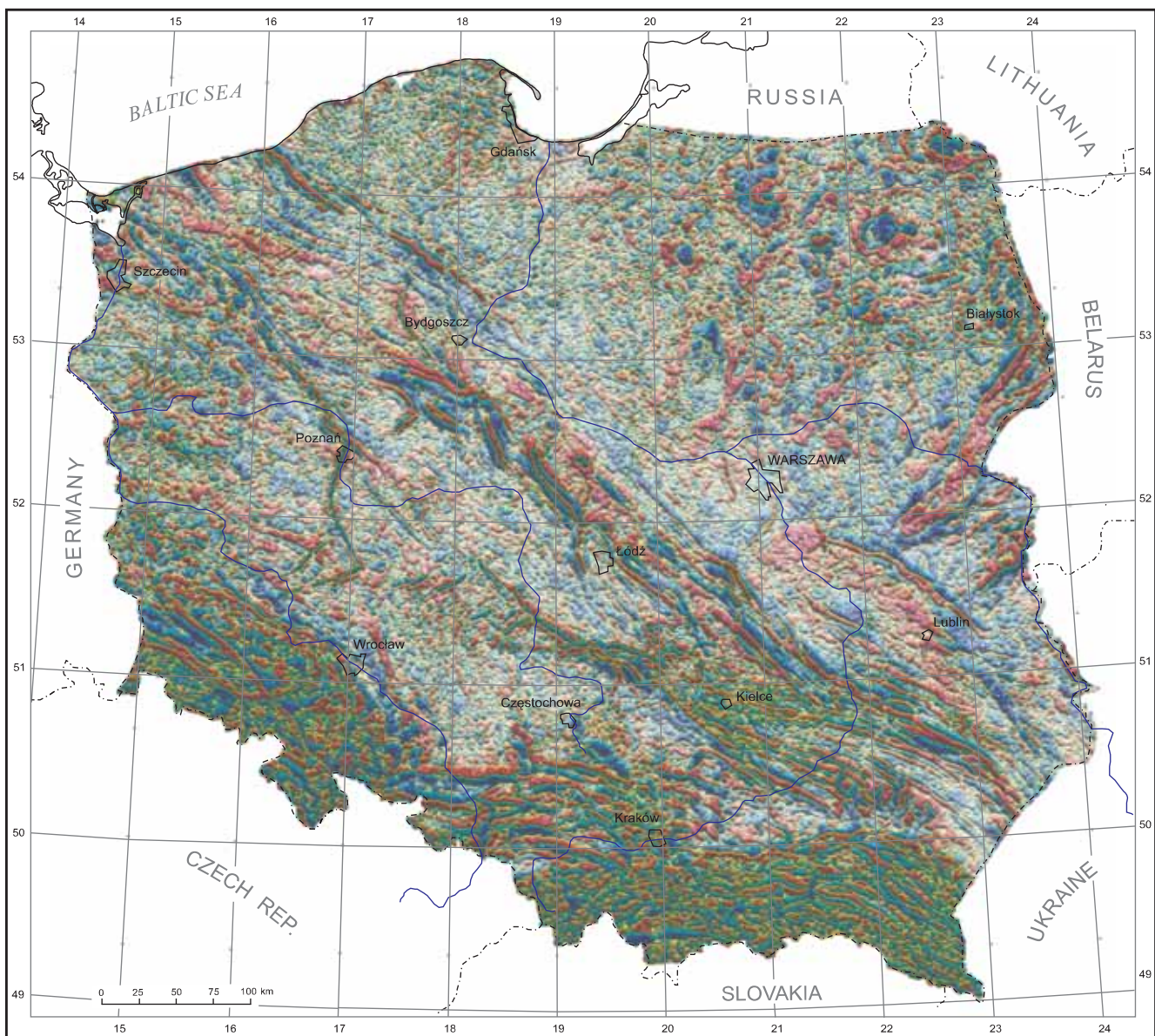


**Transformation:** local anomaly with basic wavelength range 1 to 30 km and a module of its horizontal component; **transformation technique:** as in Plate 3 and additionally: horizontal components obtained by digital filtration using x- and y-Hilbert transformers (dimension 61x61); **visualization:** vertical-horizontal vectorial image with component/component-module colour scale (intensity 1.0) with superimposed shaded relief of the module of the local anomaly illuminated from the north-east; surface mirror reflectivity: index 10, coefficient 1.0

**Remarks:** New elements on this image in comparison with Plate 5 are as follows. The base grid is here 500 x 500 m, so after using the same digital filters as in Plate 5, a basic wavelength range is 1 to 30 km, so its depth range is much smaller. Different kind of novelty is this, that quantity which shaded relief is shown here is not a local anomaly but its module. It seems, that in many instances this kind of imaging is better.

PLATE 11

Vertical-horizontal vectorial image of the first derivative Bouguer anomaly of Poland

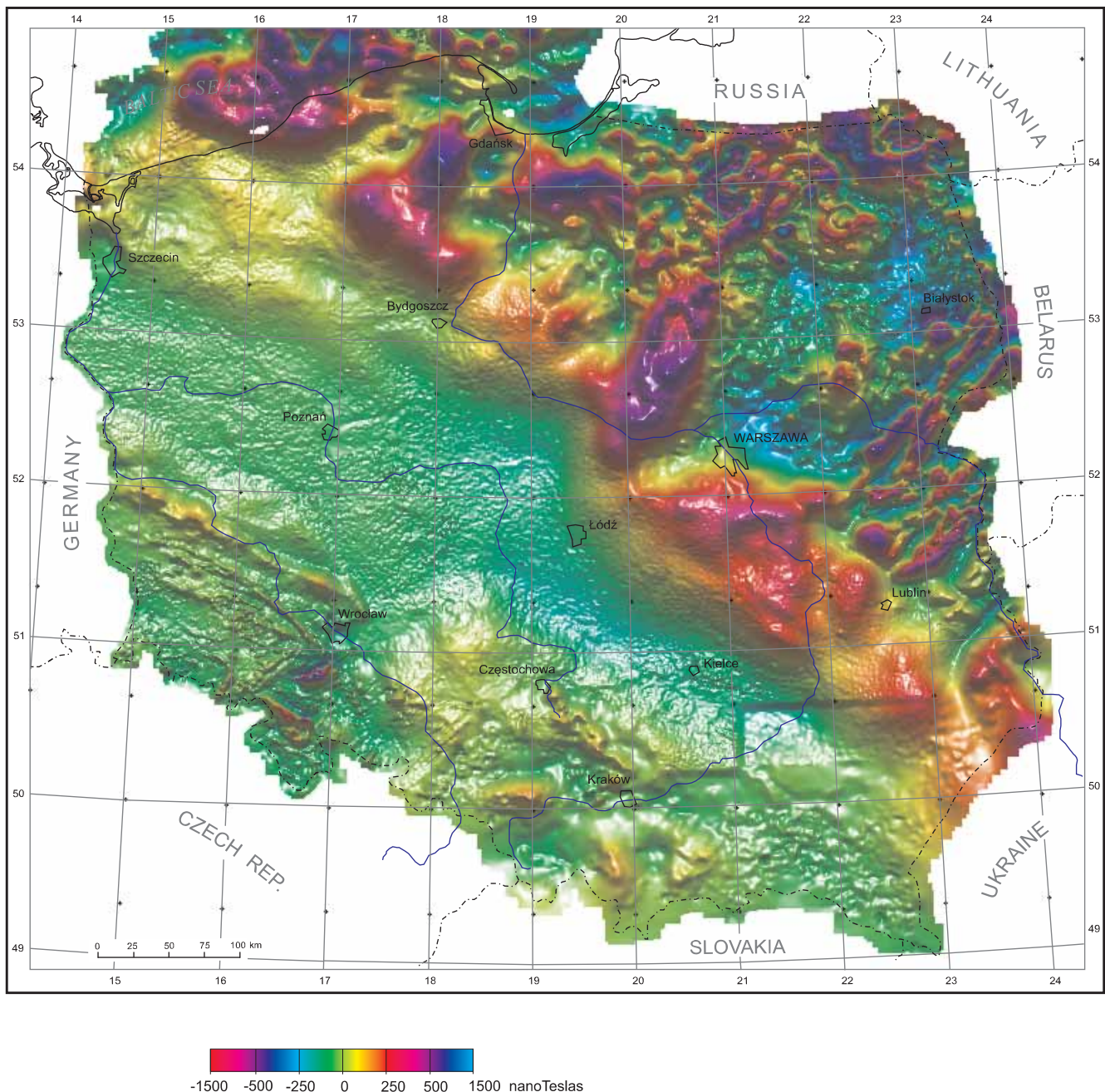


**Transformation:** vertical derivative and a module of horizontal derivative; **transformation technique:** derivatives by FFT, smoothing afterwards by averaging in a radius of 1.5 km; **visualization:** vertical-horizontal vectorial image with component/component-module colour scale (intensity 1.0) with superimposed shaded relief of the module of the vertical derivative illuminated from the north; surface mirror reflectivity: index 10, coefficient 1.0

**Remarks:** This image is similar to the previous one, but shows the shallowest elements, as first derivatives enhance the shortest wavelengths. The smoothing was used to weaken the noise.

## PLATE 12

### Image of the total magnetic field anomaly of Poland — extended full-hue colour scale

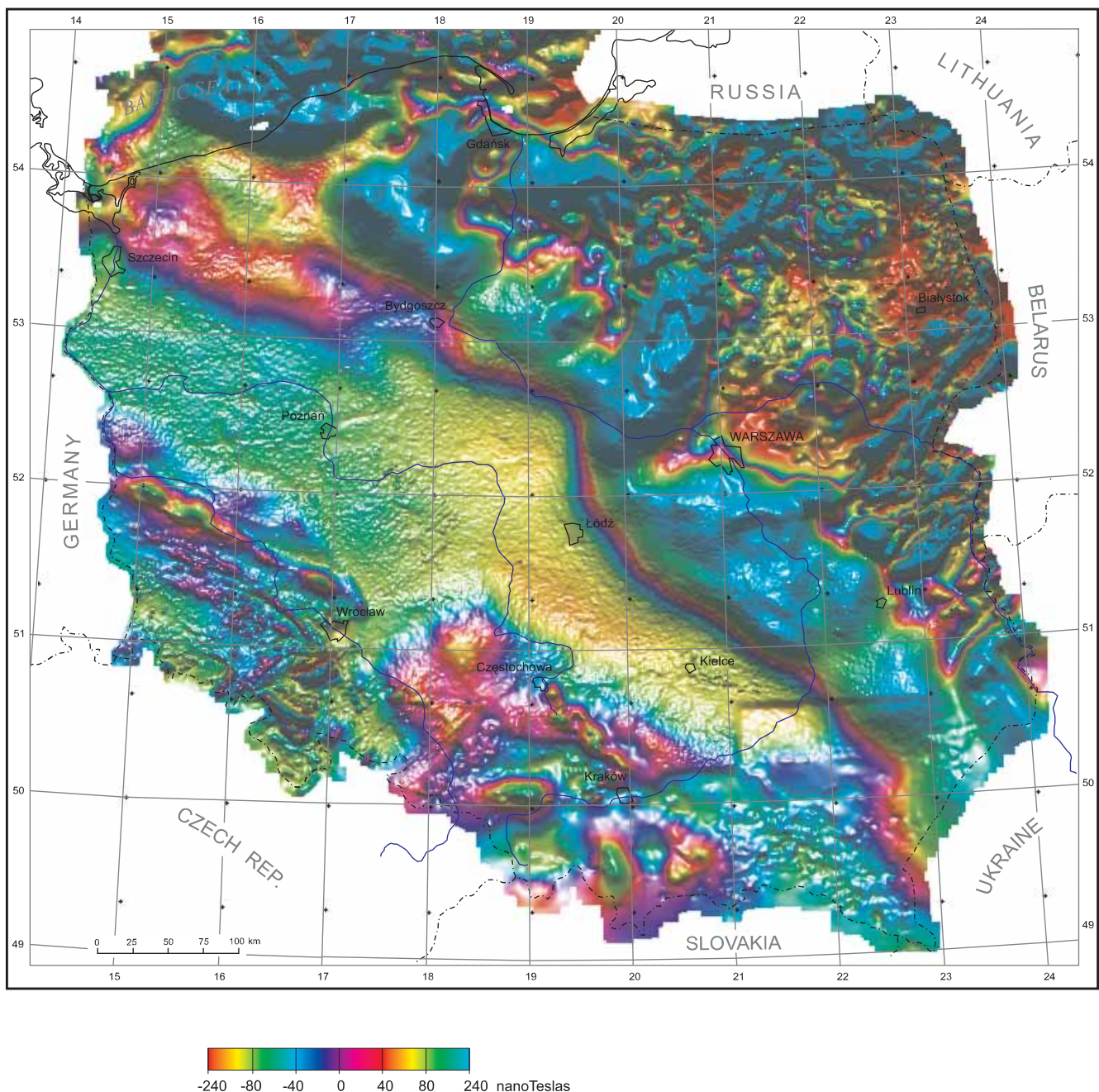


**Data source:** Polish magnetic database; aeromagnetic data from the Carpathians were not used because of their weak quality; **processing:** grid 1 x 1 km, gridding using minimum curvature algorithm — USGS's MINC-program; **transformation:** Z-component data from NE Poland and the Carpathians transformed to the total field; the step seen north of the Carpathians is caused by new data not available in the moment of transformation; **wavelength range:** minimal — 2 km; **visualization:** superposition of scalar image with extended full-hue colour scale, and shaded relief illuminated from the north-east; surface mirror reflectivity: index 10, coefficient 1.0

**Remarks:** This image of the total magnetic field of Poland shows the difficulty with imaging magnetic field. North-eastern part of Poland belongs to the Precambrian domain with strongly magnetized rocks giving strong anomalies. The rest of the country is non-magnetic or weakly magnetic, with small exceptions. It is quite impossible to show on the same image diversity in strong anomalies and weak anomalies, even using extended colour scales. The solution is using two scales (and two images) for this purpose. For comparison look on the next Plate with inverse colour scale.

PLATE 13

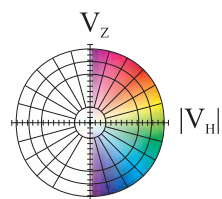
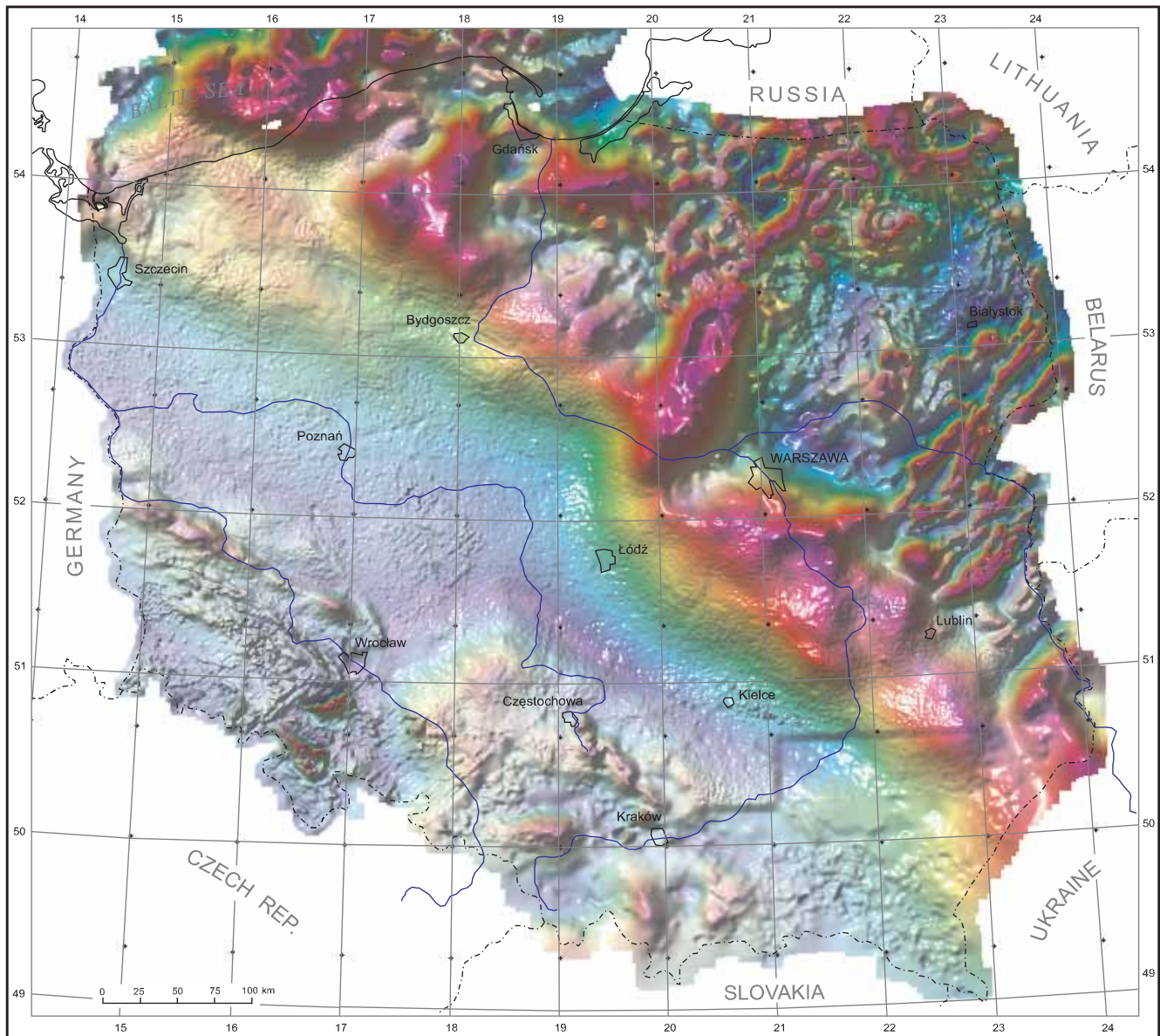
Image of the total magnetic field of Poland — extended inverse full-hue colour scale



**Transformation:** as in Plate 11; **visualization:** superposition of scalar image with extended inverse full-hue colour scale, and shaded relief illuminated from the north; surface mirror reflectivity: index 10, coefficient 1.0

**Remarks:** The resolution of weak anomalies is quite good by using extended inverse full-hue colour scale, but understanding of the area with strong anomalies is much worse.

## Vertical-horizontal vectorial image of total magnetic field anomaly of Poland

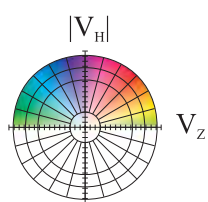
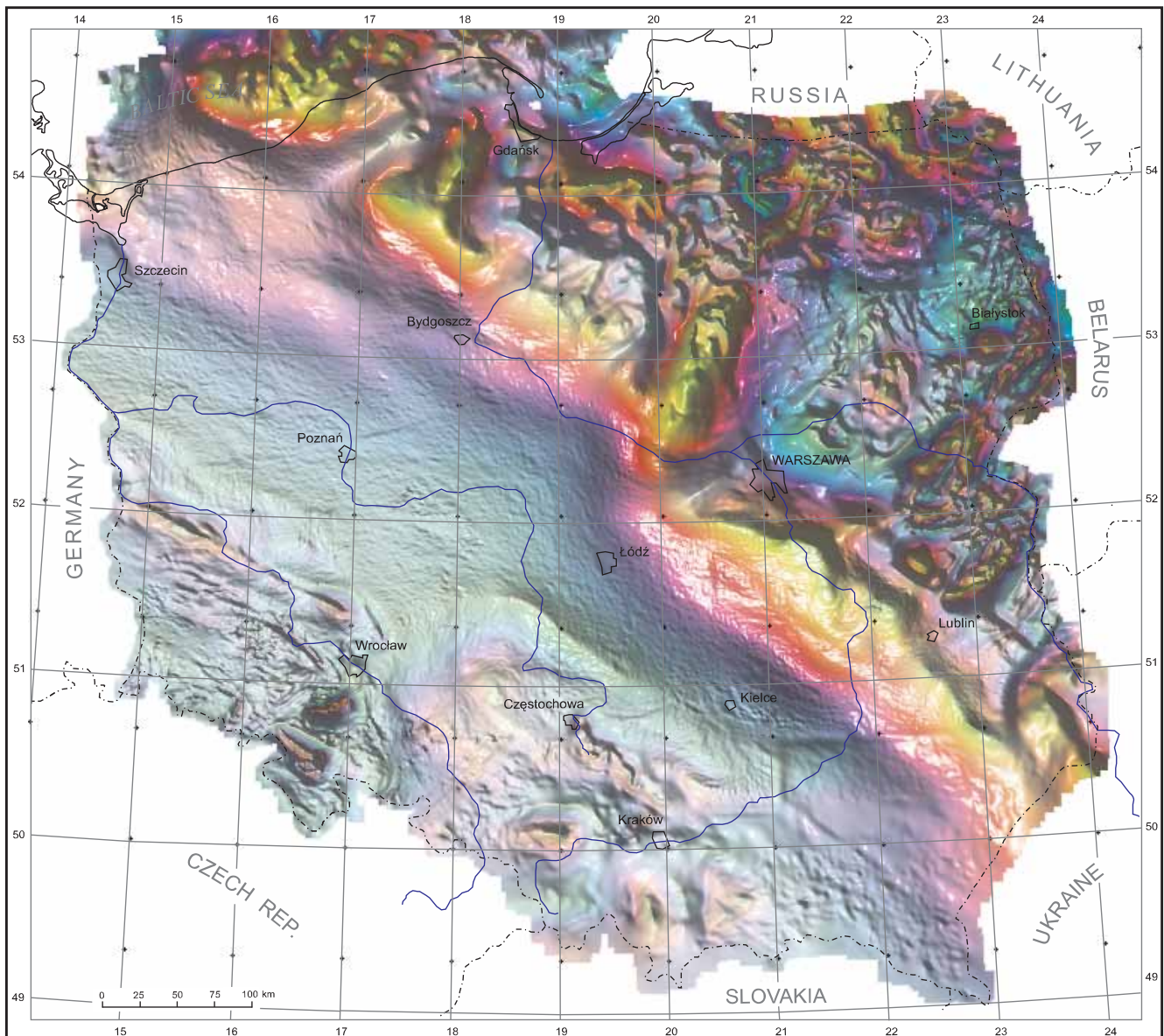


**Transformation:** module of horizontal component; **transformation technique:** Hilbert transform by FFT; **visualization:** vertical-horizontal vectorial image with component/component-module colour scale (intensity 1.0) with superimposed shaded relief of total field anomaly illuminated from the north; surface mirror reflectivity: index 10, coefficient 1.0

**Remarks:** This vectorial image is more informative when compared with scalar one on [Plate 12](#), especially in south-west of the country.

PLATE 15

Horizontal-vertical vectorial image of total magnetic field anomaly of Poland

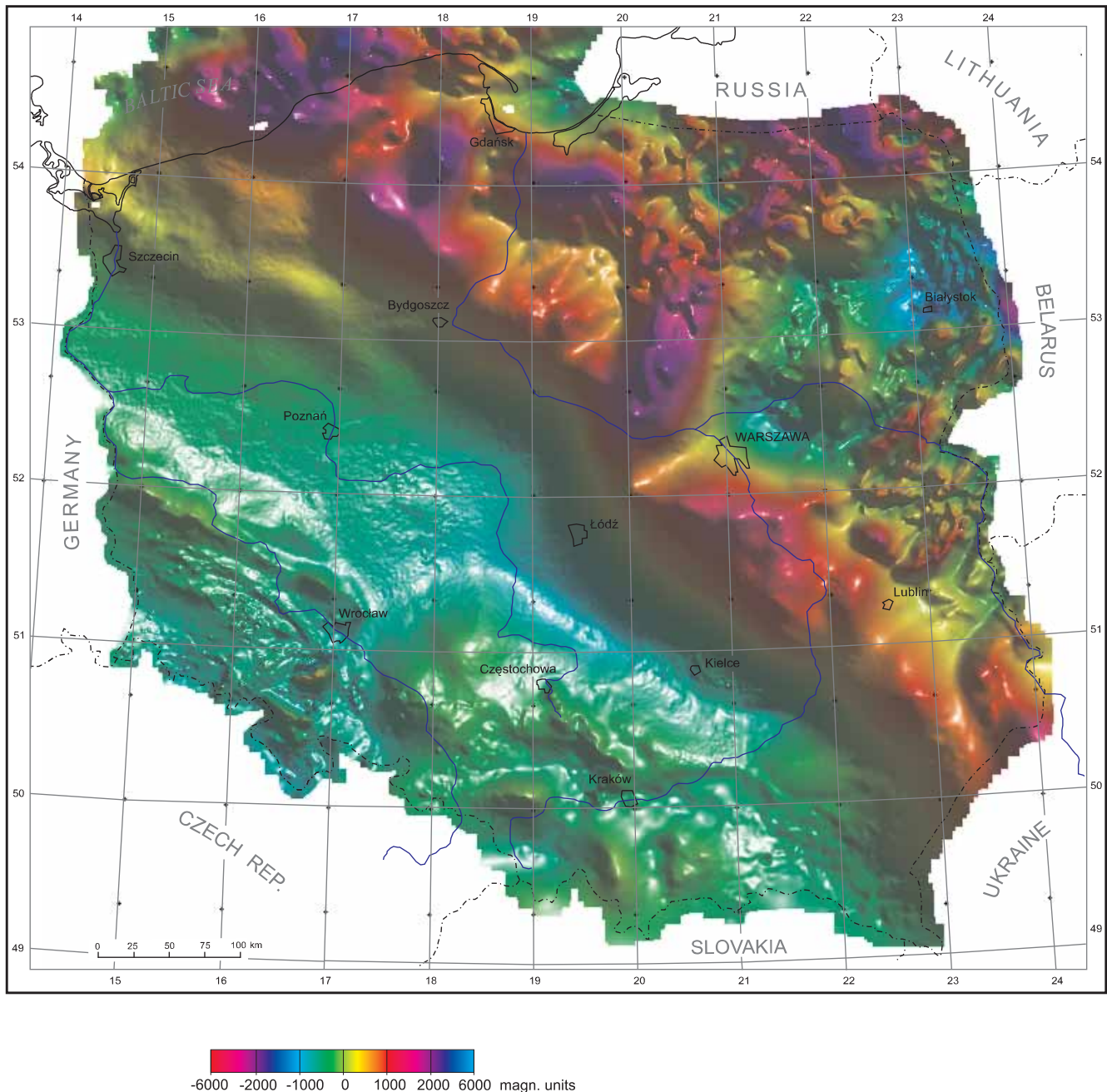


**Transformation:** as in Plate 14; **transformation technique:** Hilbert transform by FFT; **visualization:** horizontal-vertical vectorial image with component-module/component colour scale (intensity 1.0) with superimposed shaded relief of the module of horizontal component illuminated from the north; surface mirror reflectivity: index 10, coefficient 1.0

**Remarks:** This image shows clearly the magnetic boundaries in Poland. The most prominent is Teisseyre-Tornquist Line, which delimits the Sveco-fennian Platform of the East European Platform from the west.

PLATE 16

Image of the half vertical integral of the total magnetic field anomaly of Poland — extended full-hue colour scale

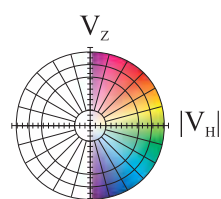
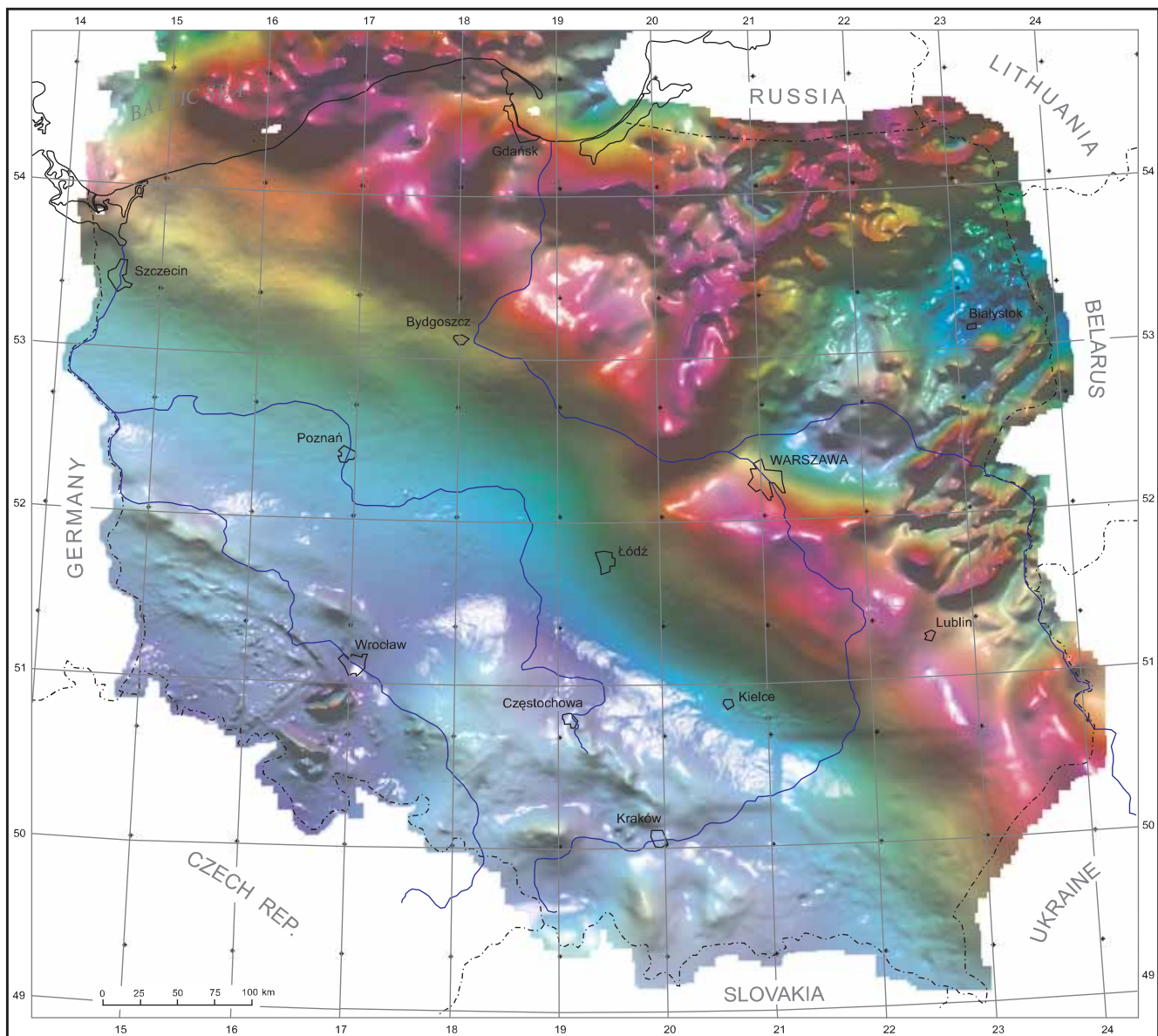


**Transformation:** 1/2 fractional vertical integral; **transformation technique:** FFT; **visualization:** superposition of scalar image with extended full-hue colour scale, and shaded relief illuminated from the north-east; surface mirror reflectivity: index 10, coefficient 1.0

**Remarks:** This is an image showing new transformation: fractional vertical integral (in this case — 1/2). It enhances low frequencies anomalies, which is suitable especially in magnetics.

PLATE 17

Vertical-horizontal vectorial image of the half vertical integral of the total magnetic field anomaly of Poland

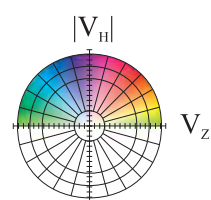
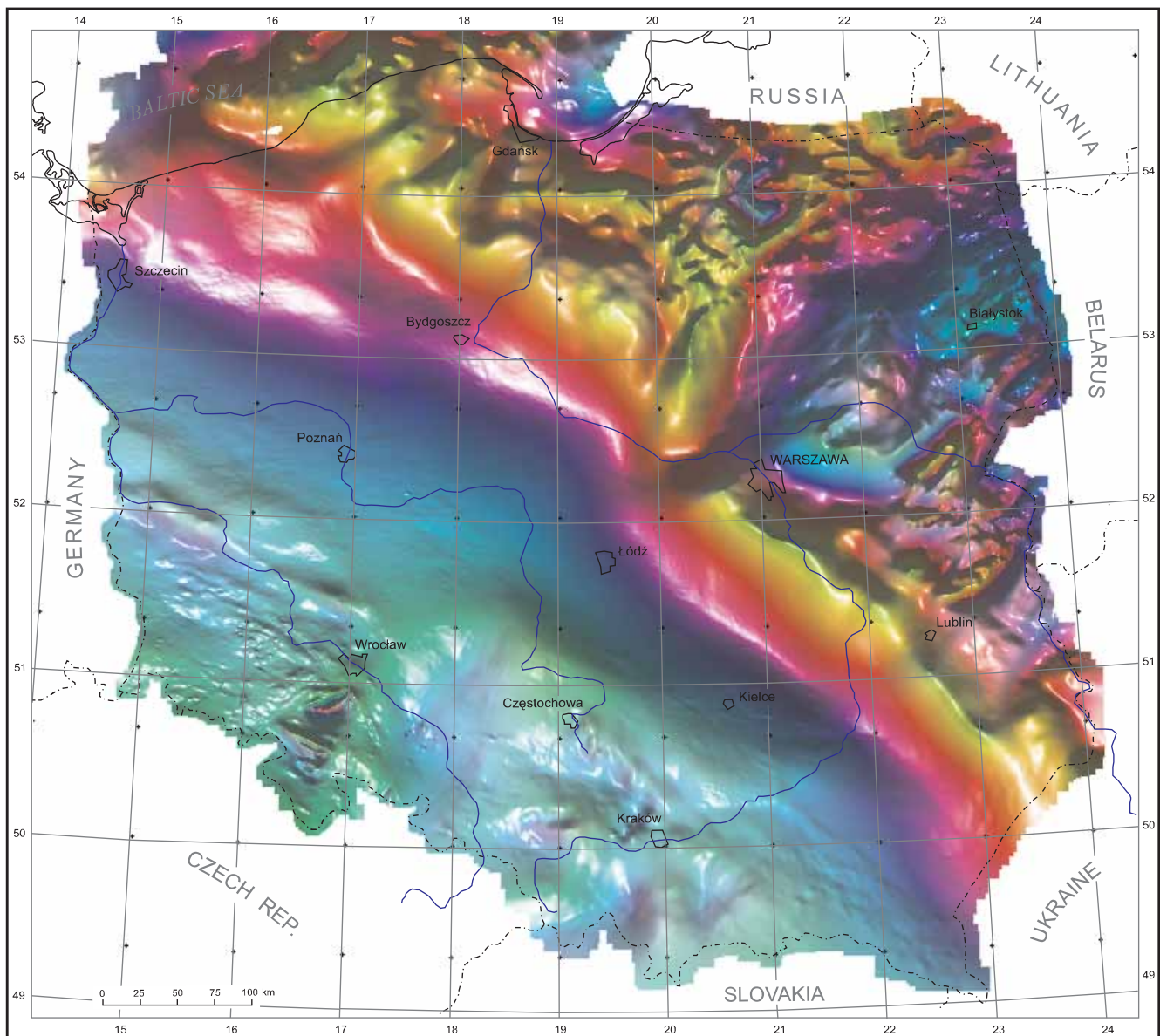


**Transformation:** 1/2 fractional vertical integral and module of its horizontal component; **transformation technique:** FFT; **visualization:** vertical-horizontal vectorial image with component/component-module colour scale (intensity 1.0) with superimposed shaded relief of total field anomaly illuminated from the north; **surface mirror reflectivity:** index 10, coefficient 1.0

**Remarks:** This vectorial image enhances anomalies connected with Teisseyre-Tornquist Line and suggests, that anomalies in S and SW Poland have local significance and are surrounded by non-magnetic rocks of regional extension.

PLATE 18

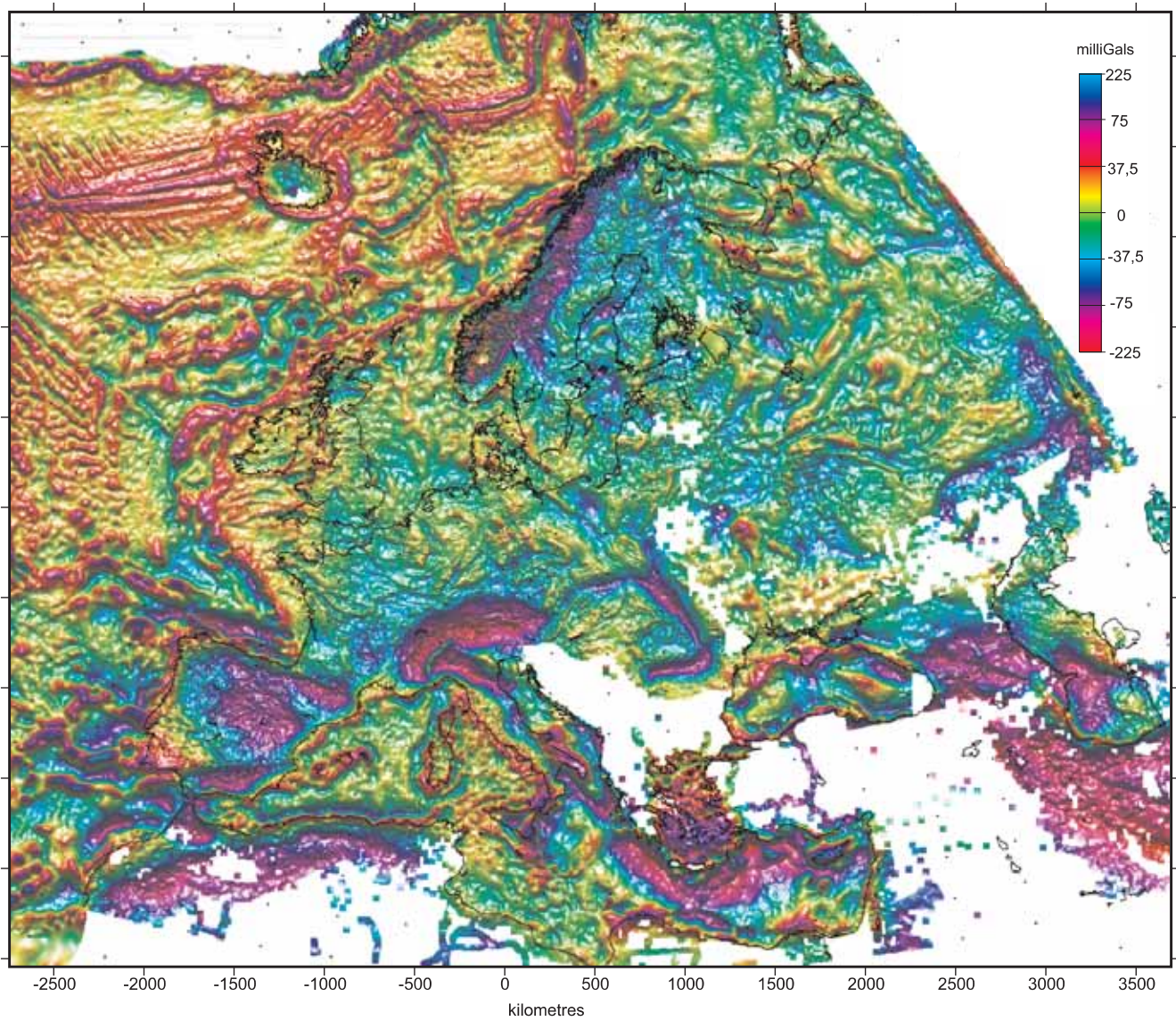
Horizontal-vertical vectorial image of the half vertical integral of the total magnetic field anomaly of Poland



**Transformation:** 1/2 fractional vertical integral and module of its horizontal component; **transformation technique:** FFT; **visualization:** horizontal-vertical vectorial image with component-module/component colour scale (intensity 1.0) with superimposed shaded relief of the module of horizontal component illuminated from the north; **surface mirror reflectivity:** index 10, coefficient 1.0

**Remarks:** On this image, which enhances magnetic boundaries, we can see the main magnetic boundary in Poland, which in the northern part splits in two parts: the northerly one, which match the known TT Line, and westerly part going to Szczecin. It seems, that these two lines delimit Precambrian domains of different origin and age.

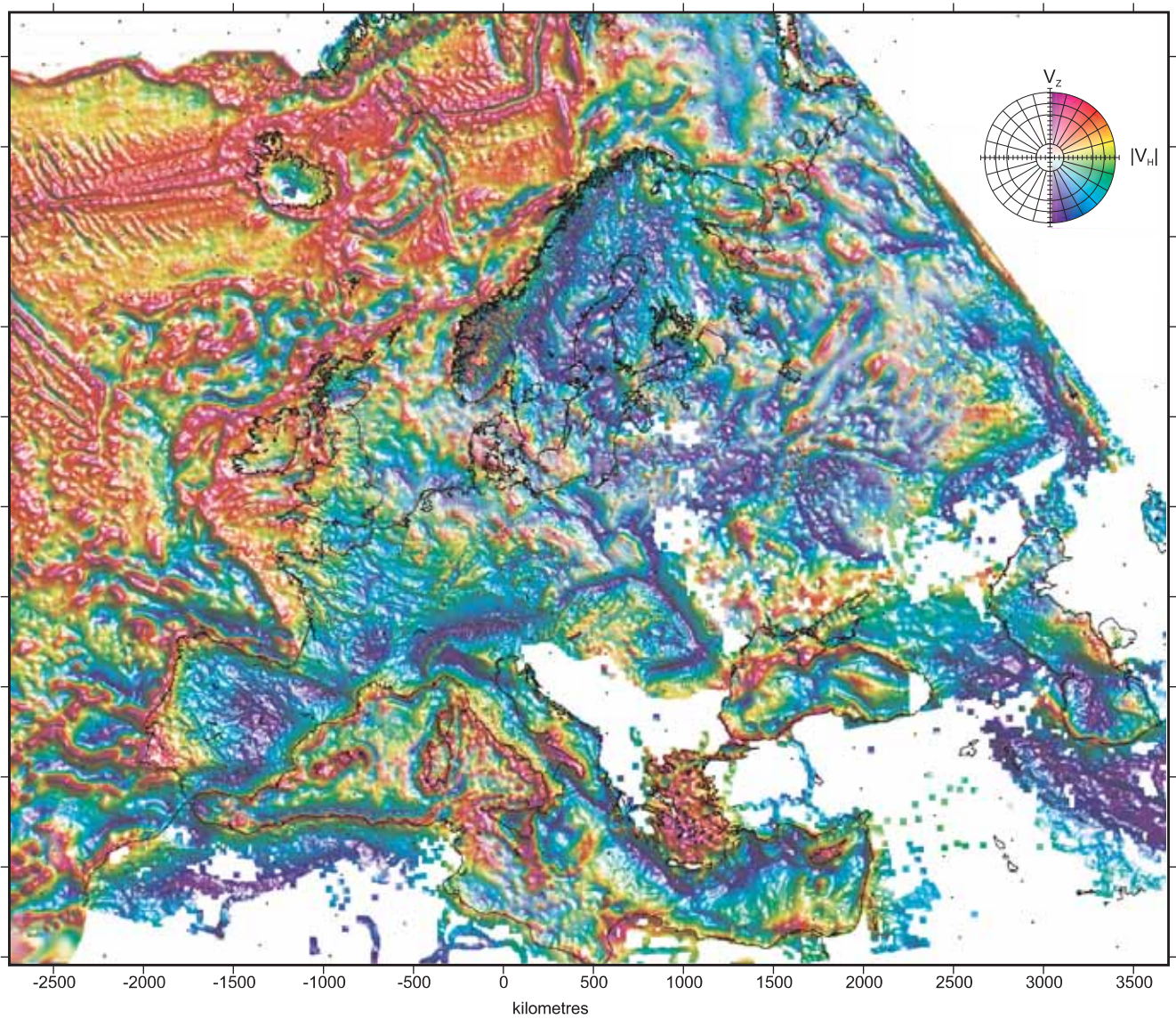
## Image of gravity anomalies of Europe — extended full-hue colour scale



**Data source:** compilation from different sources (see Wybraniec *et al.*, 1998); **land data** — Bouguer anomaly, **sea data** — satellite free-air anomaly; **processing:** grid 5 by 5 km obtained using MINC program; **visualization:** superposition of scalar image with extended full-hue colour scale, and shaded relief illuminated from the north-east; surface mirror reflectivity: index 10, coefficient 1.0

**Remarks:** This image of gravity of Europe (alas, with many blank areas, as yet) shows, that apart from the Alpine folding region and the Atlantic Ocean, the rest areas have similar gravity signature, which makes the interpretation rather difficult. We must look for other types of images for this purpose.

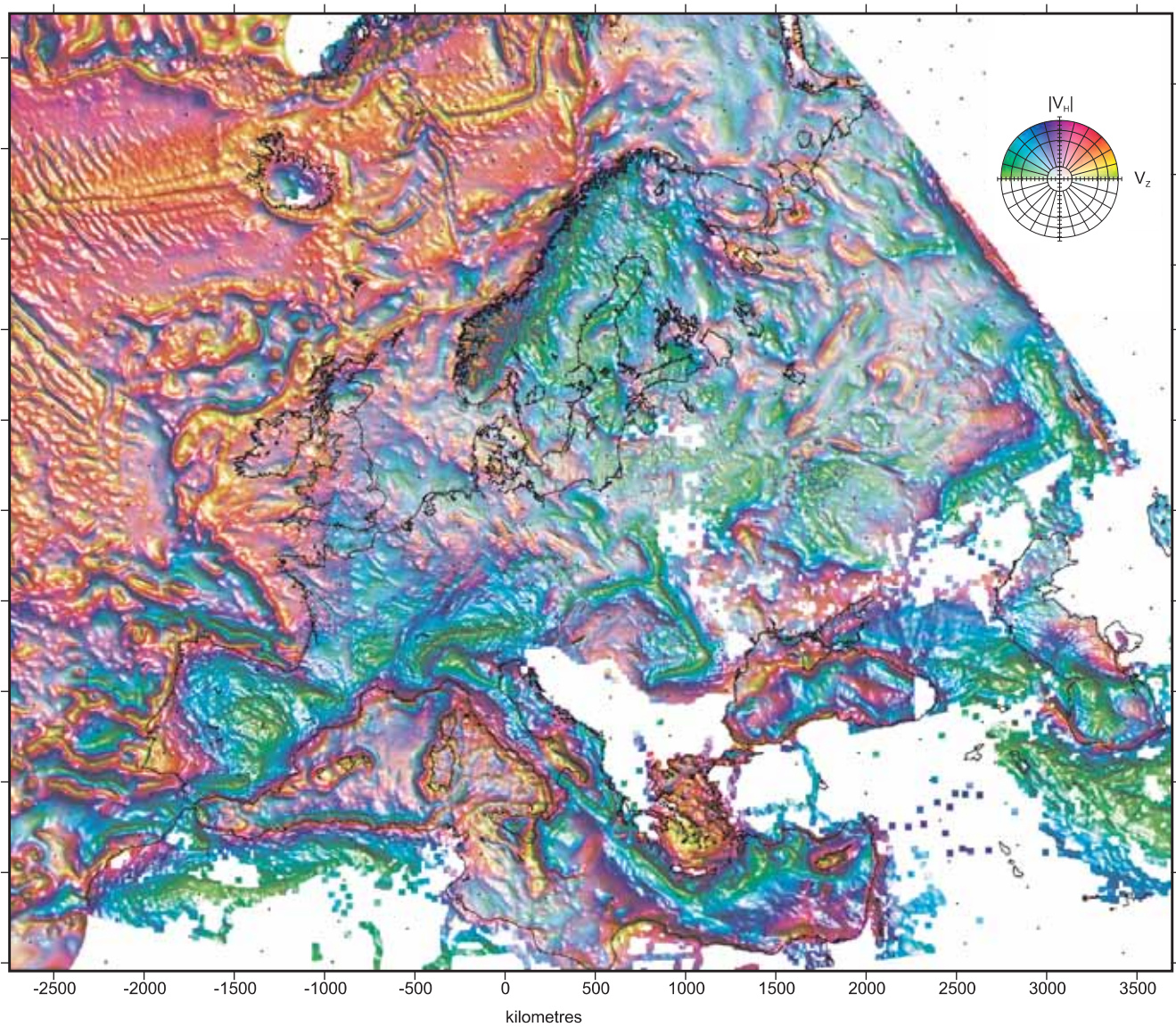
## Vertical-horizontal vectorial image of gravity anomalies of Europe



**Transformation:** module of horizontal derivative; **transformation technique:** Hilbert transform by FFT; **visualization:** vertical-horizontal vectorial image with component/component-module colour scale (intensity 1.0) with superimposed shaded relief of total field anomaly illuminated from the north; surface mirror reflectivity: index 10, coefficient 1.0

**Remarks:** This vectorial image is more informative than the previous one. There is a visible difference between East European Platform and the Palaeozoic Europe. Enigmatic position is that of Denmark and surrounding areas. It is a block with higher gravity values. It is more clearly seen on the next vectorial image.

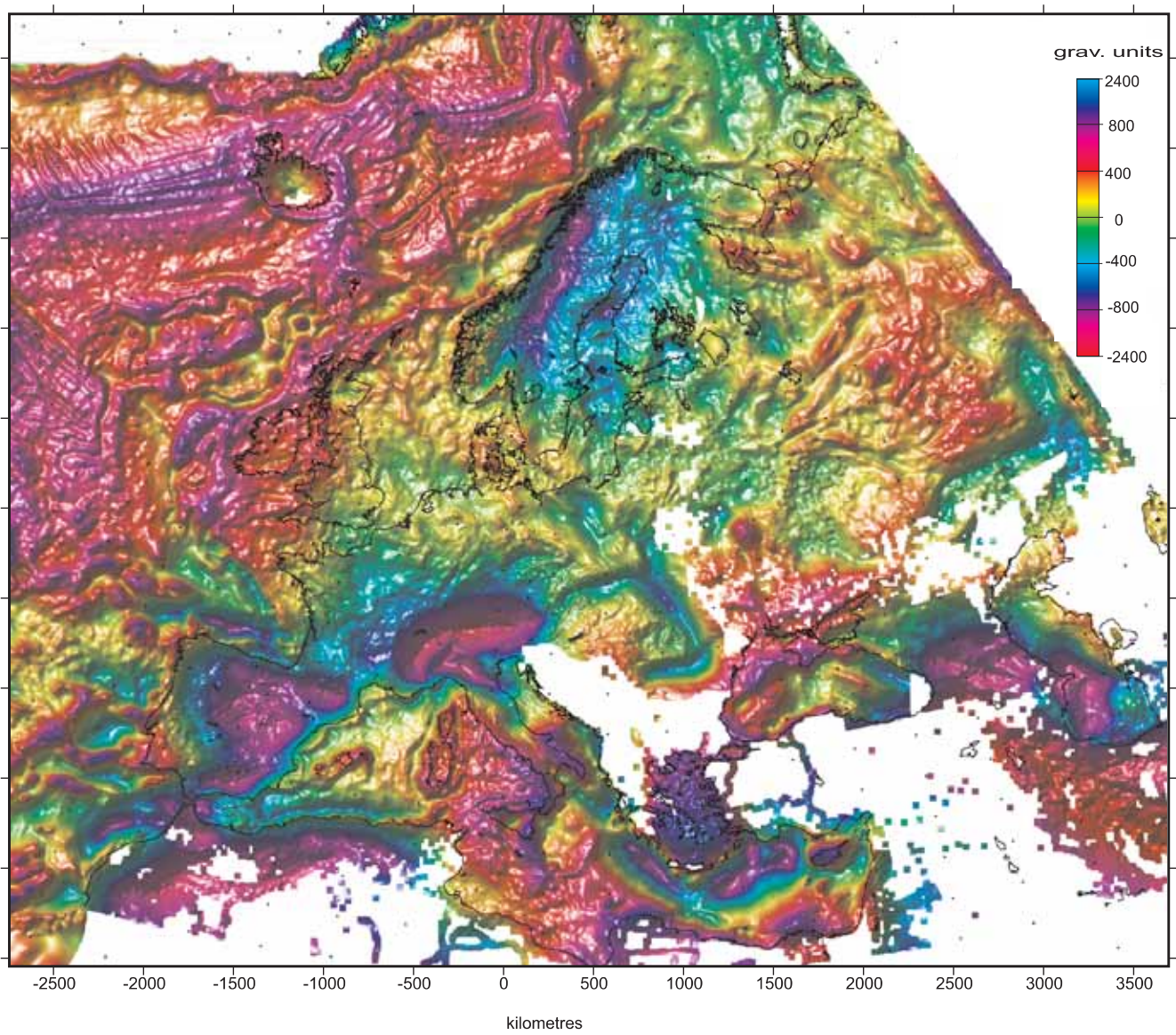
## Horizontal-vertical vectorial image of gravity anomalies of Europe



**Transformation:** module of horizontal derivative; **transformation technique:** Hilbert transform by FFT; **visualization:** horizontal-vertical vectorial image with component-module/component colour scale (intensity 1.0) with superimposed shaded relief of the module of horizontal component illuminated from the north; **surface mirror reflectivity:** index 10, coefficient 1.0

**Remarks:** This horizontal-vertical vectorial image enhances smaller anomalies which are not well seen on other images. The Denmark block is very distinctive. Also Ukrainian Shield and Irish Block (seen also on the previous image). The latter has the gravity signature rather oceanic than continental.

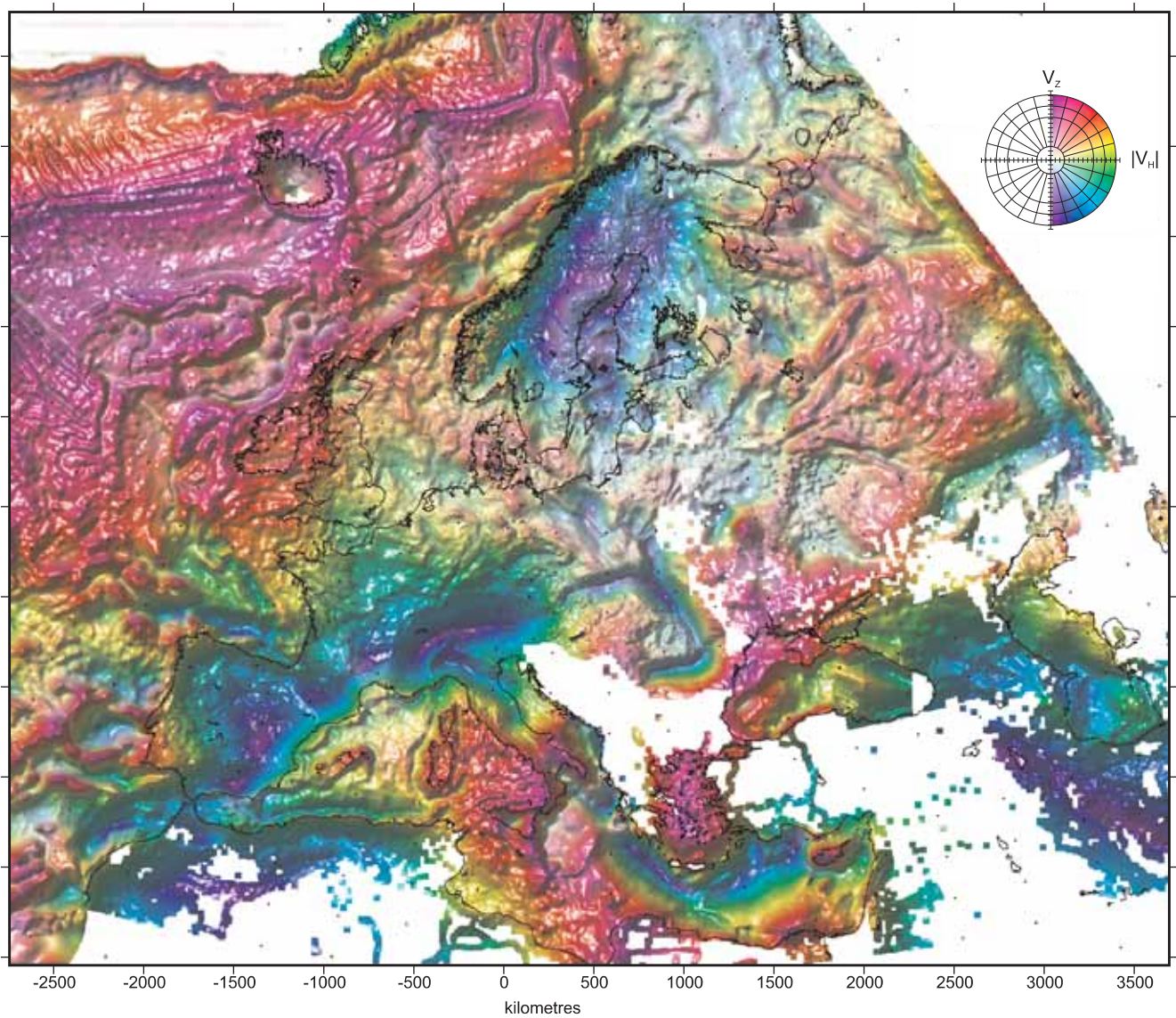
Image of the half vertical integral of gravity anomalies of Europe — extended full-hue colour scale



**Transformation:** 1/2 fractional vertical integral; **transformation technique:** FFT; **visualization:** superposition of scalar image with extended full-hue colour scale, and shaded relief illuminated from the north-east; surface mirror reflectivity: index 10, coefficient 1.0

Remarks: This image shows full possibilities of new transformation: fractional vertical integral. When we compare this image with that in Plate 19 we see advantages of using this transformation in similar cases. Very interesting partition to different regions can be seen especially in the East European Platform. All blocks mentioned earlier are clearly exposed.

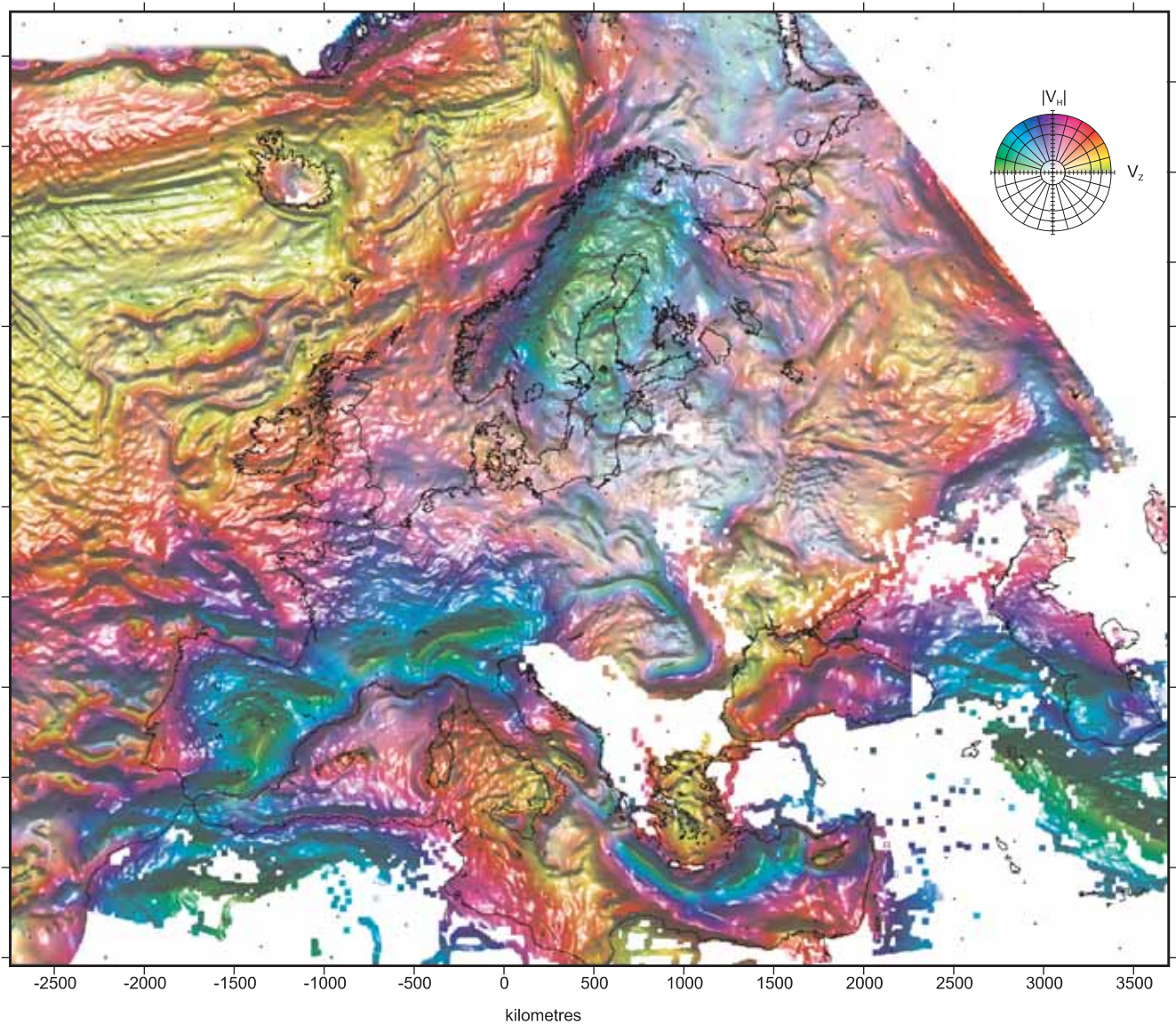
## Vertical-horizontal vectorial image of the half vertical integral of gravity anomalies of Europe



**Transformation:** 1/2 fractional vertical integral and a module of its horizontal component; **transformation technique:** FFT; **visualization:** vertical-horizontal vectorial image with component/component-module colour scale (intensity 1.0) with superimposed shaded relief of total field anomaly illuminated from the north; **surface mirror reflectivity:** index 10, coefficient 1.0

**Remarks:** This image is similar to the previous one, but the Baltic Shield is better exposed. It is worthwhile to mention situation in south-eastern Europe. The Ukrainian Shield with so called Scythian Plate and Moesian Plate (and possibly Pannonian basin) one gravity unit, together with Aegean Sea gravity high. But there are too many white spots to understand it clearly.

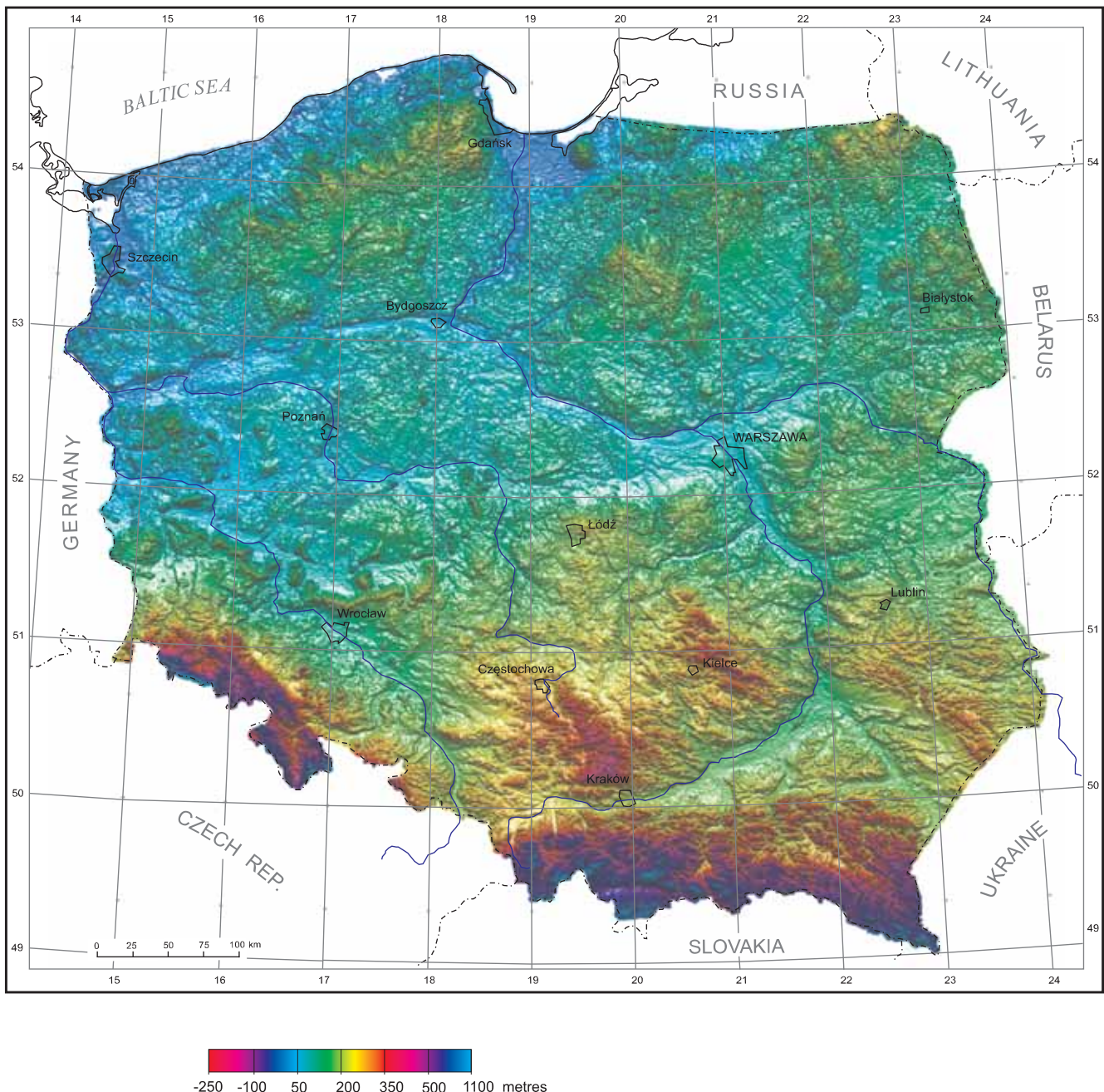
## Horizontal-vertical vectorial image of the half vertical integral of gravity anomalies of Europe



**Transformation:** 1/2 fractional vertical integral and a module of its horizontal component; **transformation technique:** FFT; **visualization:** horizontal-vertical vectorial image with component-module/component colour scale (intensity 1.0) with superimposed shaded relief of the module of horizontal component illuminated from the north; **surface mirror reflectivity:** index 10, coefficient 1.0

**Remarks:** This image sharpens boundaries seen on the previous images. The division on regional superunits can be seen.

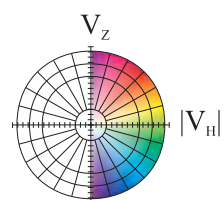
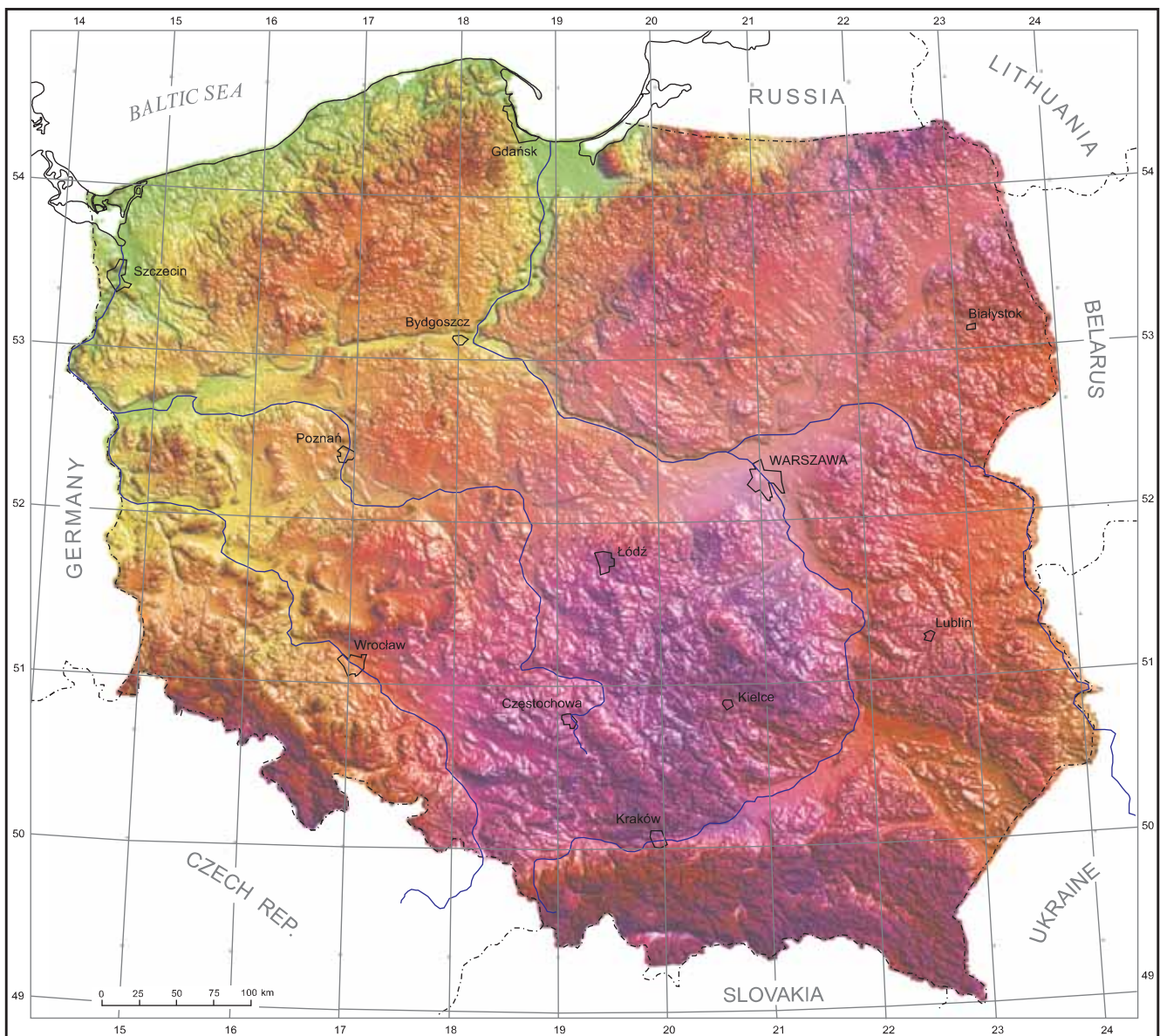
## Image of hypsography of Poland — extended full-hue colour scale



**Data source:** Polish gravity database; **processing:** grid 500 x 500 m obtained by MINC program from USGS software package; **transformation:** none; **visualization:** superposition of scalar image with extended full-hue colour scale, and shaded relief illuminated from the north; surface mirror reflectivity: index 10, coefficient 1.0

**Remarks:** This image is just plain shaded relief of Poland: mountains and plateaus are in the south. The rest of the country is a lowland. These data were treated as a vertical gradient of a certain potential field, and using Hilbert transform, a horizontal components of this field were calculated and then the module. See the next Plates for resulting vectorial images.

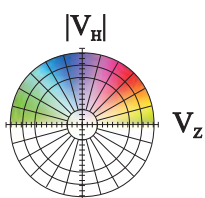
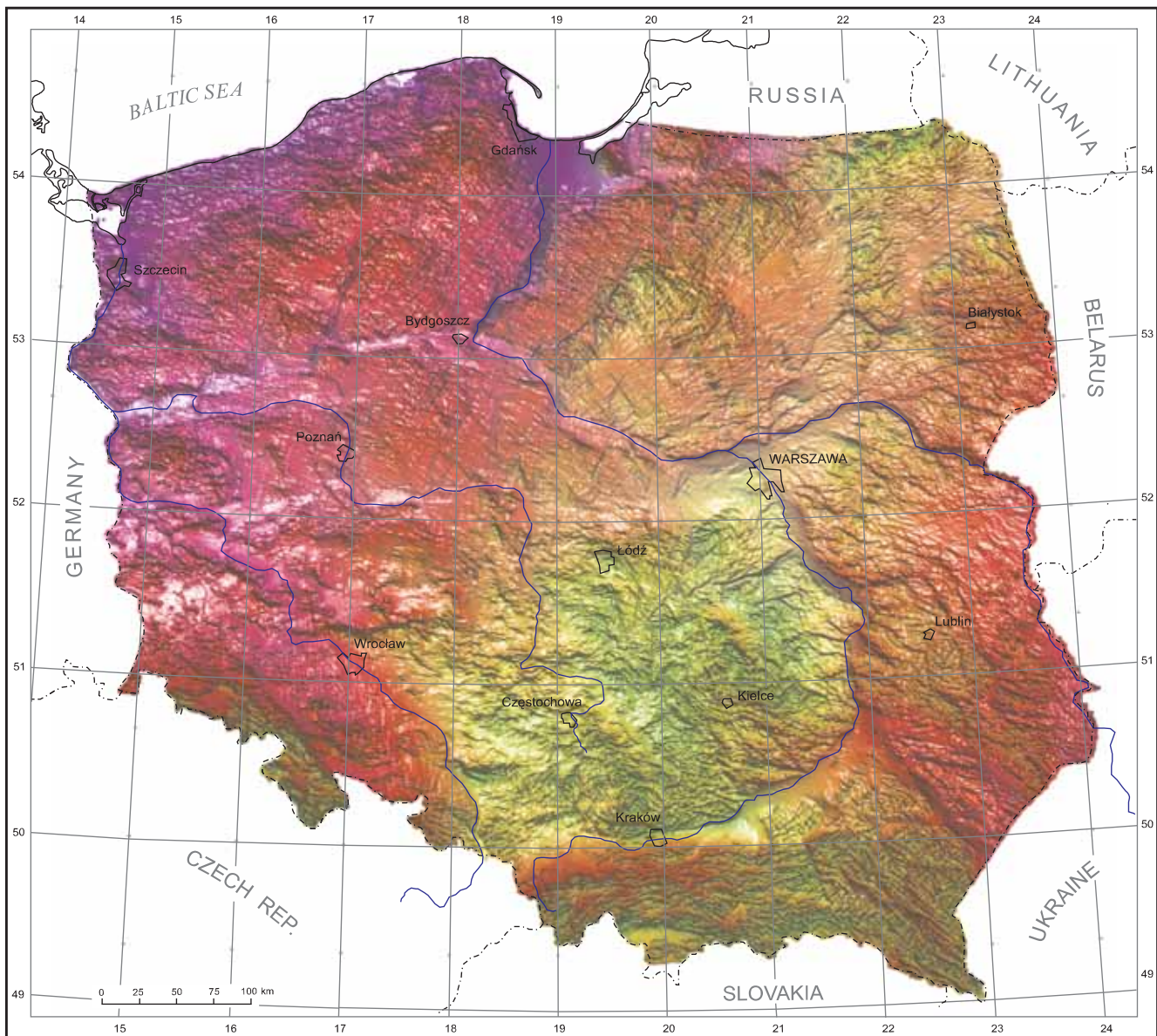
## Vertical-horizontal vectorial image of hypsography of Poland



**Transformation:** module of horizontal component; **transformation technique:** Hilbert transform by FFT; **visualization:** vertical-horizontal vectorial image with component/component-module colour scale (intensity 1.0) with superimposed shaded relief of total field anomaly illuminated from the north; surface mirror reflectivity: index 10, coefficient 1.0

**Remarks:** This vectorial image is quite unexpected. There is a difference between central highlands and eastern one. Vistula river flows just between them. It is better seen on the next image.

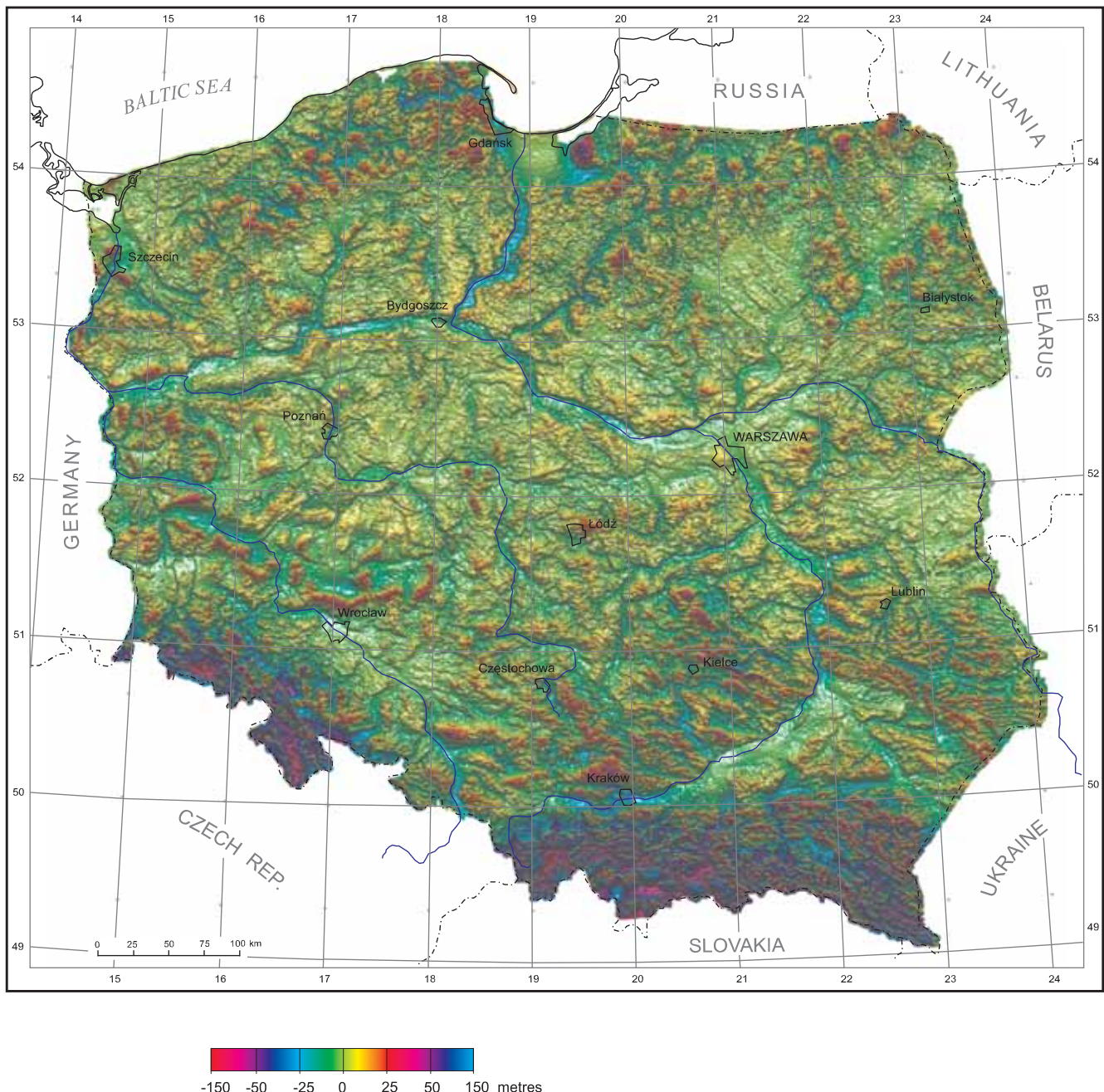
## Horizontal-vertical vectorial image of hypsography of Poland



**Transformation:** module of horizontal component; **transformation technique:** Hilbert transform by FFT; **visualization:** horizontal-vertical vectorial image with component-module/component colour scale (intensity 1.0) with superimposed shaded relief of the module of horizontal component illuminated from the north; surface mirror reflectivity: index 10, coefficient 1.0

**Remarks:** This image is more explicative than the previous one. The central highland is remarkably well delimited. It seems, that its origin is connected with Carpathian folding. Continuous stress which takes place here is upwelling the Carpathian foreland. It must be a block delimited by faults, which rivers like Odra and Vistula uses for their flows. In northern part of the country a delicate pattern of slight shadows of NNE–SSW direction can be seen. It can be connected probably with direction of flow of continental glacier in the last glaciation.

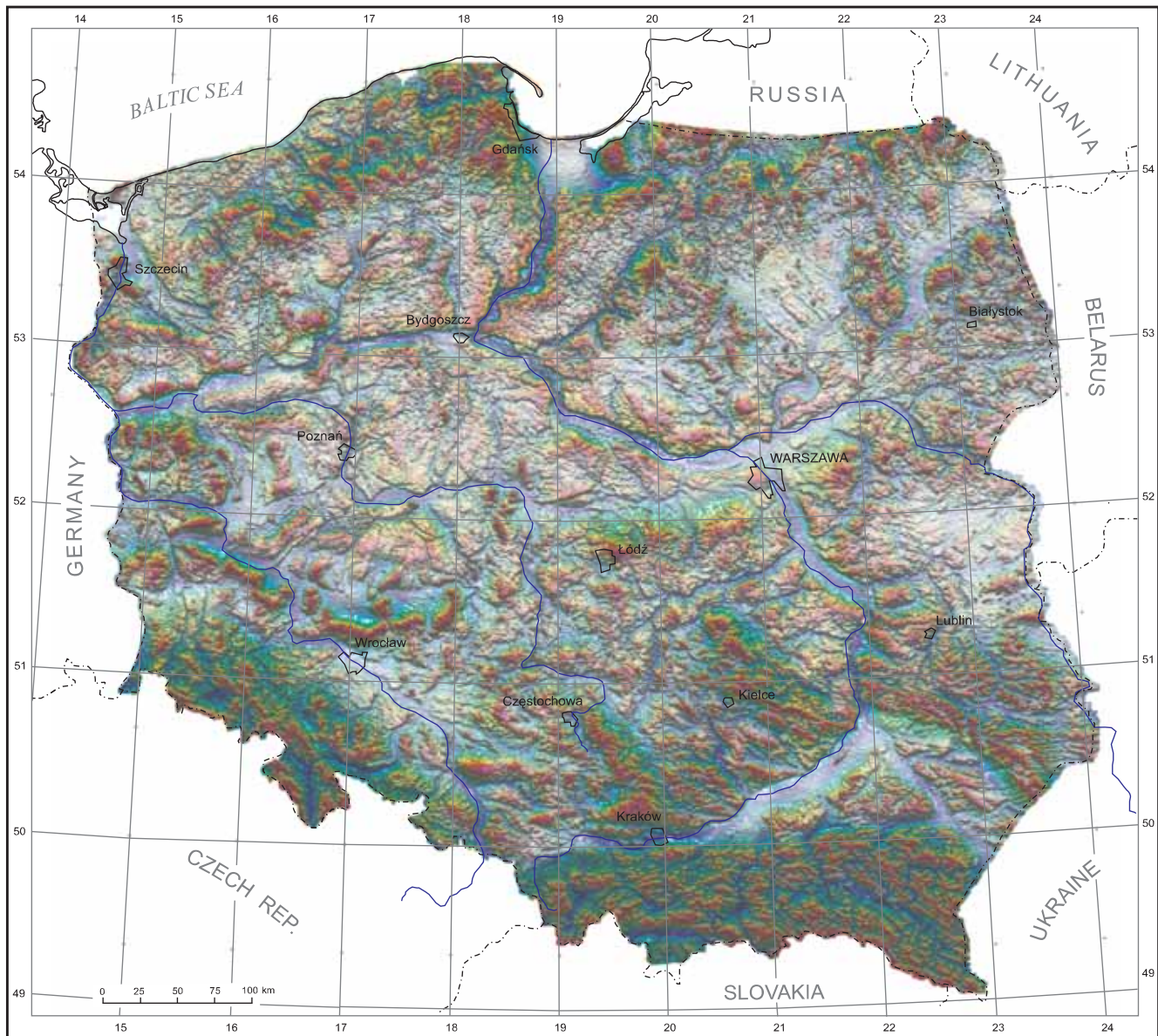
## Image of local anomaly of hypsography of Poland — extended full-hue colour scale



**Transformation:** local anomaly with basic wavelength range 1 to 30 km; **transformation technique:** sum of four directional components (every  $90^\circ$ ) obtained by digital filtering with Hilbert bi-transformer of  $61 \times 61$  dimensions; **visualization:** superposition of scalar image with extended full-hue colour scale, and shaded relief illuminated from the north; surface mirror reflectivity: index 10, coefficient 1.0; **visualization:** superposition of scalar image with extended full-hue colour scale, and shaded relief illuminated from the north-east; surface mirror reflectivity: index 10, coefficient 1.0

**Remarks:** Three following images shows “local anomaly” of Polish hypsography, as basic wavelength range is limited from 1 km to 30 km. As a result we observe strong positive and negative anomalies in the mountains.

## Vertical-horizontal vectorial image of local anomaly of hypsography of Poland

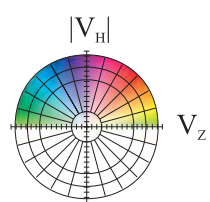
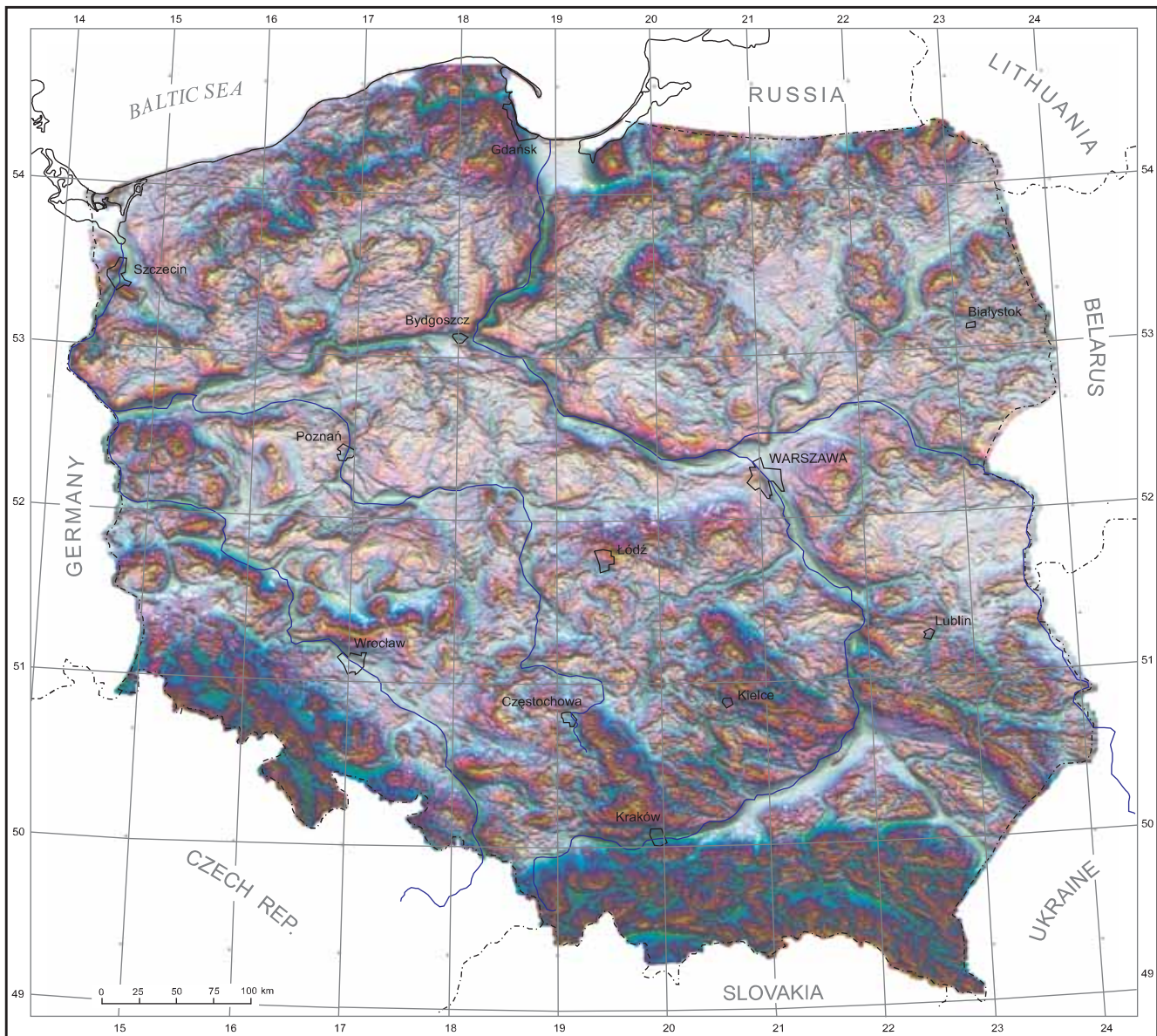


**Transformation:** local anomaly with basic wavelength range 1 to 30 km (as in Plate 28) and a module of its horizontal component; **transformation technique:** as in Plate 28 and additionally: horizontal components obtained by digital filtration using x- and y-Hilbert transformers (dimension 61x61); **visualization:** vertical-horizontal vectorial image with component/component-module colour scale (intensity 1.0) with superimposed shaded relief of total field anomaly illuminated from the north; surface mirror reflectivity: index 10, coefficient 1.0

**Remarks:** This image clearly shows great possibilities in using vectorial images in geomorphological interpretation of the relief. All flat areas, connected, as a rule, with river valleys, have blue colour, so hydrographic net is very well seen. All geomorphological objects are also well exposed. If we compare this image with its predecessor, the conclusion is evident.

PLATE 30

Horizontal-vertical vectorial image of local anomaly of hypsography of Poland



**Transformation:** local anomaly with basic wavelength range 1 to 30 km (as in Plate 28) and a module of its horizontal component; **transformation technique:** as in Plate 28 and additionally: horizontal components obtained by digital filtration using x- and y-Hilbert transformers (dimension 61x61); **visualization:** horizontal-vertical vectorial image with component-module/component colour scale (intensity 1.0) with superimposed shaded relief of the module of horizontal component illuminated from the north; surface mirror reflectivity: index 10, coefficient 1.0

**Remarks:** This image is a completion of the previous image. It enhances another aspect of terrain features. The gradient of relief is especially exposed. It seems, that it can be usefull for analysis of neogeodynamics activity. The more intense colour shows the areas where this activity is strongest. The areas with pale colours shows probably areas of subsidence or weak activity.